TABLE OF CONTENTS

Technical Papers on Drilling and Geology

International Conference on Petroleum Engineering 2016 (ICPE-2016)
Bangladesh University of Engineering & Technology (BUET)
Dhaka-1000, Bangladesh

ICPE (2016-021)

A Review on Smart Well Completion System: Route to the Smartest Recovery

Md. Nahin Mahmood[1], Md. Zayed Bin Sultan[2], Navid Yousuf[3]

[1]Lecturer, Department of Petroleum and Mining Engineering**,** Chittagong University of Engineering & Technology (CUET), Chittagong-4349

[2]Assistant Professor, Department of Petroleum and Mining Engineering, Chittagong University of Engineering & Technology (CUET), Chittagong-4349

[3]B.Sc. in Petroleum and Mining Engineering, Chittagong University of Engineering & Technology, (CUET), Chittagong-4349

ABSTRACT

Drilling and completion techniques in petroleum industries have advanced significantly over the last few decades to improve the recovery from hydrocarbon reservoirs. The conventional method of drilling followed by well completion is replaced by various intelligent ways, which effectively support the production improvement. Smart well completion is one of these intelligent or modern techniques that include permanent downhole sensors and surface-controlled downhole flow control valves, allowing to record, evaluate, and actively manage production in real time without any well interventions. In addition, smart wells provide the ability to control uncertainties associated with reservoir heterogeneity. These mitigate unexpected sand production due to fractures and hence increase the ultimate recovery. The design, selection and installation of different tools and equipments in a smart well completion are conducted in an effective manner so that the wells can be brought into production within the operator's objectives for the field development. Once a smart well is developed, valves can be used to independently control each segment / branch of the well in a reactive mode, such as shutting off a zone when it starts producing water; or in a defensive mode, which requires a prior determination of valve settings. The smart well system is comprised of different downhole sensors and valves which facilitate to improve the performance of the well, literally signifies the improvement of productivity and bypassing different unwanted occurrences. Various objectives are served like water cut minimization, and net present value maximization. Besides the sand production can also be minimized which causes serious distortion in the production scenario. So the intelligent completion methods of production well can destine towards a logical and effective stability. In this paper, the completion system of a smart well is reviewed and presented with its pros and cons. The proper arrangement structure is furnished here which will be helpful to get a clear idea about the smartest completion outlook and can be effectively used for further practical applications.

Keywords- Smart Wells, Downhole Sensors, Valves, Production Improvement, Sand Production.

* Corresponding Author address
E-mail: nahin2582@cuet.ac.bd

INTRODUCTION

Wells are being drilled in potential hydrocarbon bearing zone since the inception of earth science. These wells serve the purpose of exploration and production of hydrocarbons; significantly oil and gas. Completion systems are the components necessary to complete the well after it is drilled and prepared for production. This stage requires maximum importance for sustainable production scenario in a safe way to avoid any unwanted situations. Primitively, there were fewer scopes for completing a well after the drilling phase has done. So there were no such differences between drilling and completion phase and the well was completed with some necessary protections to avoid blowout or any other known adversity. A blow out preventer (BOP) served as the prime completing element for a well. But with the advancement of technology, well completion is categorized as a separate portion of hydrocarbon production system. And nowadays, the term 'Smart Well Completion System' is on the way to replace the conventional completion system. The system characterizes some kind of automation by using different valves and downhole sensors at the significant positions of a well. The concept of smart well system resembles with the automated alarming system which indicats the anamoly of any stable situation in any electro-mechanical system. The ultimate consequence of implementing this system is the better recovery with lesser possibility of risks. As the whole well condition can be monitored from the surface, so it is easier to interpret the production scenario along with the negative consequences in a well's life time. Besides, production of the solid particles like, sand can be monitored properly and necessary steps like using packers or isolating sand producing zone can be taken into light.

DEFINITION

Smart wells are also termed as 'Intelligent Wells' from past. And the present day technology turned this intelligent system into a smarter one. 'Smart Well Completion' is defined as "the design, selection and installation of equipment and the specification of treatment and procedures necessary to bring the well into production and thereafter, to produce in a manner which satisfies the operator's objectives for the field development. [1] Completion, in petroleum production, is the process of making a well ready for production (or injection). This principally involves preparing the bottom of the hole to the required specifications, running in the production tubing and its associated downhole tools as well as perforating and stimulating as required. Sometimes, the process of running in and cementing the casing is also included. Nowadays, a sand control device also added as a key component in the system. It shows that a properly conceived and executed sand-control strategy can be very effective in reducing or eliminating solid production without unduly restricting productivity. New integrated techniques combining sand-control technology with smart well technology emerge to initiate the renaissance of modern completion system.

ISSUES SPECIFIED FOR SMART WELLS

The challenge to the completions industry is how to effectively integrate intelligent-well technologies with modern sand-control strategies. The following issues must be considered during the implementation of an intelligent flow control and monitoring system:

Protection and Isolation of Zones or Layers

Smart well completions may be used to monitor and control flow from separate reservoirs, separate layers, or separate regions of a heterogeneous formation. Some or all of these zones may require some

form of sand control, but critical to the effectiveness of the flow control is the hydraulic isolation of one zone from the other. Isolation may be achieved by using cemented and perforated liners with blank sections between zones. [1]

Equipment Diameters and Available Space

Intelligent flow-control equipment, transducer mandrels, and flat packs or control lines all take significantly more space than conventional completion equipment and may need to be deployed directly inside the sand-control equipment. This can create conflicts when attempting to keep casing and completion equipment sizes within conventional designs while maximizing flow areas to reduce flow velocity and maximize productivity.

Fluid Velocity, Pressure Drop, and Erosion

The bane of completion equipment in a solids-producing environment is erosion, and restricted flow areas and tortuous flow paths (typical around and through flow-control equipment) contribute to the effects of high velocity causing equipment erosion. When producing compressible fluids, such as gas, the flowing pressure drop associated with high velocity and restricted flow areas result not only in lower productivity but also in higher flow velocity. Erosion/corrosion mechanisms must also be considered in the material selection. [1]

Protection of Sensors, Cables, and Control Lines

Control lines, cables, and sensors represent the nervous and circulatory system of smart well completion and damage to these elements may mean partial or total loss of the functionality of the intelligent completion. These elements must be adequately protected from, vibration, and thermal stresses by use of appropriately designed clamps and encapsulating blast joints. Some manufacturers provide systems using dual redundant control line and electronic systems capable of operating on one system in the event of failure of the other.

Mechanical Interference of Moving Components

The solids produced with the fluids can interfere with movement and sealing of dynamic components, particularly sleeves on flow-control chokes and valves. The design of these components must be sand tolerant—either they must exclude solids from entering cavities that may cause interference with movement, or they must be able to easily wipe away the solids or function despite the presence of solids. Actuators and spring returns must generate sufficient force to move the dynamic components despite buildup of solids or scale. Frequent cycling of the valves may prevent accumulation of significant amounts of solid.

Injection Wells

In multizone reservoirs where the production wells require sand control, sand control should also be considered for the injections wells. Dissolution of the natural cementing materials in water-injection wells can destabilize the formation. During shut-in of these wells, flowback and crossflow between layers at different reservoir pressures will result in significant production of solids into the wellbore, which can cause plugging and interference with flow-control devices. Closing the flow-control devices during shut-in to reduce crossflow will help alleviate the problem but may not prevent it.

DESIGN CRITERIA OF WELL COMPLETION

As intelligent or smart well completion technology matures, the field of application continues to challenge the environment increasingly such as, the poorly consolidated, high-permeability, high-productivity; clastic reservoirs are fit for the operation of intelligent-well applications-high-productivity wells, complex reservoirs, high capital investment, and high intervention costs.

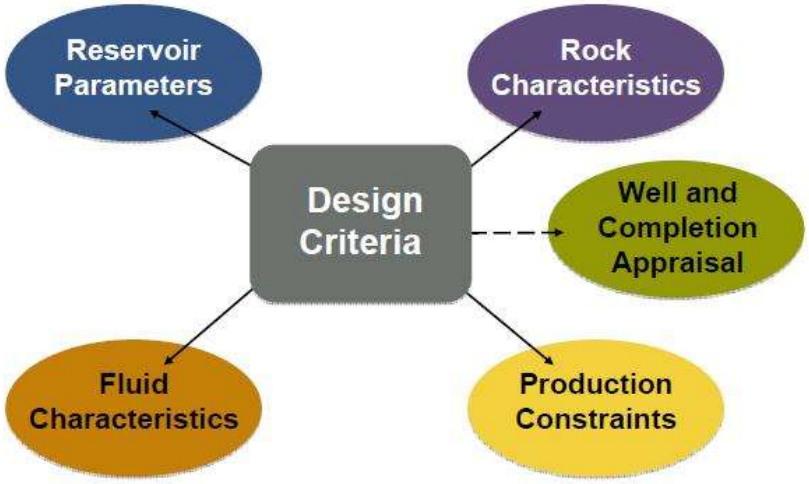

Figure 1: Design Criteria of Smart Well Completion [1]

With the increased demand for hydrocarbon as a clean energy source, many operators investigate different means of increasing performance of their field. Many design variables such as number of wells, line pressure, wellbore diameter, peak day requirements, and gathering system must be taken into account in the optimization process. Additional parameters that affect the performance of the field are formation characteristics related to geology and depositional environment.The demand for hydrocarbon changes seasonally and the desired storage reservoir should be capable of meeting the peak rates especially during the winter months. There is a need to develop more hydrocarbon storage reservoirs that are managed efficiently. The inherent problem is the maximization of production with minimum cost. The maximum production is a function of hydrocarbon volume controlled by the reservoir properties such as porosity, permeability and pressure. It is beneficial to determine the optimum combination of wells, cushion gas, and compression facilities to minimize the cost of developing a new gas storage reservoir or converting an existing gas or depleted oil reservoir.

Factors like rock characteristics, fluid characteristics, production constraints are the key issues effecting the hydrocarbon storage reservoir. But to find the best combination is a challenge. A limited improvement of formation properties can be achieved by stimulation treatments. On the other hand, decisions regarding the number, location, and type of wells, completion methods, hole size and similar decisions are the result of proper planning. The literatures presented in this study are the effects of reservoir properties on the efficiency of selected well design to meet the demand. Besides, sand and fines produced with oil and gas can cause erosion and wear of production facilities/equipments, resulting in production downtime, expensive repairs, and potentially loss of containment (serious safety risk). Erosion of choke

elements, seal surfaces, control lines, and interference with device movement can render the intelligent completion inoperable, thus losing its functionality and the ability of the operator to use the equipment to realize its long-term value.

PHASES OF WELL COMPLETION

Smart well completion systems offer a better approach for completing a well with an active management procedure. Through continuous readout data acquisition and remote control, the operator has the ability to monitor and control flow from or injection into multiple zones within real time. Producers can reconfigure a well's architecture at will and acquire real-time data without well intervention. Well completion procedure should follow some steps which are mentioned below:

Firstly, the zonal isolation is to be done. Then the flow from the desired location should be controlled. Running the casing followed by complete cementation ensures a good start in the completion phase. Finally the swell packer serves as to counter swelling of the formation.

Secondly, the solids laden fluid is replaced with the solids free fluids followed by running in the work string. Then the drilling mud is circulated with the completion brine. The brine is filtered and work string is pulled out.

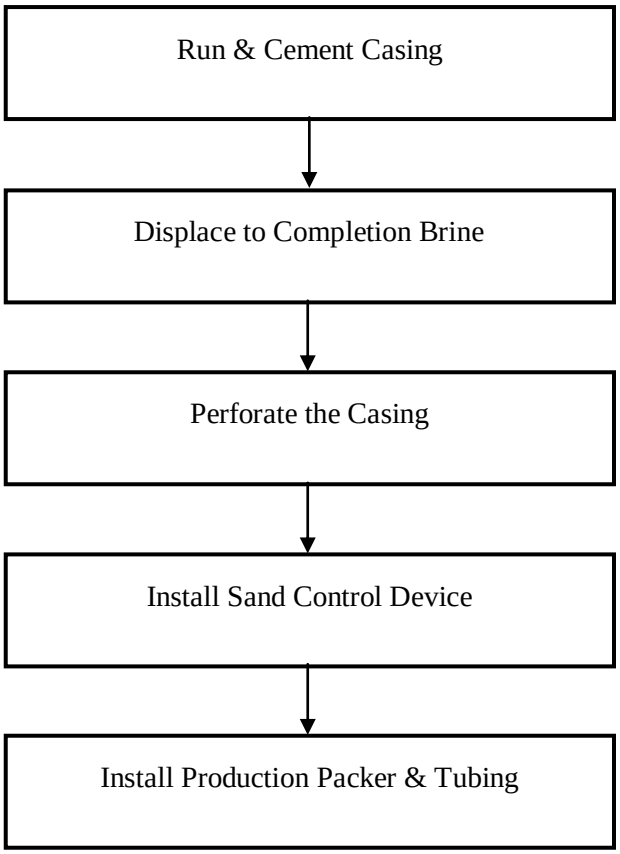

Figure 2: Flow Chart of a Well Completion

Thirdly, perforation provides a flow path from the reservoir to the well bore. In this phase, the packer is being run along with the perforating assembly. The guns in the hole being fired which creates sufficient perforations and stabilize the well. The spent guns are pulled out at last.

Fourthly, the formation materials found from the oil, gas or water production are filtered. The screen and packer assembly is run. The packer is set by dropping the ball. Gravel packs are installed which is simply a downhole filter, designed to prevent the production of unwanted formation sand. The formation sand is held in place by properly sized gravel pack sand that, in turn, is held in place with a properly-sized screen. To determine what size gravel-pack sand is required, samples of the formation sand must be evaluated to determine the median grain size diameter and grain size distribution. [2] The quality of the sand used is as important as the proper sizing. The American Petroleum Institute (API) has set forth the minimum specifications desirable for gravel-pack sand in API *RP 58*, testing sand used in gravel-packing operations. [3]

Fifthly, it is mandatory to seal and protect the casing from erosion and corrosion. The production tubing is run in the well. The inhibited packer fluids are allowed to circulate which is followed by installing production packer.

SYSTEM AND ASSEMBLY OF COMPLETION SYSTEM

There are many completion options available to oil and gas producers. Today's cased-hole completion systems vary from relatively simple single-zone low-pressure/low-temperature (LP/LT) designs to complex high-pressure/high-temperature (HP/HT) applications that were unthinkable with the technology available 50 years ago. Many of the basic components appear similar to those used in the past, yet they have been vastly improved, and their performance has been optimized to suit numerous environments. At the reservoir level, there are two types of completion methods used on wells: open-hole or cased-hole completions. An open-hole completion refers to a well that is drilled to the top of the hydrocarbon reservoir. The well is then cased at this level, and left open at the bottom. Also known as top sets and barefoot completions, open-hole completions are used to reduce the cost of casing where the reservoir is solid and well-known. But the cased hole completion system serves the purpose of maximum security and protections from undesired situations. The appropriate equipment depends on the type of completion as well as downhole conditions. Completion tools offers a wide range of products and services designed to maximize well production including swellable technology, subsurface safety systems, high-pressure packer systems, intervention solutions, flow controls, and expandable liner technology as well as intelligent completions and multilateral systems.The assembly of a smart well system possesses the following components which direct towards a stabilized and smart condition of production. It includes,

Annulus Safety System-This is a fully retrievable high performance annulus safety system integrated with an annular safety valve. The system provides annular bypass through a hydraulically operated valve array. The packer is run in association with a hydraulic system (HS) hanger in two trip applications where the ability to perform top end workover is needed in certain conditions.

Zonal Isolation Packers Setting- Packer is a single-string, retrievable, cased-hole packer that features a facility of bypassing multiple electrical and/or hydraulic control lines. Available for using as both the top production packer or as one of many lower packers isolating adjacent zones, the packer includes a specialized slip configuration and additional body lock ring, which allow it to operate under higher loads and greater pressures than standard production packers. Packers, available for both production and isolation applications, are single-string, cased-hole, retrievable packers primarily designed for use in smart well completions in marginal or mature assets. Both production and isolation packers have the facility to feed through up to eight hydraulic or electrical control lines, allowing communication with other smart well equipment without compromising the integrity of the isolated zones. [3]

Downhole Control Systems-Downhole control systems provide a method of integrating the surface control system (either manual or automated) with downhole smart well equipment. The system is a fully integrated control and data acquisition system which allows the operator to remotely control the wellbore and obtain real-time pressure/temperature data for each zone. This data feedback and accurate flow control capability allow the operator to optimize reservoir performance and enhance reservoir management. [3]

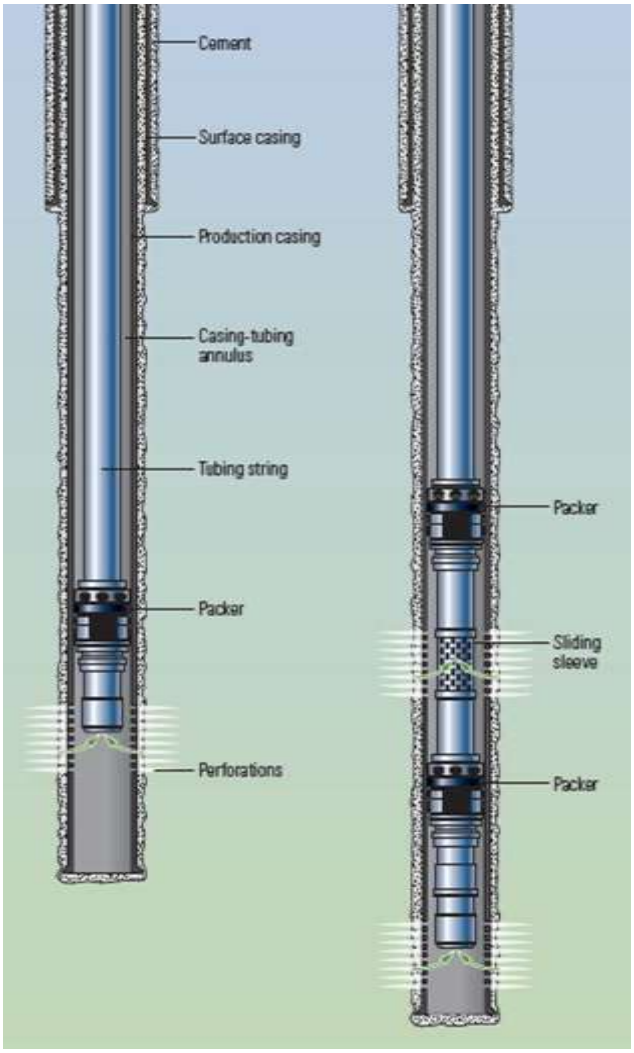

Figure 3: Single Zone and Multi Zone Well Completion [4]

Surface Control System-The surface equipment for the digital hydraulics system is designed as part of the digital infrastructure system. A fully automated surface hydraulic system (SHS), controlled from a central location allows control of the digital hydraulics system from a local or remote control station. The smart well master application translates digital hydraulics system logic into standard central control room operations. This translation allows the operator to easily monitor and control multiple digital hydraulics completion systems as well as an individual zone within an intelligent well completion.

Swell Technology Systems-Swell technology systems are based on the swelling properties of elastomers. The swelling process creates effective seals in both open and cased hole applications. Some isolation

systems used above top of cement (TOC) will prevent pressure migration to surface (sustained casing pressure) from lower reservoirs without compromising the competency of the original cement job. [3]

SAND CONTROL SEQUENCES IN A SMART WELL

Sand production is one of the major problems associated with smart well completion system. Use of smart well completion elements can significantly contribute to the management and prevention of sand production while maximizing hydrocarbon productivity. In below, here is a flow chart regarding the management of sand control methodology, which shows the complete scenario of sand management. [5]

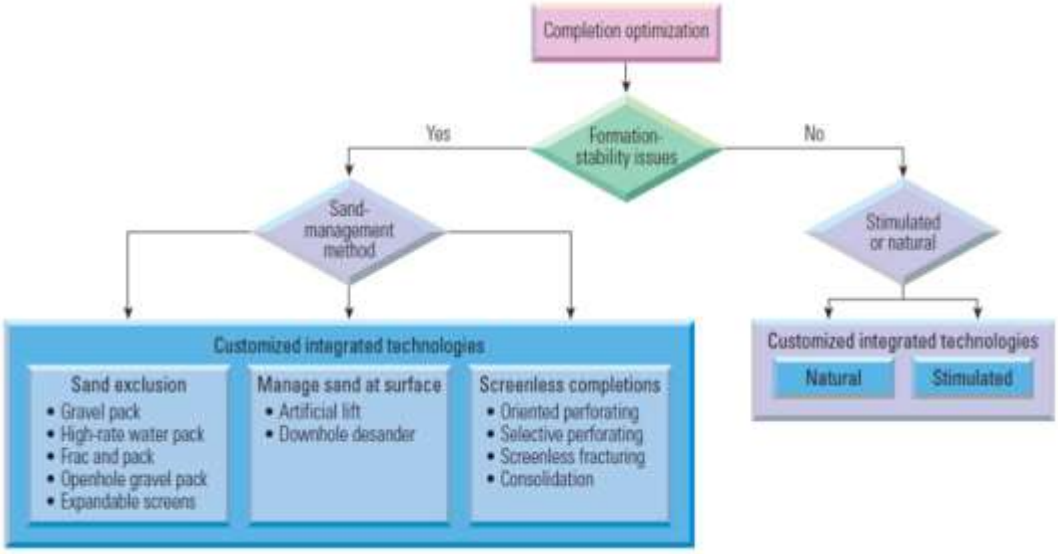

Figure 4: Sand Management Methodology [5]

The first step decides about formation stability issues. If the stability criterion is fulfilled, then the sand management procedure can be adopted. Otherwise the process of completion should go for further stimulation of the formation. In the sand management procedure there are notably three types of procedure to follow. Like, a) Sand Exclusion b) Manage Sand at Surface c) Screenless completion.

Here, the technologies are applied on the basis of various factors like the formation geology, stratigraphy, and completion types (vertical or horizontal). The most promising solution is the use of smart well equipment with expandable screens. This solution maximizes flow areas in both the annulus and the production conduit. Installation of several dip-tube-type completions around the world has been successful.

Besides, the sequence chart also shows that, if the stability issues are not satisfactory, customized integrated technologies should be adopted. Here, the approach consists of natural and stimulated technologies.

The sand management procedure can generally be classified into two ways; either it is done by implementing a completion system which will monitor and control the flow rate or in other way, it will allow the sand to come in production and then disposed. Using garvel pack or maintaining the flow velocitybelow critical point can be the most effective starategy of sand exclusions in a well. Although formation solids are not always sand, in the petroleum industry, the production of any solids from a well is generally called sand production.It is not often anticipated that, produced solids can accumulate in the

well or in subsea or surface flow lines, destroy a downhole pump, or erode various well hardware including slotted liners or screens, gas-lift valves, the surface choke, or any bends in surface pipe. At a low enough flow velocity, formation solids will remain in the formations. The critical sanding rate is the production rate at or below which sand production is avoided. The critical sanding rate may drop over time due to changes in the completion or the flow stream. For example, many wells do not produce formation fines until water breakthrough.

A smart well is best drilled in reservoirs where wellbore hydraulics (water coning) and heterogeneity (fractures causing early water breakthrough) exist. Therefore, eliminating water coning and delaying water breakthrough by determining the best ICV (Inflow Control Valves) configuration provides considerable scope for improving oil and gas production. By monitoring actual inflow conditions and controlling and restricting fluid flow into the wellbore, smart wells can maintain the flow below critical rates that would otherwise destabilize the formation matrix or gravel pack. Zones that develop a propensity for water production can be choked back or closed in, also reducing the tendency for sand production aggravated by multiphase flow and aqueous dissolution of natural cements. One of the simplest solutions for controlling two zones with sand control is the dip tube or siphon tube solution. [6] The well is completed with a conventional two-stage gravel pack (or screens), isolating the two zones from each other with a section of blank pipe and a packer. A second solution for controlling multiple zones with sand control is done where each zone is completed with (from top to down) a hydraulic set, hydraulic feed-through isolation packer, a gravel slurry placement sleeve, a shrouded ICV with the shroud attached to the gravel-pack screen base pipe and the ICV attached to an internal, concentric, through-wellbore, production conduit, which ties into the isolation packer of the next lower interval.And the third and most promising solution is the use of intelligent-well equipment with expandable screens. [7] This solution maximizes flow areas in both the annulus and the production conduit.

CONVENIENCES OF SMART WELL

Though the concept of intelligent or smart wells has been in existence for over a decade, it continues to receive a lot of attention and research grants, due to the enormous amount of accruable benefits, if effectively applied. Foremost on the list of benefits are the accelerated hydrocarbon production rates and upsurge in reservoir recovery factor. [1] The functions of smart well completion are considered two-pronged i.e.: monitoring and control. Both the monitoring and control sectors must work in synergy for a well to be truly considered smart or intelligent. As is evident thus far, the benefits of optimal application of smart well completion technology are numerous. These include:

1. Reduction or elimination of extra wells, surface facilities, and intervention procedures **2.** Reduction in the water cut **3.** Reduction in operational expenses (OPEX) **4.** Extends the life of wells and reserves **5.** Crossflow elimination and back allocation of commingled production for economic exploitation of marginal reserves **6.** Augmentation or replacement of wireline services, particularly in inaccessible wells **7.** Maximization of injection sweep efficiency by regulating injection rates **8.** Reduction of geological uncertainty by higher reservoir characterization 9. Real time measurement and transmission of reservoir properties for better reservoir management 10. Reduced risk of personnel accidents, since there is reduced requirement for their presence on the well site.The advantages of smart wells have been demonstrated in practical applications for both single and multiple reservoir production (non-commingled production). Because of their ability to control production from each lateral or segment through ICV adjustment and manipulation, smart wells can mitigate water production by allocating the optimum production rate and therefore factorize in the production improvement.

A discussion on complete screening exercises has proved to be the most convenient way to highlight intelligent-completion value and intelligent completion's ability to enhance asset-value in terms of production acceleration, increased ultimate recovery, and reduced operating expenditure (OPEX) and

capital expenditure (CAPEX). Most of the recent oil and gas field developments in the word are furnished with smart wells. They provide the desired production target with lower capital and operating costs. Figure 5 shows a comparison between vertical, horizontal, and smart wells that were deployed in different developments within the same field. Desired production target is achieved with 48 smart wells as opposite to 150 vertical wells and 66 horizontal wells. [7]

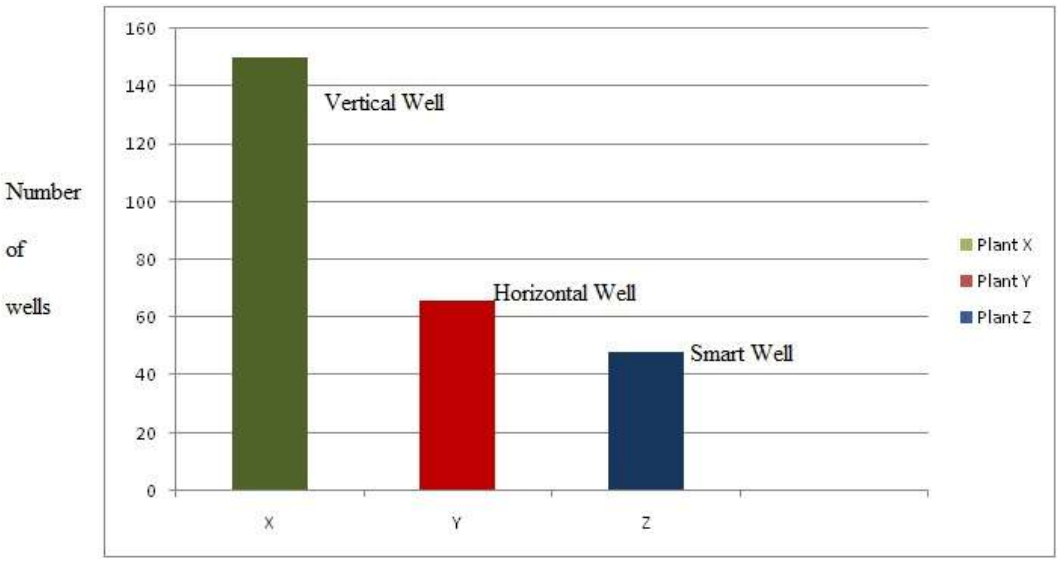

Figure 5: Number of Wells Reduction in Smart Well Operation [7]

CONCLUSION

The concept of Smart well completion has been investigated from different perspectives, ranging from its applicability under different conditions and multiple scenarios, to the benefits and challenges encountered in operation. Extensive knowledge sharing on application of smart well completion technology has bolstered its growth. A review has been carried out here on previous smart well completion research and applications. The service industry and field operators are actively pursuing remote completion monitoring and control. Initial indications have indicated the benefits and scope for this technology, but only limited quantification of benefits has been made. Based also on experience with manual intervention techniques, it is concluded that up to 10% of accelerated or incremental recovery is a reasonable target for this new technology in the early years of well life. Intervention savings provide further payback, particularly for subsea or unattended platform wells.

ACKNOWLEDGEMENT

The extreme gratitude goes to the Almighty who enable us to fulfill the job perfectly within the assigned time frame. We are highly thankful to the entire Petroleum and Mining Engineering Department, CUET; Especially to Mr. Tareq-Uz-Zaman, Assistant Professor, Department of Petroleum and Mining Engineering, CUET for his unconditional support and assistance throughout the research procedure. He contributed with all the corrections, suggestions and makes the review paper come into the light. Besides, heartiest gratitude and thanks go to different unmentioned people in different phases of the work.

REFERENCES

[1]. Yeten, B. & Jalali, Y., (2001). Effectiveness of Intelligent Completions in a Multiwell Development Context, [SPE-68077-MS]. Paper presented at the SPE Middle East Oil Show, Bahrain, 03-04.

[2]. Adekunle & Aderemi, Olajide, (September 2012). Master's thesis on Intelligent Well Applications in Production Wells, University of Aberdeen, 06-07.

[3].Brown, Emie, Thomas, Ron. & Milne, Aurthur, (2011). Analysis of the challenges of well completion. Proceedings of the National Conference on Drilling, Texas.

[4]. Flatern, Van. Rick Senior Editor, (Winter 2011-12). Schlumberger; Oil field Review, 53-54.

[5]. Jorge López-de-Cárdenas, Masatoshi Nishi, Andrew Acock, Allan Wilson, et al. (Spring 2004). Practical Approaches to Sand Management, 17-18.

[6].Michael J. Economides A, Daniel Hill Christine, Ehlig-Economides, Ding Zhu, (2013). Petroleum Production Systems, [SBN-13: 978-0-13-703158-0], Pearson Education, Inc. Westford, Masscachusetts, Second Edition, 623-649.

[7]. Al-Ghareeb, M. Zeid., (June 2009). Monitoring and Control of Smart Wells, 02-03.

International Conference on Petroleum Engineering 2016 (ICPE-2016)
Bangladesh University of Engineering & Technology (BUET)
Dhaka-1000, Bangladesh

ICPE (2016-022)

Wellbore Instability Issues While Drilling Wells in Bangladesh: A Case Study

Evana Tinny*[1], Shahriar Mahmud[1], Howleder Ohidul Islam[2]
Petroleum and Mineral Resources Engineering Department, Bangladesh University of Engineering and Technology, Dhaka,Bangladesh[1], Bangladesh Petroleum Exploration and Production Company Limited, Dhaka, Bangladesh[2]

ABSTRACT

Wellbore instability is one of the most prevalent downhole challenges since oil well drilling began. Each year issues related to this cause momentous amount of non productive time (NPT) and cost. In some cases fishing operations are necessary which results in further financial loss. The Drilling Industry in Bangladesh has also experienced wellbore related issues especially stuck pipe cases from time to time. While the problem is quite common all around the world including Bangladesh, there is a lack of in-depth analysis of these incidents. The Exploratory well Mubarakpur-1, in sathia of Pabna, was spudded on August 2014 by BAPEX (Bangladesh Petroleum Exploration and Production Company Limited). There was not much prior Geological knowledge of the region available before the Drilling Programme commenced. Hence the degree of uncertainty was higher than usual for the company. During the drilling operation the crew experienced problems like hole pack-off, excessive tight spot, overpull, cavings, high torque and drag, inability to run logging tool due to reduced wellbore size etc.. Finally pipe got stuck at around 4175 m MD. A good amount of time was spent to recover the BHA without any success. Ultimately the BHA was lost. Later they had to sidetrack to reach Target Depth. The primary focus of this study was to analyze the operational sequences and subsequently to find out the root causes which led to this Stuck Pipe incident. Our study shows that the Stuck Pipe situation occurred for multiple reasons e.g. unusual formation characteristic compared to other areas in Bangladesh (Illite rich Shale formation) which led to creating cavings at high in-situ stresses, less hydrostatic pressure, long time exposure to open hole, inadequate hole cleaning etc. Due to cavings formation there was also issue with proper cementing job. After the investigation the authors have highlighted on the lessons learned and made an effort to give recommendations which could be useful for planning for future drilling operations within this region.

Keywords: Stuck Pipe, Mubarakpur-1, Exploration well drilling, Illite rich formation, Cavings.

* Corresponding Author address
Email: evanatinny@gmail.com

INTRODUCTION

Mubarakpur exploratory well-1 is located in Santhia Upazilla of Pabna district in Bangladesh. The well lies southeast of Singra-1 and southwest of Hazipur x-1. On completion of a five-year joint seismic survey by Petrobangla (Bangladesh Oil, Gas & Mineral Corporation) and German company Prakla Seismos in 1984, Mubarakpur, was identified as a prospective site. The drilling project started on August 2014. Expected reservoirs of the site are Stratigraphic Trap (delineated as onlap closure), onlap features (a bunch of sand beds) pinching out against the slope channel sequences towards the northwest. The aim of the Mubarakpur Well-1 was to penetrate a wide slope channel sequence of Miocene age and to test the hydrocarbon potentiality in a geologically new province.

Mubarakpur exploratory well-1 was spud on 29 August, it's TD was 4624 m RKB. It was one of the most problematic drilled well of recent times. Wellbore instability manifested in many ways like hole pack-off, tight spot, overpull, excessive cavings, high torque and drag, inability to log the well, poor cementing and finally leading towards pipe stuck, tools lost in hole, that required side tracking. Other problems like rig centering, top drive problem etc with several others minor problems made the hole a challenging one to drill.

GEOLOGICAL ASPECT

The tectonic framework of Bangladesh may be broadly divided into two main units: 1) Stable platform in the northwest 2) Deep basin to the southeast. There is also a narrow northeast-southwest trending zone called "Hinge zone" separates the above two units diagonally almost through the middle of the country. The geology of Mubarakpur area is associated with stable to transitional (Hinge zone) tectonic setting. The zone is about 25km wide northeast-southwest zone that separates Precambrian platform in the northwest from deep basin to the southeast. There is no surface expression of this unit but it is marked by the sudden increase of dip in subsurface sedimentary layers as shown strongly by the seismic marker (seismic line PK-01, 8426, 8316, 8424, 8425, HC-01) at the top of the Sylhet limestone unit of Eocene age. The hinge zone is not a tectonic hinge but represents Eocene shelf edge / slope break i.e. a paleocontinental slope. It extends more than 500 km from Calcutta, India, north-eastward to Bangladesh's northern border. Its equivalent continues into the Assam basin of India for an additional 300 km, defining the eastern limit of the Indian continent during the Eocene. It may be noted that the western part of Bengal Basin is marked by a series of migrating shelf break with the most prominent being the Eocene shelf edge. That is why it is known as Eocene hinge zone.[1]

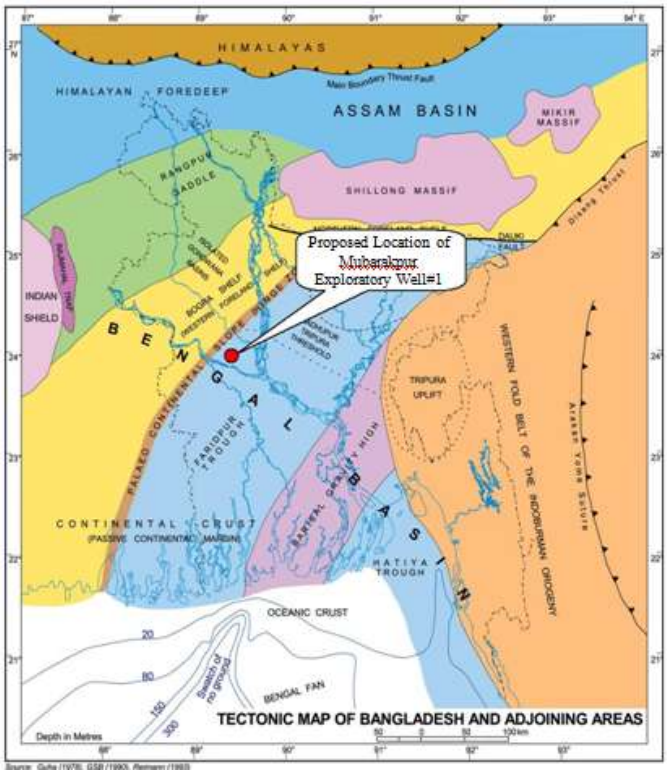

Fig 01: Mubarakpur Exploratory Well#1 on Tectonic Map of Bengal Basin

Normal hydrostatic pressure was expected in Mubarakpur area upto 3500m. Below this depth anticipated pressure gradient of Mubarapur exploratory well#1 was 0.52 psi/ft. Geological setting and environment of deposition is different from the above 3500m section.(Fig 02)

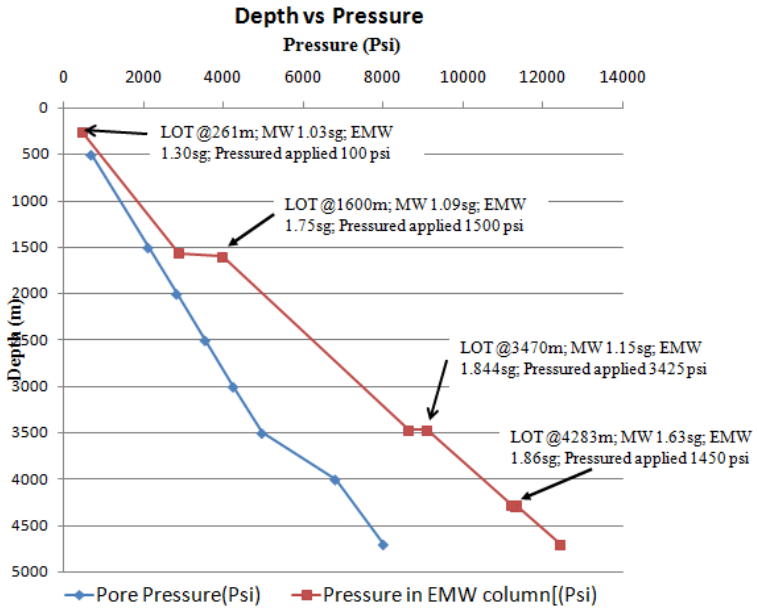

Fig 02: Pore pressure and Fracture gradient from LOT[5]

SUMMARY OF OPERATIONS

The design of this well was 30″ False Conductor Casing (0 - 33m) X 20″ Surface Casing (0 – 256m) X 13 ⅜″ Intermediate Casing (0 – 1588 m) X 9 $^{5}/_{8}$″ Intermediate Casing (0 – 3465 m) X 7" Liner Casing (3360 – 4278 m) X 5" Liner Casing (4233– 4623 m).

Operation sequences are as follows:

- Spud in, run 30” false conductor Casing and Cemented.
- Cement tag, worked on BOP, Bell Nipple, Rig testing, Rig Engine, Mud System, Draw works and others
- RIH with 26" Bit and drilled.
- 20" Casing run and Cemented, WOC, Repairing work on VFD house, work on well head.
- Made up New BHA with 17 ½” bit, Top drive repaired.
- Wireline Logging, run 13 3/8” Casing and Cemented, WOC and Work on Well head
- RIH with 12 ¼” PDC bit, drilled, wiper tripped, reaming up and down.
- Wireline Logging, run and cemented 9 5/8” Casing, Work on Well Head
- Rig Centering and Civil work for it
- Made up 8 ½” bit, RIH, top drive problem
- Drilling progressed, reaming, pipe stuck at 4190m during circulation, got free by downward jamming.
- Reaming, Failed to pass wireline logging tools.
- Wiper tripped, 10 attempt failed to run logging tools, KCL polymer mud used.
- Reaming continued, power system shut down for 20 minutes, got again but pipe stuck at 4175m, lost circulation.
- Stuck free operation, fishing operation, string lost, Cement dumping.
- Side track started from 3495m with 8 ½” bit.
- Reaming, failed to run Wireline logging, Mud weight increase
- 7” Liner run, Cemented, WOC, Wireline Logging completed
- Drilling resumed with 6 ½” bit.
- 5” Liner run in, Cemented, WOC, Cement Drilling and Wireline Logging completed
- DST Operation[5]

FUNDAMENTALS OF STUDY

In Geological aspect Mubarakpur area was quite different from others gas field area. The problematic shale zones were Illites which do not show interlayer swelling. The compensating cations of illite are primarily the potassium ion (K+) (Fig: 03). Ca and Mg can also sometimes substitute for K. The ionic diameter allows the K+ to fit snugly between unit layers forming a bond that prevents swelling in the presence of water. Mixed layers of Illite and Smectite often cause various problems in borehole stability and drilling fluid maintenance. The troublesome nature of these clay minerals can be related to the weakly-bonded interlayer cations and weak layer charges that lead to swelling and dispersion upon contact with water. With increasing burial depths, the smectite gradually converts into illite/smectite mixed-layer clays and finally to illite and mica. As a result, shale formations generally become less swelling but more dispersive in water with increasing depth.[3]

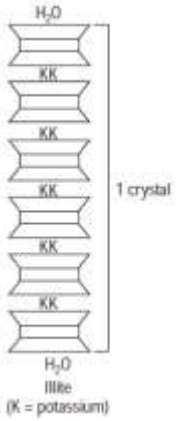

Fig 03: Non swelling clay, Illite structure.[3]

All rocks are subjected to stresses at any depth. Vertical principle stress($\sigma_{a)}$, usually the overburden stress, results from the cumulative weight of the sediments above a given point, two horizontal stresses (σ_r & σ_h) and pore pressure(P). The total load on the wellbore wall is the mud pressure(Pi) inside the bore hole and this load is taken up by the stresses in the rock matrix plus pore pressure. [2]

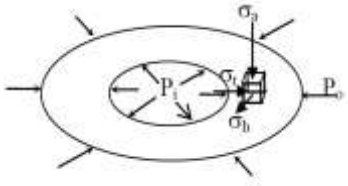

Fig 04: Stresses acting on the borehole wall

During drilling the rock that was in the hole is replaced with drilling mud. If the drilling mud creates the same stress, there is no disturbance in stress. The mud density in a well section is constant, but the stresses and pore pressure change with depth. The mud weight is therefore a compromise over a depth interval. The low permeable shale zones without optimal mud weight often cannot reach to the point to support the total overlying rock column. As a result the high stress contrast between the high hoop stress and the low borehole pressures gives rise to borehole collapse. [2]

The not equilibrium stress condition sometimes result in tight spots , which may require frequent wiper trips or reaming. A tight spot and borehole collapse are similar events; in one case, the hole may yield, while in the latter case, an abrupt failure may occur. Rock cavings in the mud returns are the effect of more hoop stress[2]

In exploration wells, sometimes the mud weight is kept close to the pore pressure (Fig 05). shows three mud weight selection principles: low mud weight, median-line mud weight, and high mud weight. Aadnoy (1996)[4] reports a reduction in tight holes and back reaming after invoking that the median-line principle is a simple tool to establish an optimal mud-weight schedule. [2]

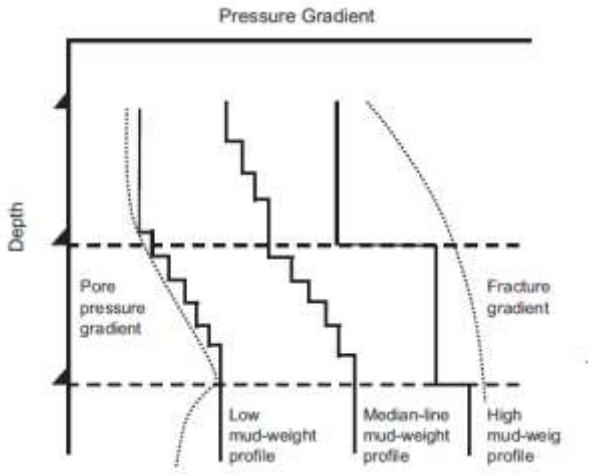

Fig 05: Alternative mud-weight schedules.[2]

PROBLEM ANALYSIS

There were several challenges the drilling team encountered before the pipe eventually got stuck. All these issues have been enumerated below:

Stuck Pipe: Before entering the 17 ½" section, drilling process ran smoothly. As the drilled zone was an over pressured illite shale area, with the increase of depth and exposure time, higher internal pressured weakly bonded shales dispersed in mud, started sloughing into the wellbore due to less hydrostatic pressure. After reaching the TD (Total Depth) and several failed attempts for wireline logging, continuous reaming were done to make the hole free. But with the attempt to go down without rotation & without pump out the open hole exposure could not resist the already over pressured formation wall. That promoted high torque, mud circulation fully lost and finally pipe stucked at a depth 4175m.

Excessive tight spots: In Mubarakpur-1 first tight spot was found at 937m. That was the start of many (more than 60) tight spots, observed across sections containing shale. Due to inadequate mud weight resulted in sloughing the shales and tight spots occured. Thus wellbore diameter reduced and increased drag while pulling up and down into the hole.

Cavings: Cavings observed in shale shakers while drilling in the sand and shale mixed zones. Polymer mud encapsulates shale cuttings and the well bore wall to prevent sloughing. But with extended exposure time while excessive reaming and tripping, this type of system, most notably KCL systems could not stop sloughing in many shale zones which results in huge cavings in shale shaker. After drilling 3500m, huge cavings of average 1-1.5″ were observed at shale shaker continuously. Cuttings and cavings were not hydrate or mushy as the shale zones were illites. (see Fig 06)

Fig 06: Cavings found in Mubarakpur-1 with in depth 3505-3530m.

High torque and drag: Due to tight hole conditions, sloughing hole, cutting build up caused by poor hole cleaning increased the pulling force than buoyancy effect resulted high drag and decreased RPM with increased torque.

Logging problem: Lowering logging tool inside the hole failed several times after the depth 3475m. Logging probe has only weight for itself, the sloughing shale pack off the hole and tools failed to pass through the held up zone.

Poor cementation: Excessive cavings lead to washout of formation of different depth, during cementing linear flow could not remove mud from the washout area. That's why at certain point poor or bad cementation found. For this need turbulent flow but it doesn't possible. Good hole condition is the precondition of good cementing. If there is no good cement in between water sand and gas sand, after some production due to pressure deplation there must cross flow started, so it will hamper the production.

To get rid from hole filling and preventing all pipe stucking indications drillers continued wiper trip with reaming, back reaming to lose the packed hole, pumped hi-vis mud, increased mud weight. Also changed mud system from gel polymer to LSND (Low Solid Non Dispersed) and finaly add KCL polymer. But non swelling clays could not stop sloughing and pipe stuck. With several failed attempts of jarring actions, sidetrack decision was taken with back off operation. Sidetrack started from 3495m and after 3549m drilling continued with Clay-seal Polymer mud system with increased mud weight than planned ones to stabilize the shale formation with the long exposure time.[5][9]

CONCLUSION

As this was the first well drilled in Mubarakpur area which has a different geological structure compared to other parts in Bangladesh which already have been explored, there was no offset data and hence lack of knowledge about the formation. The problematic zones were high in illite, the shales were chemically inactive, inhibitive mud was not needed. Otherside the overpressured zone, calculated after 3500m (Fig 02), could not stop sloughing due to insufficient hydrostatic pressure (Fig: 07). It is also imporatant to clean the hole in proper manner with the up going trends of cavings. All these causes leds to the wellbore instability of Mubarakpur-1 which resulted in pipe sticking took large amount downtime and maintenance costs and schedule delays.

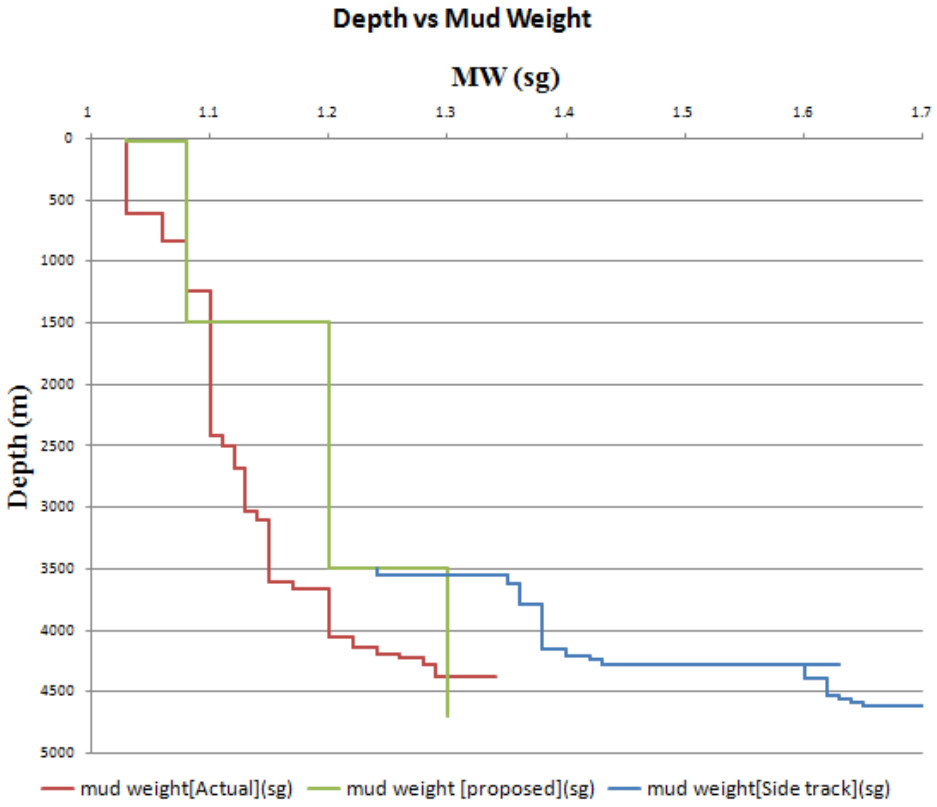

Fig 07: Comparison between Planned and Actual MW[5]

RECOMMENDATIONS

To drill a well without any obligations is quiet impossible. But a proper planned drilling program and quick arrangement to take preventive actions considering possible challenges can reduce the NPT (Non Productive Time).

From this chapter following suggestions have been made which can be considered during planning and execution phase of future drilling programs within that region:

- Non Invasive Fluid (NIF) can be recommended to reduce above issues. It can seal heterogeneous permeable formations (including microfractured shale formation), increase fracture pressure of the formation in a certain degree, widen the window of drilling fluid density, drill formations with different pressures using the same fluid system and remarkably reduce downhole troubles and formation damage. Its application is found worldwide like Assam field wells in India, Shengke 1, Bogu 1, Bogu 2, Bo 930 , Pai 2-7, Pai 2-10,Pai 2-14, Pai 2-Ping 41 wells in China.[6][7][8]
- When drilling operation stopped for maintenance work or other purposes and hole exposed to formation, continuous circulation is needed to keep the hole free from blockage. It can provide through by-pass line like cementing pipe.
- For proper hole cleaning both low-viscous and hi-viscous pill can be applied successively.
- Solid removal system must be followed properly. Shale shaker, disilter, desander, centrifuge. And circulation until the hole is clean will be continued.
- Circulate at maximum recommended flow rate for hole size.
- Minimize open hole time as wellbore instability conduct with time depent factors.
- Optimize reaming and back-reaming practice.

ACKNOWLEDGEMENT

Authors express their heartiest gratitude to both Petrobangla (Bangladesh Oil, Gas and Mineral Corporation) and BAPEX (Bangladesh Petroleum Exploration and Production Company Limited) to allow to study on Mubarakpur-1 well.

REFERENCES

[1] Klaus U. Reimann, .1993.Geology of Bangladesh.
[2] Robert F. Mitchell; Stefan Z. Miska, .2011. Fundamentals of Drilling Engineering.
[3] MI SWACO Drilling Fluid Manual.
[4] Aadnoy, B.S., .1996. Modern Well Design. Rotterdam, The Netherlands: A.A. Balkema.
[5] BAPEX, .2016.Well Completion Report of Mubarakpur-1 well.
[6] K.K. Borah and S.K. Mishra, .2009. Deep drilling Challenges in Oil's Assam Field- a Case Study. SPE/IADC 125337.
[7] Xue Yu-zhi, Li Gong-rang, Liu Bao-fang, and Zhang Jinghui,.2010. Application of super high density drilling fluid under ultra high temperature on well Shengke-1.SPE 131189.
[8] Shengli Drilling Technology Reasearch Institute of Sinopec, webpage: *http://www.sldti.com/eng/TechnologiesandServices/DrillingFluidandFormationDamageControlTechnologies.aspx*
[9]BAPEX,.2016. GR+CCL+CBL+VDL(Main log).

International Conference on Petroleum Engineering 2016 (ICPE-2016)
Bangladesh University of Engineering & Technology (BUET)
Dhaka-1000, Bangladesh

ICPE (2016-025)

New Approach to Monitor the Wellbore Condition Using Hydraulic Lift Phenomenon during Casing While Drilling

***Saiful Islam*[*1], *Shahriar Mahmud*[2], *Mohammad Mojammel Huque*[3], *Mubarak Hossen*[4]**
Bangladesh University of Engineering and Technology

ABSTRACT

Casing while Drilling (CwD) is a process of simultaneously drilling and casing a well. This novel technique has been practiced successfully for the past decade; however, due to narrow annulus problems like packing or caving in the wellbore often restricts the fluid flow and reduces hole cleaning capacity. Hydraulic lift can be used to examine the wellbore for such restrictions during drilling. The purpose of this paper involves development of a theoretical hydraulic lift model during CwD and subsequent evaluation of the wellbore condition in real time. Usually small annulus in CwD creates higher fluid frictional pressure drop and thus higher upward drag force on casing wall. Another force acts upwards at the bottom of the bit face as high velocity fluid exits through the nozzles. In this paper fluid hydraulic principles have been used to develop the theoretical model to predict overall hydraulic lift. Trend of this predicted hydraulic lift value has then been compared with field measured value from hookload data. Deviation of the field measured value from the predicted value is an indicator of wellbore conditions. To validate the model, hydraulic lift for different depth intervals and flow rates of a particular field is calculated based on the field data which then graphically compared with the theoretically predicted values and matched up with the field observation. During CWD operation evaluation of the wellbore condition using hydraulic lift will enable the operators to take required measures to wellbore issues and reduce drilling time.

Keywords: CwD, Hydraulic Lift, Hookload, Friction, Wellbore

INTRODUCTION

Globally rising demand for oil and natural gas, and an increasing rate of depletion in producing reserves, lead the oil and gas industry continuously to find new techniques to improve drilling technology. Casing while Drilling (CwD) technology stands as a response to practical needs of the industry. The innovative CwD method eliminates the need for wiper trips prior to casing/cementing operations, because the casing string is already run in the hole as the well is being drilled. Therefore, it helps to reduce risk, nonproductive time and cost in the drilling operations (Lopez et al., 2010 and Tessari et al., 2006). CwD introduces new benefits that modify conventional practices and offer a safer engineering design (Karimi 2011). However, as CwD process utilizes large diameter casing to drill narrow annulus often hinders the mud flow and lead to poor wellbore condition.

* Corresponding Author address
Email: saiful.pge13@gmail.com

To drill consistently it is always important to maintain better wellbore condition. Poor wellbore often reduces the hole cleaning efficiency and causes the reduction of ROP. In order to mitigate these challenges hydraulic lift mode will be a useful tool to monitor the wellbore condition.

MODEL DESCRIPTION

The small annulus brings about higher friction which leads to higher equivalent circulating density (ECD) in comparison to conventional drilling. During drilling operations as fluid circulates through large casing and narrow annulus several forces act upwards on the casing **Figure 1**. Major contributing lifting forces are

a. Drag Forces: Upward frictional forces of fluids on casing wall during CwD operation as fluid passes through narrow annulus.
b. End Forces: Upward force of fluids as it exits the nozzles and acts upward on the bit face. This force consists of frictional pressure loss through annulus and the hydrostatic pressure required balancing the mud column.

Considering the assumptions that sections of open hole are circular in shape and of known diameter, no effect of casing eccentricity on frictional pressures loss and incompressible drilling fluid, overall hydraulic lift can be expressed as

Hydraulic Lift = Frictional drag force on casing wall (F_1)
+ End Forces at the bottom (F_2)

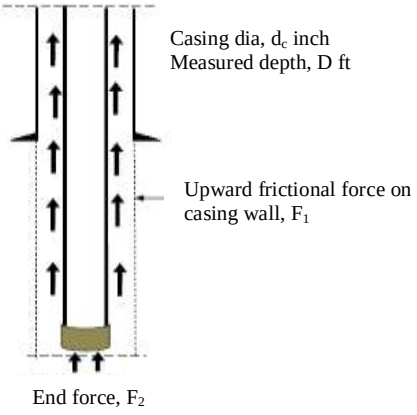

Figure 1: Contributing forces on hydraulic lift (Vertical well uniform hole size)

MODEL DERIVATION FOR VERTICAL WELL WITH SINGLE DIAMETER CASING AND UNIFORM HOLE

Figure 1 shows the lifting forces of a vertical well with single diameter casing. To model the overall hydraulic lift these two forces are derived.

Frictional force on casing wall (F_1)

Frictional force on casing wall occurs due to fluid flow through annulus along with cuttings. Knowing the cuttings concentration, effect of cutting is included in the calculation by considering effective mud density (Bourgoyne et al. 1986). In this paper to calculate cuttings concentration, particles slip velocity is determined using Chiens correlation (Chien 1971). Annular frictional pressure drop can be computed using narrow slot approximation

method for various fluid types and flow pattern, (Bourgoyne et al. 1986). Frictional force on casing wall F_1 then can be calculated by shear stress on casing wall.

$$F_1 = \tau_w \times \text{casing area}$$

$$= \left(\frac{d_h - d_c}{4}\right) \times \left(\frac{d_p}{d_l}\right) \times 2\pi \times \frac{d_c}{2} \times D$$

End forces at the bottom of the casing (F_2)

Amount of pressure contained at the bottom of the casing is the sum of annular frictional pressure and the hydrostatic pressure differential between different mud densities. it can be written as

F_2 = Fluid pressure contained at the bottom × Area of the bottom of the casing

$$= \left\{\frac{d_p}{d_l} + 0.052(\rho_e - \rho_m)\right\} \times D \times \frac{\pi}{4} \times d_c^2$$

Combining F_1 and F_2 Hydraulic lift can be expressed by following equation,

$$\text{HL} = \frac{\pi}{4} \times D \times \left\{\left(\frac{d_p}{d_l}\right) \times d_h \times d_c + 0.052 \times d_c^2 (\rho_e - \rho_m)\right\}$$

MODEL DERIVATION FOR VERTICAL WELL WITH SINGLE DIAMETER CASING AND FOR VARIOUS HOLE SIZE

Vertical well with varying hole size such as drilling with liner operation where the casing is at the bottom of the string and the end section of the casing extends to the surface **Figure 2**.

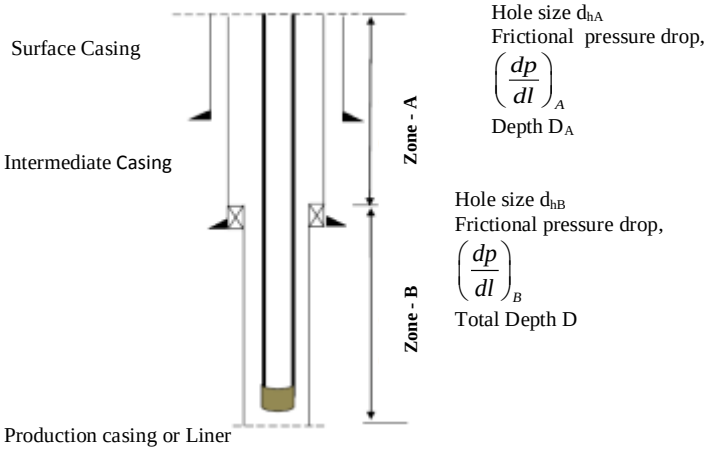

Figure 2: Contributing forces on hydraulic lift (Vertical well various hole size)

Due to the variation of the hole diameter annular frictional pressure drop also varies for different section. Similarly hydraulic lift for this case can be expressed as

$$\text{Hydraulic Lift} = \left\{\left(\frac{d_{hA} - d_c}{4}\right) \times \left(\frac{d_p}{d_l}\right)_A \times 2\pi \times \frac{d_c}{2} \times D_A\right\} + \left\{\left(\frac{d_{hB} - d_c}{4}\right) \times \left(\frac{d_p}{d_l}\right)_B \times 2\pi \times \frac{d_c}{2} \times (D - D_A)\right\}$$

$$+ \left[\left\{\left(\frac{d_p}{d_l}\right)_A \times D_A\right\} + \left\{\left(\frac{d_p}{d_l}\right)_B \times (D - D_A)\right\} + \left\{0.052 \times d_c^2 (\rho_e - \rho_m) \times D\right\}\right] \times \frac{\pi}{4} \times d_c^2$$

FIELD MEASUREMENT PROCEDURE OF HYDRAULIC LIFT

In field at first record the hookload with off bit bottom, pump off and rotating the casing slowly. Afterwards engage the mud pump(s) and bring flow rate up to drilling speed and measure the hookload again. Finally, the difference between hookload having pump off and on will be the overall hydraulic lift.

The principle used to monitor the well is that frictional pressure drop increases with fluid velocity and fluid velocity is proportional to the flowing area. While HL is modeled as a function of annular frictional pressure drop, change of this pressure drop will reflect on overall HL. Thus, any flow restriction in wellbore will essentially increase the hydraulic lift (HL). Therefore, following criteria can be used in comparisons of field measured value and predicted value.

- $HL_{Measured} > HL_{Predicted}$ poor well bore condition
- $HL_{Measured} \leq HL_{Predicted}$ improved well bore condition

Result analysis of the predicted and field measured value

In order to validate the model a casing drilling operation in a well is considered. The operator started drilling with casing after 8700 ft drilled by conventional method. Casing was run to drill up to depth 9205 ft **Figure 3**. Summary of the well parameters are shown in **Table 1**. Hydraulic lift is predicted by the model using the following parameters and field values are measured using the hookload calculation for different sections with different flow rate. These values are graphically compared to examine wellbore and validate the model.

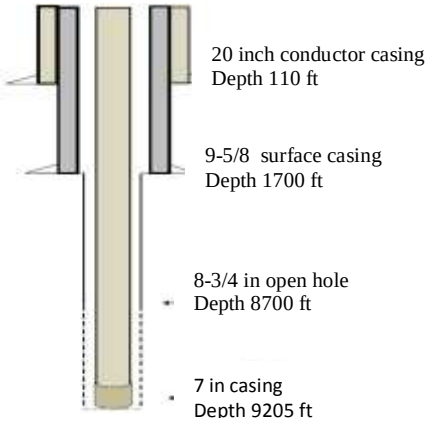

Figure 3: Geometry of the considered wellbore

Table 1: Summary of casing drilling

Depth in	8700 ft
Depth out	9204ft
RPM	40-100
WOB	4-20 kips
Mud Weight	8.8 lbm/gal
PV	6.6
YP	10

In Figure**. 4** for depth 8710 -8735 ft field measured values are found significantly higher than the predicted values. These variations occurred due to poor wellbore conditions. While hole cleaning is not sufficient packing tend to form which reduces the flowing area of the annulus and causes the increment of frictional pressure drop. However, using the model calculation is performed considering uniform annulus. Field observation implies incompatible drilling operation in terms of poor hole cleaning and lower ROP for first two joints up to nearly 8780 ft. As a result the operator had to clean the BHA and pump down additives in order to improve the wellbore stability. It can be relates that the inconsistency of drilling was due to poor wellbore condition which also reflected from the comparison of HL. **Figure. 5** shows within depth 8770 ft to 9180 ft real field measured values are considerably lower than the predicted values throughout the distance. This variation is due to some natural down hole fluid loss during mud circulation. In prediction, calculation was performed with constant flow rate but this fluid loss causes minor reduction of fluid volume and reduced the frictional forces on casing wall. It can be interpreted that wellbore was smooth with less friction having no obstacles to restrict flow. Field observation also

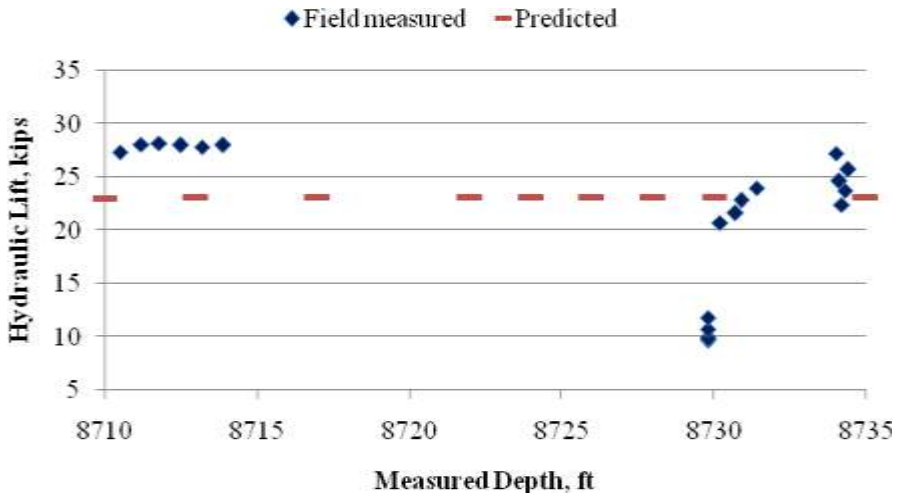

Figure 4: Comparison between measured and predicted HL for depth 8710ft –8735 ft with flow rate 293 gpm

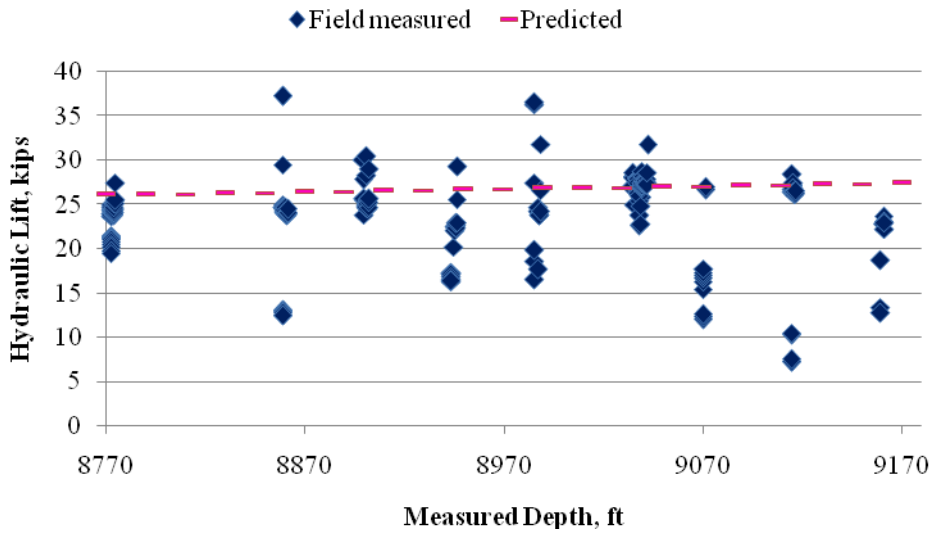

Figure 5**:** Comparison between measured and predicted HL for depth 8770ft –9180 ft with flow rate 318 gpm

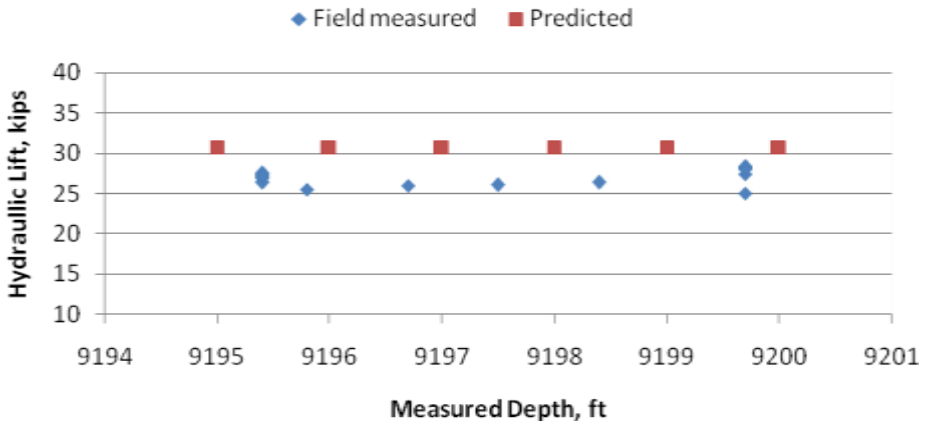

Figure 6: Comparison between measured and predicted HL for depth 9190-9204 ft with flow rate 343 gpm

indicates after using additives and cleaning the BHA drilling was quite consistent with sufficient hole cleaning from depth 8780 ft prior to reach 9204 ft. And there was no indication of significant loss circulation. **Figure. 6** fro further analysis also shows all the way through the distance within 9190 to 9204 ft field measured values comparing with the predicted value is lower for most of the interval. Therefore, from this analysis derived HL model can be considered valid for this case as well to examine the wellbore scenario.

CONCLUSION

In this study focus has been given to derive the theoretical model of overall hydraulic lift force and its application for vertical well during CwD operation. Upon studying different cases of a vertical well it can be summarized that according to the hydraulic lift principles fluid velocity rises with the reduction of flowing area which leads to higher frictional pressure drop. Thus, higher lifting force compared to the predicted value using theoretical model for a certain interval depth is an indicator of wellbore irregularities and poor hole cleaning as well. Conversely, if there is no hindrance in the flowing area predicted values should be equal or slightly lower than the field measured values. This phenomenon also has been verified with the real field case.

NOMENCLATURES

CwD = Casing while drilling

D = Measured depth, ft
d_c = Diameter of the casing, inch
d_h = Diameter of the hole, inch
$\frac{dp}{dl}$ = Frictional pressure drop, psi/ft
HL = Hydraulic lift, kip

τ_w = Shear stress, psi
ρ_m = Mud density, lbm/gal
ρ_e = Effective mud density, lbm/gal

REFERENCES

Bourgoyne Jr, A.T., Millheim, K.K., Chenevert,M.E. and Young Jr, F.S. (1986) Applied Drilling Engineering Vol. 2 143P, 177P.

Chien S. F., (1971) Annular velocity for Rotary Drilling Operation. In: SPE Fifth Conference on Drilling and Rock mechanics, Austin, Texas (Jan 5-6, 1971) 5-16 .

Karimi, M., Moellendick, E., and Pena, C. (2012). Casing drilling allows for safer engineering design,"Paper. In: AADE Drilling Fluids Technical Conference, Houston, Texas, 10-11 April.

Lopez, E.A., Bonilla, P.A.,(2010) Casing Drilling Application in the Depleted La Cira Infantas Mature Field Colombia. In: SPE Latin American & Caribbean Petroleum Engineering Conference, Peru.

Tessari, R.M., Warren, T.M., and Jo, J.Y. (2006). Drilling with casing reduces cost and risk. In: SPE Russian Oil and Gas Technical Conference and Exhibition, Moscow, Russia, October 3-6.

International Conference on Petroleum Engineering 2016 (ICPE-2016)
Bangladesh University of Engineering & Technology (BUET)
Dhaka-1000, Bangladesh

ICPE (2016-028)

Sensitivity Analysis of a CFD Model for Simulating Slurry Flow through Pipeline

Rasel A Sultan*[*, a], Mohamed Aziz Rahman[a], Sohrab Zendehboudi[a], Vandad Talimi[b], Vassilios C. Kelessidis[c]

[a]Faculty of Engineering and Applied Science, Memorial University of Newfoundland, St. John's, NL, Canada

[b] C-CORE, St. John's, NL, Canada

[c]Faculty of Petroleum Engineering, Texas A&M University at Qatar, Doha, Qatar

ABSTRACT

Three-dimensional CFD modeling of two-phase slurry flows is shown in this paper through 26mm diameter horizontal pipe for mixture velocity range of 3.5–4.7m/s and overall volumetric concentration range of 9.95%–34% with three grain sizes viz. 0.165, 0.29 and 0.55 mm. Eulerian model with Reynolds Stres Model (RSM) turbulence closure is adopted to analyze the monodispersed sand particles of varying granular diameters and density 2650 kg/m^3. The objective of this work is to analyze the sensitivity slurry flow using CFD simulation and validating the simulation with experimental studies available in the literature. The simulated local solid concentration values and pressure gradients are found to be in good agreement with experimental results at different conditions. Pressure drop per meter or pressure gradient increases with flow velocity of mixture. Effects of grain size on various slurry flow parameters especially on local solid concentration distribution is also studied.

Keywords: CFD; Slurry flow; Pressure gradient; Solid concentration; Pipeline.

* Corresponding Author address
Email: ras380@mun.ca

INTRODUCTION

Liquid-solid and liquid-gas two-phase flow in pipeline or annuli are of great importance in different industries with transport requirement. In recent years, solid transportation in liquid through pipelines or annuli has become increasingly popular due to its numerous application in different industries and enormous focus of society on reduction in environmental pollution. Usually slurry flow has been applied to transport raw materials, wastes and sludges which are in solid form (Soliman and Collier, 1990), beneficiation in extractive metallurgy and mining plants (Roco and Shook, 1983), coal processing plants (Choi et al., 2001), fluidized beds (Huilin et al., 2002), food and chemical plants, petroleum industries and many more. Slurry transportation system helps to reduce traffic, air pollution, noise, accidents along with saving on energy consumption and lesser ecological disturbance.

Two-phase slurry flow through pipeline is researched from the beginning of third decade of 20th century, aiming towards developing general solutions based on available experimental data for solid volumetric or mass concentration profiles, pressure gradient and slurry velocity profile, which are primarily required for better understanding of whole slurry flow process. Among the initial researches, O'Brien (1933) and Rouse (1937) contributed their work of slurry flow in open channel with low solid concentration, they use diffusion model to predicted the concentration distribution. Also Durand (1951), Durand and Condolios (1952), Newitt et al. (1955) are considered as the pioneers to describe friction pressure losses in slurry flow. Correlations established by Einstein (1906), Thomas (1965) and Krieger (1972) for homogeneous distribution of slurry and model by Ling et al. (2003) for heterogeneous slurry distribution gave a new dimension in the study of predicting pressure gradient of slurry flow. Some other works on empirical correlations for slurry pressure gradient are Govier and Aziz (1972), Vocadlo and Charles (1972). Aude et al. (1974), Aude et al. (1975), Seshadri (1982) and Seshadri et al. (1982) studied on long distance slurry flow in pipeline and showed this can be used as a reliable mode of transportation of solid. Many researches took place aiming at predicting concentration distribution for slurry flow in pipelines. A few notables of them are Shook and Daniel (1965), Shook et al. (1968), Karabelas (1977), Seshadri et al. (1982), Roco and Shook (1983), Roco and Shook (1984), Gillies et al. (1991), Gillies and Shook (1994), Gillies et al. (1999), Kaushal and Tomita (2002), Kaushal and Tomita (2003), Kumar et al. (2003), Kaushal et al. (2005). Apart from this, several studies for predicting pressure drop over the length also took place for slurry flows. A few notables of them are Wasp et al. (1970), Wilson (1976), Wasp et al. (1977), Doron et al. (1987), Gillies et al. (1991), Sundqvist et al. (1996), Mishra et al. (1998), Ghanta and Purohit (1999), Wilson et al. (2002), Kaushal and Tomita (2002), Kumar (2002), Kaushal and Tomita (2003), Skudarnov et al. (2004), Kaushal et al. (2005), Kumar et al. (2008), Vlasak et al. (2012), Pouranfard (2014). These empirical correlations and experimental studies are based on limited scope, data and application range (Lahiri and Ghanta, 2007). CFD simulation models have been utilized to minimize these limitations. CFD studies by Hernández et al. (2008), Chen et al. (2009), Kumar and Kaushal (2015), Kumar and Kaushal (2016) on slurry flow in pipeline have provided a new dimension in this field.

The approach of this study is to perform several comparisons of CFD simulation with experimental and empirical studies at different conditions and ranges for different industrial purposes. A parametric study is conducted using CFD simulation with versatile range of variables to minimize limitation in applications. Furthermore, different variables like modelling pressure loss, measuring/modeling concentration profile, analyzing the physics that control the hydrodynamics of fluid flow in annuli or pipeline is studied.

MATHEMATICAL MODELS

The Eulerian model of granular version has been adopted as multiphase model for present study. The selection of appropriate multiphase model depends mainly on the range of volume fraction (α) of solid phase under consideration. Since high value of volume fraction is used in this study this model is taken into account. Granular version helps in capturing the effects of friction and collusions between particles which is especially important in higher concentration slurries having varying grain sizes.

1. Multiphase Model

The Eulerian multiphase model allows for the modeling of multiple separate, yet interacting phases. The phases can be liquids, gases, or solids in nearly any combination. The Eulerian treatment is used for each phase, in contrast to the Eulerian-Lagrangian treatment that is used for the discrete phase model.

1.1. Volume Fractions

The description of multiphase flow as interpenetrating continua incorporates the concept of phasic volume fractions, denoted here by a_q. Volume fractions represent the space occupied by each phase, and the laws of conservation of mass and momentum are satisfied by each phase individually. The derivation of the conservation equations can be done by ensemble averaging the local instantaneous balance for each of the phases (Anderson and Jackson, 1967) or by using the mixture theory approach (Bowen, 1976).

The volume of phase q, V_q, is defined by

$$V_q = \int a_q dV \tag{1}$$

Where,

$$\sum_{q=1}^{n} a_q = 1 \tag{2}$$

The effective density of phase q is,

$$\hat{\rho}_q = a_q \rho_q \tag{3}$$

Where ρ_q is the physical density of phase q.

1.2. Conservation Equations

The equations for fluid-fluid and granular multiphase flows, are presented here for the general case of an n -phase flow.

1.2.1. Continuity Equation

The volume fraction of each phase is calculated from a continuity equation as below –

$$\frac{1}{\rho_{rq}}\left\{\frac{\partial}{\partial t}\left(a_q \rho_q\right) + \nabla.\left(a_q \rho_q \overrightarrow{\vartheta_q}\right) = \sum_{p=1}^{n}\left(\dot{m}_{pq} - \dot{m}_{qp}\right)\right\} \tag{4}$$

Where ρ_{rq} is the phase reference density, or the volume averaged density of the q^{th} phase in the solution domain, $\dot{m}_{pq}$ characterizes the mass transfer from the p^{th} to q^{th} phase and $\dot{m}_{qp}$ characterizes the mass transfer from the q^{th} to p^{th} phase.

1.2.2. Fluid-Fluid Momentum Equations

The conservation of momentum for a fluid phase q is –

$$\frac{\partial}{\partial t}\left(a_q \rho_q \overrightarrow{\vartheta_q}\right) + \nabla.\left(a_q \rho_q \overrightarrow{\vartheta_q}\overrightarrow{\vartheta_q}\right) = -a_q \nabla \mathrm{p} + \nabla.\bar{\bar{\tau}}_q + a_q \rho_q \vec{g} + \sum_{p=1}^{n}\left\{K_{pq}\left(\overrightarrow{\vartheta_p} - \overrightarrow{\vartheta_q}\right) + \dot{m}_{pq}\overrightarrow{\vartheta_{pq}} - \dot{m}_{qp}\overrightarrow{\vartheta_{qp}}\right\} + Fq + Flift,q + Fvm,q \quad (5)$$

Here $\vec{g}$ is the acceleration due to gravity, $\bar{\bar{\tau}}_q$ is the q^{th} phase stress-strain tensor, $\overrightarrow{F_q}$ is an external body force, $\vec{F}_{lift,q}$ is a lift force and $\vec{F}_{vm,q}$ is a virtual mass force.

1.2.3. Fluid-Solid Momentum Equations

Following the work of Alder and Wainwrigh (1960), Chapman and Cowling (1970) and Syamlal et al. (1993), a multi-fluid granular model is used to describe the flow behavior of a fluid-solid mixture.

The conservation of momentum for the fluid phases is similar to Equation (5), and that for the s^{th} solid phase is –

$$\frac{\partial}{\partial t}\left(a_s \rho_s \overrightarrow{\vartheta_s}\right) + \nabla.\left(a_s \rho_s \overrightarrow{\vartheta_s}\overrightarrow{\vartheta_s}\right) = -a_s \nabla \mathrm{p} - \nabla p_s + \nabla.\bar{\bar{\tau}}_s + a_s \rho_s \vec{g} + \sum_{l=1}^{N}\left\{K_{ls}\left(\overrightarrow{\vartheta_l} - \overrightarrow{\vartheta_s}\right) + \dot{m}_{ls}\overrightarrow{\vartheta_{ls}} - \dot{m}_{sl}\overrightarrow{\vartheta_{sl}}\right\} + \left(\overrightarrow{F_s} + \vec{F}_{lift,s} + \vec{F}_{vm,s}\right) \quad (6)$$

Where p_s is the s^{th} solids pressure, $K_{ls} = K_{sl}$ is the momentum exchange coefficient between fluid or solid phase l and solid phase s, N is the total number of phases.

1.3. Solids Pressure

For granular flows in the compressible regime (i.e., where the solids volume fraction is less than its maximum allowed value), a solids pressure is calculated independently and used for the pressure gradient term, ∇p_s in the granular-phase momentum equation. Because a Maxwellian velocity distribution is used for the particles, a granular temperature is introduced into the model, and appears in the expression for the

$$p_s = a_s \rho_s \Theta_s + 2\rho_s(1 + e_{ss})a_s^2 g_{0,ss}\Theta_s \quad (7)$$

Where, e_{ss} is the coefficient of restitution for particle collisions, $g_{0,ss}$ is the radial distribution function, and Θ_s is the granular temperature. Here a default value of 0.9 for e_{ss} is used, but the value can be adjusted to suit the particle type. The granular temperature Θ_s is proportional to the kinetic energy of the fluctuating particle motion. The function $g_{0,ss}$ is a distribution function that governs the transition from the "compressible"

condition with $a < a_{s,max}$, where the spacing between the solid particles can continue to decrease, to the "incompressible" condition with $a = a_{s,max}$, where no further decrease in the spacing can occur. A value of 0.63 is the default for $a_{s,max}$, but it can be modify during the problem setup.

1.4. Solids Shear Stresses

The solids stress tensor contains shear and bulk viscosities arising from particle momentum exchange due to translation and collision. A frictional component of viscosity can also be included to account for the viscous-plastic transition that occurs when particles of a solid phase reach the maximum solid volume fraction.

The collisional and kinetic parts, and the optional frictional part, are added to give the solids shear viscosity-

$$\mu_s = \mu_{s,col} + \mu_{s,kin} + \mu_{s,fr} \tag{8}$$

Where, $\mu_{s,col}$ is shear viscosity due to collision, $\mu_{s,kin}$ is kinetic viscosity and $\mu_{s,fr}$ frictional viscosity.

The collisional part of the shear viscosity is modeled as Gidaspow et al. (1991) and Syamlal et al. (1993) –

$$\mu_{s,col} = \frac{4}{5} a_s \rho_s d_s g_{0,ss} (1 + e_{ss}) \left(\frac{\Theta_s}{\pi}\right)^{1/2} \tag{9}$$

The default expression of kinetic viscosity is from Syamlal et al. (1993):

$$\mu_{s,kin} = \frac{a_s d_s \rho_s \sqrt{\Theta_s \pi}}{6(3 - e_{ss})} \left[1 + \frac{2}{5}(1 + e_{ss})(3e_{ss} - 1) a_s g_{0,ss}\right] \tag{10}$$

The frictional viscosity is included using Schaeffer's (1987) expression –

$$\mu_{s,fr} = \frac{p_s \sin \emptyset}{2\sqrt{I_{2D}}} \tag{11}$$

2. Turbulence Model

Turbulent quantity for fluid flow are assumed using Reynolds Stress Model (RSM) (Launder et al., 1975, Gibson and Launder, 1978 and Launder, 1989). This is the most elaborate turbulence model. Abandoning the isotropic eddy-viscosity hypothesis, the RSM closes the Reynolds-averaged Navier-Stokes equations (Chorin, 1968) by solving transport equations for the Reynolds stresses, together with an equation for the dissipation rate. Here five additional transport equations are required in 2D flows and seven additional transport equations must be solved in 3D.

The exact transport equation for the Reynolds Stress Model (RSM) is as below –

$$\underbrace{\frac{\partial}{\partial t}\left(\rho \overline{u_i' u_j'}\right)}_{Local\ Time\ Derivative} + \underbrace{\frac{\partial}{\partial x_k}\left(\rho u_k \overline{u_i' u_j'}\right)}_{Convection\ (C_{ij})} = \underbrace{-\frac{\partial}{\partial x_k}\left[\rho \overline{u_i' u_j' u_k'} + \overline{p\left(\delta_{kj} u_i' + \delta_{ik} u_j'\right)}\right]}_{Turbulent\ Diffusion\ (D_{T,ij})}$$
$$+ \underbrace{\frac{\partial}{\partial x_k}\left[u \frac{\partial y}{\partial x_k}\left(\overline{u_i' u_j'}\right)\right]}_{Molecular\ Diffusion\ (D_{L,ij})} \underbrace{-\rho\left(\overline{u_i' u_k'} \frac{\partial u_j}{\partial x_k} + \overline{u_j' u_k'} \frac{\partial u_j}{\partial x_k}\right)}_{Stress\ Prouction\ (P_{ij})} \underbrace{-\rho\beta\left(g_i \overline{u_j' \theta} + g_i \overline{u_i' \theta}\right)}_{Buoyancy\ Production\ (G_{ij})}$$

$$+ \underbrace{\overline{p\left(\frac{\partial u_i'}{\partial x_j}+\frac{\partial u_j'}{\partial x_i}\right)}}_{Pressure\ \ Strain\ \ (\emptyset_{ij})} - \underbrace{2\mu\overline{\frac{\partial u_i'}{\partial x_k}\frac{\partial u_j'}{\partial x_k}}}_{Dissipation\ \ (\epsilon_{ij})} \quad (12)$$

$$\underbrace{-2\rho\Omega_k\left(\overline{u_j'u_m'}\epsilon_{ikm}+\overline{u_i'u_m'}\epsilon_{jkm}\right)}_{Production\ \ by\ system\ \ Rotation\ \ (F_{ij})} + \underbrace{S_{user}}_{User-Defined\ \ Source}$$

Of the various terms in these exact equations, C_{ij}, $D_{L,ij}$, P_{ij} and F_{ij} do not require any modeling. However, $D_{T,ij}$, G_{ij}, $\emptyset_{ij}$ and ϵ_{ij} need to be modeled to close the equations $D_{T,ij}$ can be modeled by the generalized gradient-diffusion model of Daly and Harlow (1970), which is –

$$D_{T,ij} = C_s\frac{\partial}{\partial x_k}\left(\rho\frac{k\overline{u_k'u_i'}}{\epsilon}\frac{\partial\overline{u_i'u_j'}}{\partial x_l}\right) \quad (13)$$

However, this equation can result in numerical instabilities (Launder, 1989), so it has been simplified in this study to use a scalar turbulent diffusivity as follows (Launder, 1989) –

$$D_{T,ij} = \frac{\partial}{\partial x_k}\left(\frac{\mu_t}{\sigma_k}\frac{\partial\overline{u_i'u_j'}}{\partial x_k}\right) \quad (14)$$

Lien and Leschziner (Lien and Leschziner, 1987) derived a value of adjustable constant $\sigma_k = 0.82$.
Where, turbulent viscosity (μ_t) is computed as –

$$\mu_t = \rho C_\mu\frac{k^2}{\epsilon}\ and\ C_\mu = 0.09 \quad (15)$$

Where, C_μ is an adjustable constant.
Expression for G_{ij} for ideal gases is as follows –

$$G_{ij} = -\frac{\mu_t}{\rho Pr_t}\left(g_i\frac{\partial\rho}{\partial x_j}+g_j\frac{\partial\rho}{\partial x_i}\right) \quad (16)$$

Where Pr_t is the turbulent Prandtl number for energy, with a default value of 0.85 used in simulation.
The pressure-strain term, $\emptyset_{ij}$ is modeled according to the proposal by Gibson and Launder (1978), Fu et al. (1987), and Launder (1989).
The classical approach to modeling $\emptyset_{ij}$ uses the following decomposition –

$$\emptyset_{ij} = \emptyset_{ij,1} + \emptyset_{ij,2} + \emptyset_{ij,w} \quad (17)$$

Where, $\emptyset_{ij,1}$is the slow pressure-strain term, also known as the return-to-isotropy term, $\emptyset_{ij,2}$ is called the rapid pressure-strain term, and $\emptyset_{ij,w}$ is the wall-reflection term.
The slow pressure-strain term, $\emptyset_{ij,1}$, is modeled as -

$$\emptyset_{ij,1} \equiv -C_1\rho\frac{\epsilon}{k}\left[\overline{u_i'u_j'}-\frac{2}{3}\delta_{ij}k\right] \quad (18)$$

With, $C_1 = 1.8$.
The rapid pressure-strain term, $\emptyset_{ij,2}$, is modeled as –

$$\emptyset_{ij,2} \equiv C_2 \left[\left(P_{ij} + F_{ij} + G_{ij} - C_{ij}\right) - \frac{2}{3}\delta_{ij}(P + G - C)\right] \quad (19)$$

Where $C_2 = 0.60$, P_{ij}, F_{ij}, G_{ij} and C_{ij} are defined as in Equation (12), $P = \frac{1}{2}P_{kk}$, $G = \frac{1}{2}G_{kk}$, $C = \frac{1}{2}C_{kk}$.
The wall-reflection term, $\emptyset_{ij,w}$ is responsible for the redistribution of normal stresses near the wall. It tends to damp the normal stress perpendicular to the wall, while enhancing the stresses parallel to the wall. This term is modeled as –

$$\emptyset_{ij,w} \equiv C_1' \frac{\epsilon}{k}\left(\overline{u_k' u_m'} n_k n_m \delta_{ij} - \frac{3}{2}\overline{u_i' u_k'} n_j n_k - \frac{3}{2}\overline{u_j' u_k'} n_i n_k\right)\frac{C_l k^{\frac{3}{2}}}{\epsilon d} + C_2'\left(\emptyset_{km,2} n_k n_m \delta_{ij} - \frac{3}{2}\emptyset_{ik,2} n_j n_k - \frac{3}{2}\emptyset_{jk,2} n_i n_k\right)\frac{C_l k^{\frac{3}{2}}}{\epsilon d} \quad (20)$$

Where $C_1' = 0.5, C_2' = 0.3, n_k$ is the x_k component of the unit normal to the wall, d is the normal distance to the wall, and $C_l = \frac{C_\mu^{\frac{3}{4}}}{k}$, where $C_\mu = 0.09$ and k is the von Kármán constant (= 0.4187) (Karman, 1937).
The dissipation tensor, ϵ_{ij}, is modeled as –

$$\epsilon_{ij} = \frac{2}{3}\delta_{ij}(\rho\epsilon + Y_M) \quad (21)$$

Where $Y_M = 2\rho\epsilon M_t^2$ is an additional "dilatation dissipation" term according to the model by Sarkar (1991). The turbulent Mach number in this term is defined as –

$$M_t = \sqrt{\frac{k}{a^2}} \quad (22)$$

3. Solution Method

For Eulerian multiphase calculations, the phase coupled SIMPLE (PC-SIMPLE) algorithm (Vasquez and Ivanov, 2000) is used for the pressure-velocity coupling. PC-SIMPLE is an extension of the SIMPLE algorithm (Patankar, 1980) to multiphase flows. The velocities are solved coupled by phases, but in a segregated fashion. The block algebraic multigrid scheme used by the density-based solver described in (Weiss et al., 1999) is used to solve a vector equation formed by the velocity components of all phases simultaneously. Then, a pressure correction equation is built based on total volume continuity rather than mass continuity. Pressure and velocities are then corrected so as to satisfy the continuity constraint.

3.1. Pressure-Correction Equation

For incompressible multiphase flow, the pressure-correction equation takes the form of-

$$\sum_{k=1}^{n} \frac{1}{\rho_{rk}}\left\{\frac{\partial}{\partial t} a_k \rho_k + \nabla . a_k \rho_k \vec{v}_k' + \nabla . a_k \rho_k \vec{v}_k^* - \left(\sum_{l=1}^{n}(\dot{m}_{lk} - \dot{m}_{kl})\right)\right\} = 0 \quad (23)$$

Where ρ_{rk} is the phase reference density for the k^{th} phase (defined as the total volume average density of phase k), $\vec{v}_k^{'}$ is the velocity correction for the k^{th} phase, and $\vec{v}_k^{*}$ is the value of $\vec{v}_k$ at the current iteration.

3.2. Volume Fractions

The volume fractions are obtained from the phase continuity equations. In discretized form, the equation of the k^{th} volume fraction is –

$$a_{p,k}a_k = \sum_{nb}\left(a_{nb,k}a_{nb,k}\right) + b_k = R_k \tag{24}$$

In order to satisfy the condition that all the volume fractions sum to one,

$$\sum_{k=1}^{n} a_k = 1 \tag{25}$$

SIMULATION METHODOLOGY

1. Geometry and mesh generation

In the present study, a 13.15m long and 26.0mm internal diameter pipe is selected for the sensitivity analysis. The computational grids for this horizontal pipe is generated using ANSYS Fluent meshing with 1,86,767 elements with 82,827 nodes volume cells finalized conducting proper mesh independency check. Ten layers of Inflation near wall is added to observe more preciously the characteristics of different parameters near wall. Shear stress between wall surface and gas molecules are much higher and this inflation helps to create denser meshing near wall. Also it is more time consuming and reliable to use unsymmetrical meshing rather symmetrical meshing. The length of the pipe is sufficient enough to achieve a fully developed

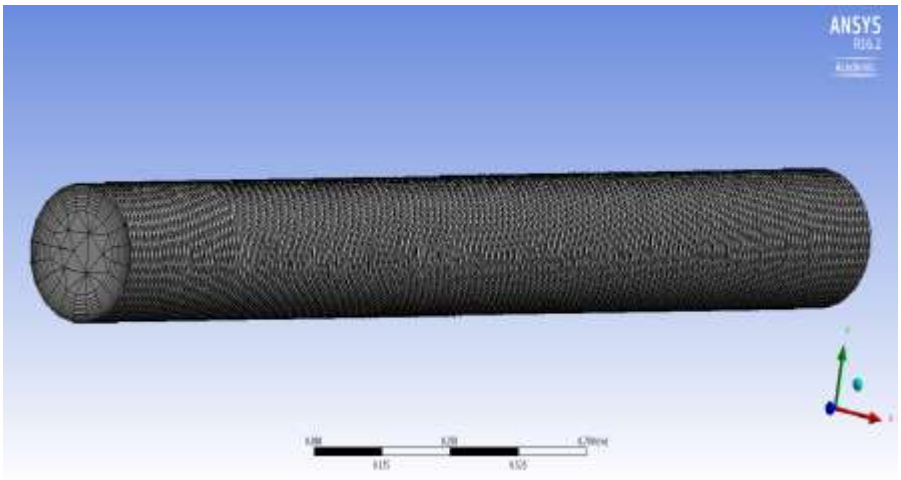

Fig.1. Mesh distribution in the pipe geometry

flow at the outlet as minimum flow development section should be at least 50D (D = internal diameter of pipe) (Wasp et al., 1977, Brown and Heywood, 1991) and here this length is maintained. Comutational grid distribution of geometry is shown in Figure 1.

2. Boundary conditions

There are three boundaries available in the given flow domain namely the inlet boundary, the wall boundary and the outlet boundary. Here, inlet velocity range of 3.5–4.7m/s and overall volumetric concentration range of 9%–34% with three grain sizes viz. 0.165, 0.29 and 0.55 mm have been considered as boundary input. A 0.2 mm of pipe wall roughness is adopted during simulation. As the nature of wall-particle collisions influences the shear stress and turbulent energy flux at the walls, a specularity coefficient is defined for solid phase at the walls. a value of 0.5 is selected which corresponds to wall quality between smooth frictionless walls and very rough walls. No slip for liquid phase has been adopted at walls. Inlet and outlet pressure are assumed same.

3. Solution process and convergence criteria

Fluent, ver. 16.2, ANSYS Inc. is used to build a CFD simulation model of pipeline flow of water-sand slurry. A convergence value of 10^{-5} has been adopted for termination of iteration, this value is slelected with optimizing analysis to have most satisfactory accuracy with less time. A second order upwind discretization for momentum equation and first upwind discretization for volume fraction, turbulent kinetic energy and its dissipation are adopted to ensure stability and convergence of iterative process.

VALIDATION OF SIMULATION

1. Comparison of pressure gradient

Pressure gradient of water-sand slurry flow from simulation is compared with Skudarnov et al. (2004) experimental data. In the experiment, length of pipe is 17m, diameter of pipe is 0.023m, fluid taken water (density 9982 Kg/m^3, viscosity 0.001003 Kg/m-s) and slurry taken glass spheres slurry (double-species slurry with densities of 2490 kg/m^3 and 4200 kg/m^3, 50%

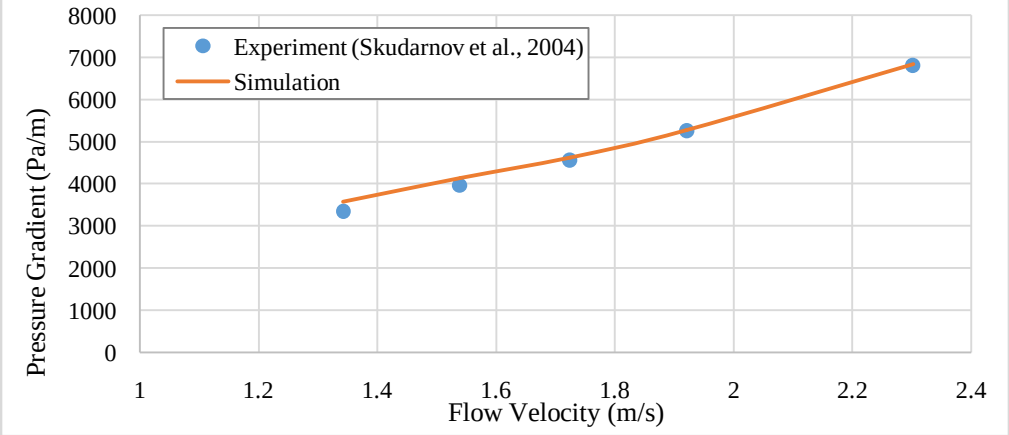

Fig.2. Comparison of pressure gradient from simulation with experimental data of Skudarnov et al. (2004) for double-species slurry with d_m = 140 µm and C_v = 15%.

by 50% by volume mixtures), wall material is stainless steel (density 8030 kg/m^3, roughness 32 µm). Figure 2 shows the comparison of pressure gradient with dm = 140 µm and Cv = 15%. Where, d_m = mean particle diameter (µm) C_v = volume concentration (%).

The result shows very good aggrement with experiemntal values with less than 10% error at each point. The small errors that are arising may be due to experimental errors (it was estimated in the reference paper that the

accuracy of the pressure gradient is ±50 Pa/m.) and numerical error of mathematical equations while applying simulation.

2. Comparison of local solid concentration profile

Local solid concentration profile of water-sand slurry flow from simulation is compared with Gillies and Shook, (1994) experimental data. In the experiment, length of pipe is 2.7m, diameter of pipe is 53.2mm, fluid taken water (density 9982 Kg/m^3, viscosity 0.001003 Kg/m-s) and slurry taken Silica (chemical formula SiO_2, density 2650 Kg/m^3, wall material is aluminum (density 2800 kg/m^3, roughness 0.2mm). Here, grain size or mean partical diameter is 0.18 mm, mixture velocity 3.1 m/s and three different solid volumetric concentration 14%, 29% and 45% is considered from experiment. Figure 3 shows the comparison of volumetric concentration of solid particles with particle sizes 0.18 mm.

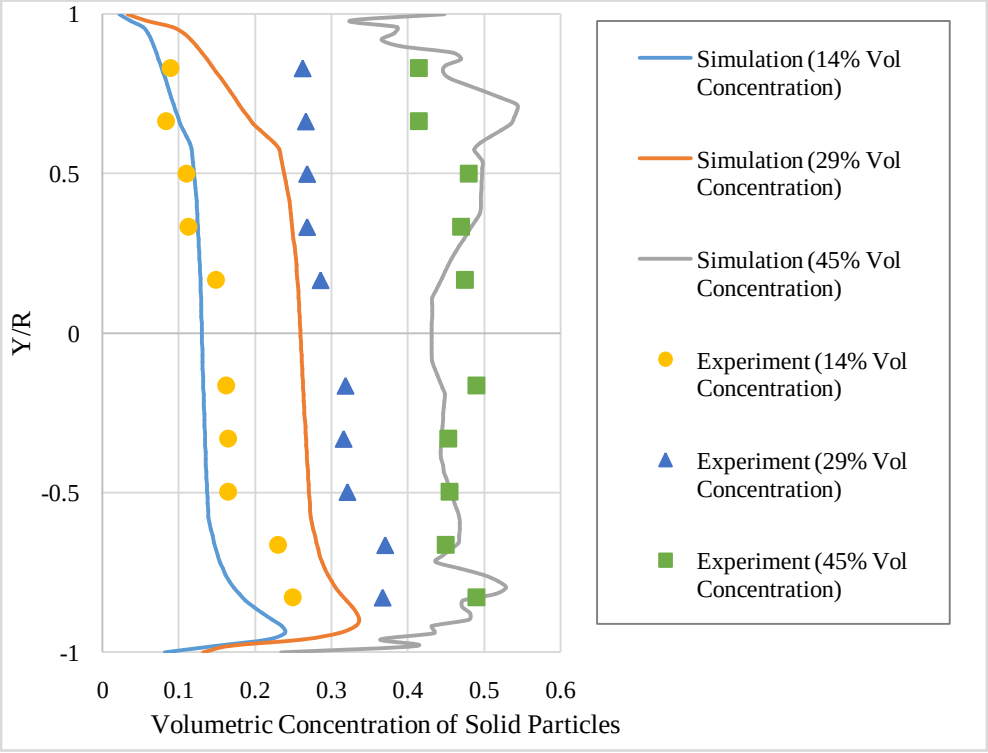

Fig. 3. Comparison of simulated and measured values of local volumetric concentration of solid across vertical centerline for particle sizes 0.18 mm.

Simulated results are in good agreement with experimental values for grain sizes 0.18mm. However, simulated values deviate from experimental values near the wall especially in the lower half of the cross-section. One of the possible reasons could be abrasive rounding of these large size particles by repeated passages during experiment, resulting significant quantities of fines were generated which were distributed uniformly within the pipe. This would have led to possible increase in carrier density. Since information of this aspect was not available in the reference research, the same is not incorporated while doing simulations.

Apart from this, another possible reason for these deviations could be approximate value of static settled concentration (packing limit) used during simulations, as the value of 0.63 used is best suited for finer grain sizes only.
However, it is also necessary to analyze newer boundary conditions at the wall for slurry pipeline flows with larger grain sizes to minimize deviations with experimental results.

SENSITIVITY ANALYSIS

1. Solid Concentration Profile Analysis

Figures 4–7 shows simulated local volumetric concentration distribution of solid phase along vertical centerline at outlet cross-section. Geometry, mesh and boundary condition details are discussed in simulation methodology chapter. Both length and diameter of this analysis are taken within range of two validated work geometry. These figures indicate that lower portion of pipe cross section contaion more solid particles than upper portion. This happens due to gravity effect and more dense solid particle than water. It means slurry flow in horizontal pipe is not uniform and theres a probabilty to have particle deposition at a certain mixture velocity and solid volumetric concentration which can create blockage of smooth flow. Figures 8 shows contours of local volumetric concentration distribution of solid phase in the vertical plane at outlet cross-section for particle size of 0.165 mm and mixture velocity of 3.5 m/s at different

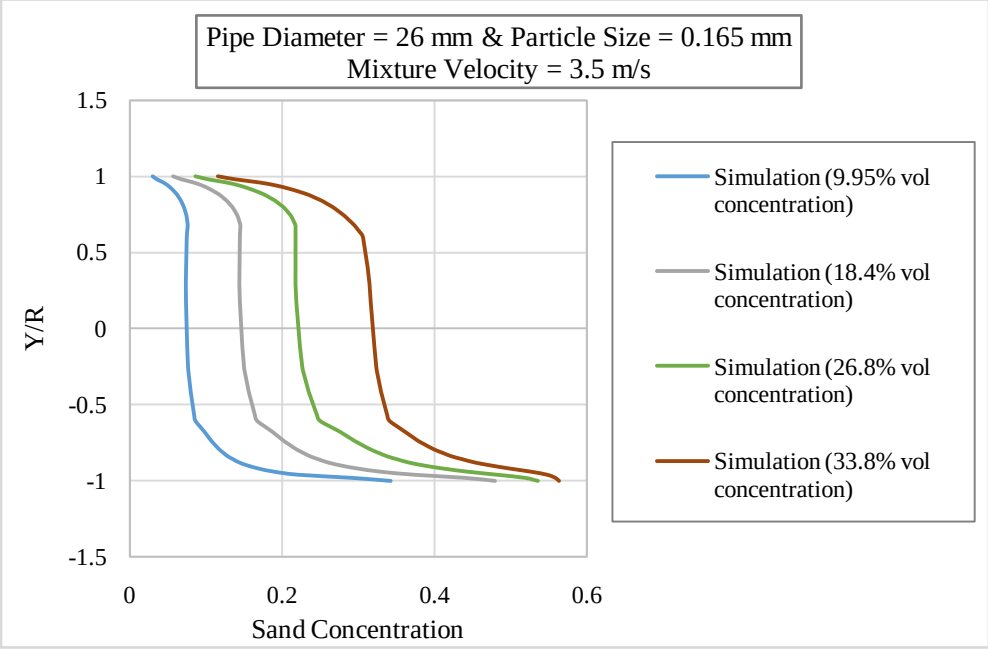

Fig.4. Simulated local volumetric sand concentration across vertical centre line of pipe outlet for particle size of 0.165 mm and mixture velocity of 3.5 m/s at different efflux concentrations.

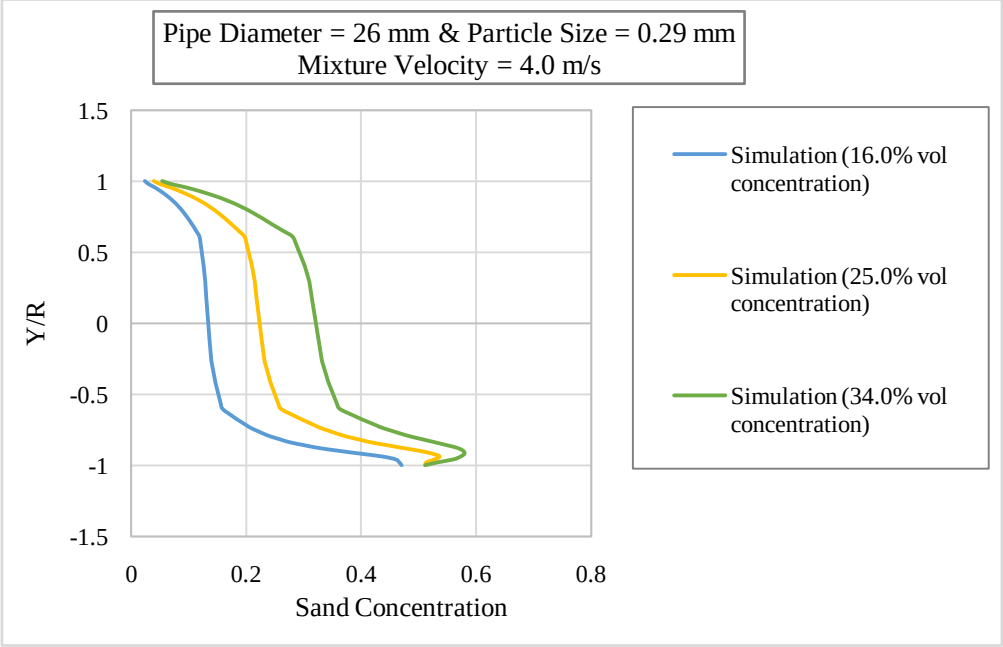

Fig.5. Simulated local volumetric sand concentration across vertical centre line of pipe outlet for particle size of 0.29 mm and mixture velocity of 4.0 m/s at different efflux concentrations.

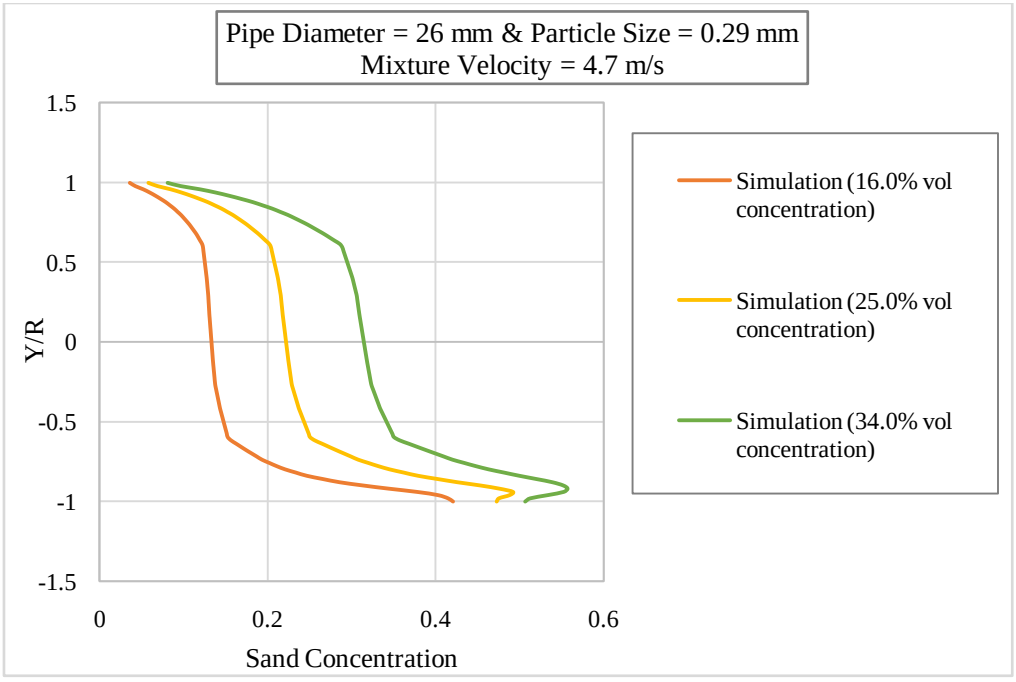

Fig.6. Simulated local volumetric sand concentration across vertical centre line of pipe outlet for particle size of 0.29 mm and mixture velocity of 4.7 m/s at different efflux concentrations.

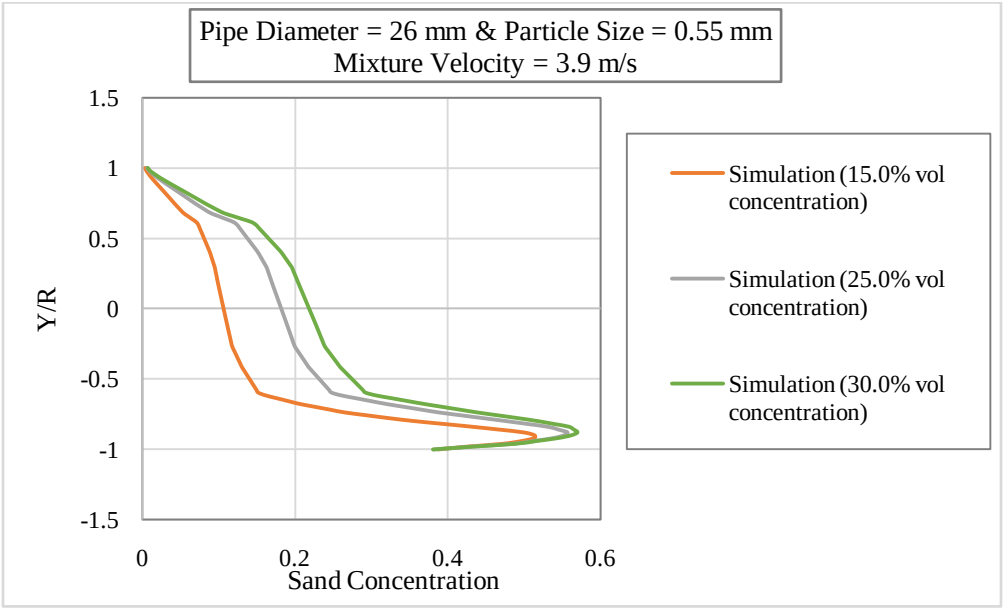

Fig.7. Simulated local volumetric sand concentration across vertical centre line of pipe outlet for particle size of 0.55 mm and mixture velocity of 3.9 m/s at different efflux concentrations.

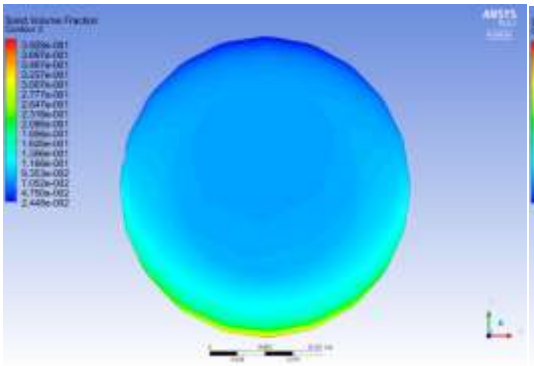

(a) solid volumetric concentration 9.95%

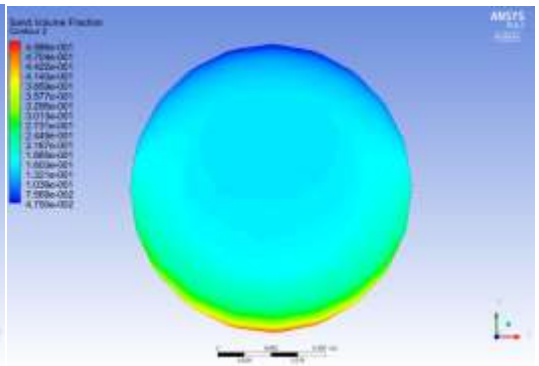

(b) solid volumetric concentration 18.4%

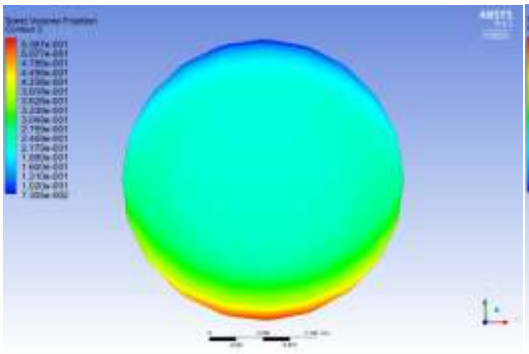

(c) solid volumetric concentration 26.8%

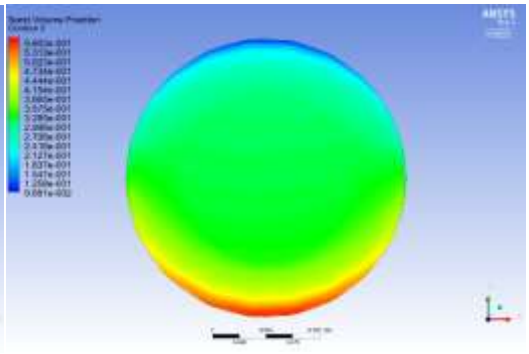

(d) solid volumetric concentration 33.8%

Fig.8. Solid concentration distribution in the vertical plane at outlet for particle size 0.165mm and at 3.5 m/s of mixture velocity.

efflux concentrations. From contour analysis it is clear that the region of highest solid concentration locates very near to the wall in the lower half of pipe cross section.

It is also observed that the spread of highest solid concentration region increases with increase in efflux concentration, particle grain size and mixture velocity but with reduced intensity. Due to similar trends, contours at other velocities and particle sizes have not been shown.

CONCLUSION

Keeping in mind to develope a widely accepted, reliable, efficient CFD model this paper analyze CFD simulation of two phase (sand-water) slurry flows through 26 mm diameter pipe in horizontal orientation for flow velocity range of 3.5-4.7 m/s and efflux concentration range of 9.95-34% with three particle sizes viz. 0.165 mm, 0.29 mm and 0.55 mm with density 2650 kg/m^3. Local volumetric concentration of solid particle at pipe outlet is very well simulated for different combinations of particle size, mixture velocity and efflux concentrations under consideration. Before these analysis, this simulation model is validated with two different experimental results having different boundary conditions from available literatures. This comparison process shows very good aggrement with experimental result and validate our model over certain range of operating condition. Mathematical equations of multiphase flow and turbulence models is also added to explain our simulation process with its acceptancy at certain operating conditions.

This study helps to understand two phase slurry flows for different applications. The analysis of local solid concentration can give idea of selecting optimizing range of particle size, volumetric concentration of slurry and mixture velocity during operation. This study can lead to find out ‘deposition velocity’ in slurry flow. However, scatter in simulation data of various flow parameters especially with bigger particle sizes of slurry indicates that the model used in the present study needs further development. Also it can be seen from figures 3, 6 and 7 that sudden reduction of solid concentration is occuring near wall with higher efflux concentration and particle size, which is not expected practically. This indicates simulation instability near lower wall over a range of efflux concentration and particle size, this needs to be solved. The choice of different coefficients and constants such as coefficient of lift, coefficient of drag, restitution coefficient and wall boundary conditions needs to be further researched. Also introducing three phase flow adding gas can lead to new findings and benifits with this two phase slurry flow.

REFERENCES

Alder, B. J., & Wainwright, T. E. (1960). Studies in molecular dynamics. II. Behavior of a small number of elastic spheres. *The Journal of Chemical Physics*, *33*(5), 1439-1451.

Anderson, T. B., & Jackson, R. (1967). Fluid mechanical description of fluidized beds. Equations of motion. *Industrial & Engineering Chemistry Fundamentals*, *6*(4), 527-539.

Aude, T. C., Thompson, T. L., & Wasp, E. J. (1974). Economics of slurry pipeline systems. *Publication of: Cross (Richard B) Company*, *15*(Proc Paper).

Aude, T. C., Thompson, T. L., & Wasp, E. J. (1975). Slurry-pipeline systems for coal; other solids come of age. *Oil Gas J.; (United States)*, *73*(29).

Bowen, R. M. (1976). Theory of mixtures. *Continuum physics*, *3*(Pt I).

Brown, N. P., & Heywood, N. I. (Eds.). (1991). *Slurry Handling: Design of solid-liquid systems*. Springer Science & Business Media.

Chapman, S., & Cowling, T. G. (1970). *The mathematical theory of non-uniform gases: an account of the kinetic theory of viscosity, thermal conduction and diffusion in gases*. Cambridge university press.

Chen, L., Duan, Y., Pu, W., & Zhao, C. (2009). CFD simulation of coal-water slurry flowing in horizontal pipelines. *Korean journal of chemical engineering*, *26*(4), 1144-1154.

Choi, Young-Chan, Park, Tae-Jun, Kim, Jae-Ho, Lee, Jae-Goo, Hong, Jae-Chang, & Kim, Yong-Goo. (2001). Experimental studies of 1 ton/day coal slurry feed type oxygen blown, entrained flow gasifier. *Korean Journal of Chemical Engineering*, *18*(4), 493-498.

Chorin, A. J. (1968). Numerical solution of the Navier-Stokes equations. *Mathematics of computation*, *22*(104), 745-762.

Daly, B. J., & Harlow, F. H. (1970). Transport equations in turbulence. *Physics of Fluids (1958-1988)*, *13*(11), 2634-2649.

Doron, P., Granica, D., & Barnea, D. (1987). Slurry flow in horizontal pipes—experimental and modeling. *International Journal of Multiphase Flow*, *13*(4), 535-547.

Durand, R. (1951). Transport hydraulique de graviers et galets en conduite. *La Houille Blanche*, 609-619.

Durand, R., & Condolios, E. (1952, November). The hydraulic transport of coal and solid material in pipes. In *Proceedings of Colloquium on Hydraulic Transportation, France*.

Durand, R., & Condolios, E. (1952). Experimental study on conveying solids in pipes, 2 emes journees de l'hydraaulique. *Soc. Hydrotech. Fr*, *29*.

Einstein, A. (1906). Zur theorie der brownschen bewegung. *Annalen der physik*, *324*(2), 371-381.

Fu, S., Launder, B. E., & Leschziner, M. A. (1987). Modelling strongly swirling recirculating jet flow with Reynolds-stress transport closures. In *6th Symposium on Turbulent Shear Flows* (pp. 17-6).

Ghanta, K. C., & Purohit, N. K. (1999). Pressure drop prediction in hydraulic transport of bi-dispersed particles of coal and copper ore in pipeline. *The Canadian Journal of Chemical Engineering*, *77*(1), 127-131.

Gibson, M. M., & Launder, B. E. (1978). Ground effects on pressure fluctuations in the atmospheric boundary layer. *Journal of Fluid Mechanics,86*(03), 491-511.

Gidaspow, D., Bezburuah, R., & Ding, J. (1991). *Hydrodynamics of circulating fluidized beds: kinetic theory approach* (No. CONF-920502-1). Illinois Inst. of Tech., Chicago, IL (United States). Dept. of Chemical Engineering.

Gillies, R. G., Shook, C. A., & Wilson, K. C. (1991). An improved two layer model for horizontal slurry pipeline flow. *The Canadian Journal of Chemical Engineering*, *69*(1), 173-178.

Gillies, R. G., & Shook, C. A. (1994). Concentration distributions of sand slurries in horizontal pipe flow. *Particulate science and technology*, *12*(1), 45-69.

Gillies, R. G., Hill, K. B., Mckibben, M. J., & Shook, C. A. (1999). Solids transport by laminar Newtonian flows. *Powder Technology*, *104*(3), 269-277.

Gopaliya, M. K., & Kaushal, D. R. (2015). Analysis of Effect of Grain Size on Various Parameters of Slurry Flow through Pipeline Using CFD.*Particulate Science and Technology*, *33*(4), 369-384.

Govier, G., & Aziz, K. (1972). *The flow of complex mixtures in pipes*. New York: Van Nostrand Reinhold.

Hernández, F. H., Blanco, A. J., & Rojas-Solórzano, L. (2008, January). CFD modeling of slurry flows in horizontal pipes. In *ASME 2008 Fluids Engineering Division Summer Meeting collocated with the Heat Transfer, Energy Sustainability, and 3rd Energy Nanotechnology Conferences* (pp. 857-863). American Society of Mechanical Engineers.

Huilin, Gidaspow, & Bouillard. (2002). Chaotic behavior of local temperature fluctuations in a laboratory-scale circulating fluidized bed. *Powder Technology*, *123*(1), 59-68.

Karabelas, A. J. (1977). Vertical distribution of dilute suspensions in turbulent pipe flow. *AIChE Journal*, *23*(4), 426-434.

Karman, T. V. (1937). The fundamentals of the statistical theory of turbulence. *Journal of the Aeronautical Sciences*, *4*(4), 131-138.

Kaushal, D. R., & Tomita, Y. (2002). Solids concentration profiles and pressure drop in pipeline flow of multisized particulate slurries. *International journal of multiphase flow*, *28*(10), 1697-1717.

Kaushal, D. R., & Tomita, Y. (2003). Comparative study of pressure drop in multisized particulate slurry flow through pipe and rectangular duct. *International Journal of Multiphase Flow*, *29*(9), 1473-1487.

Kaushal, D. R., Sato, K., Toyota, T., Funatsu, K., & Tomita, Y. (2005). Effect of particle size distribution on pressure drop and concentration profile in pipeline flow of highly concentrated slurry. *International Journal of Multiphase Flow*, *31*(7), 809-823.Krieger, I. M. (1972). Rheology of monodisperse latices. *Advances in Colloid and Interface Science*, *3*(2), 111-136.

Kumar, U. (2002). *Studies on the flow of non-uniform particulate slurries through straight pipes and bends* (Doctoral dissertation).

Kumar, U., Mishra, R., Singh, S. N., & Seshadri, V. (2003). Effect of particle gradation on flow characteristics of ash disposal pipelines. *Powder technology*, *132*(1), 39-51.

Kumar, U., Singh, S. N., & Seshadri, V. (2008). Prediction of flow characteristics of bimodal slurry in horizontal pipe flow. *Particulate Science and Technology*, *26*(4), 361-379.

Kumar Gopaliya, M., & Kaushal, D. R. (2016). Modeling of sand-water slurry flow through horizontal pipe using CFD. *Journal of Hydrology and Hydromechanics*, *64*(3), 261-272.

Lahiri, S. K., & Ghanta, K. C. (2007). Computational technique to predict the velocity and concentration profile for solid-liquid slurry flow in pipelines. In*The 17th International Conference on the Hydraulic Transport of Solids, Capetown, Southern African*.

Launder, B. E., Reece, G. J., & Rodi, W. (1975). Progress in the development of a Reynolds-stress turbulence closure. *Journal of fluid mechanics*, *68*(03), 537-566.

Launder, B. E. (1989). Second-moment closure: present… and future?. *International Journal of Heat and Fluid Flow*, *10*(4), 282-300.

Launder, B. E. (1989). Second-moment closure and its use in modelling turbulent industrial flows. *International Journal for Numerical Methods in Fluids*, *9*(8), 963-985.
Lien, F. S., & Leschziner, M. A. (1994). Assessment of turbulence-transport models including non-linear RNG eddy-viscosity formulation and second-moment closure for flow over a backward-facing step. *Computers & Fluids*,*23*(8), 983-1004.

Ling, J., Skudarnov, P. V., Lin, C. X., & Ebadian, M. A. (2003). Numerical investigations of liquid–solid slurry flows in a fully developed turbulent flow region. *International Journal of Heat and Fluid Flow*, *24*(3), 389-398.

Mishra, R., Singh, S. N., & Seshadri, V. (1998). Hydraulic Conveying-Improved Model for the Prediction of Pressure Drop and Velocity Field in Multi-Sized Particulate Slurry Flow through Horizontal Pipes. *Powder Handling and Processing*, *10*(3), 279-288.

Newitt, D. M., Richardson, J. F., Abbott, M., & Turtle, R. B. (1955). Hydraulic conveying of solids in horizontal pipes. *Transactions of the institution of Chemical Engineers*, *33*, 93-110.

O'Brien, M. P. (1933). Review of the theory of turbulent flow and its relation to sediment-transportation. *Eos, Transactions American Geophysical Union*, *14*(1), 487-491.

Patankar, S. (1980). *Numerical heat transfer and fluid flow*. CRC press.

Pouranfard, A. R., Mowla, D., & Esmaeilzadeh, F. (2014). An experimental study of drag reduction by nanofluids through horizontal pipe turbulent flow of a Newtonian liquid. *Journal of Industrial and Engineering Chemistry*, *20*(2), 633-637.

Roco, M. C., & Shook, C. A. (1983). Modeling of slurry flow: the effect of particle size. *The Canadian Journal of Chemical Engineering*, *61*(4), 494-503.

Roco, M. C., & Shook, C. A. (1984). Computational method for coal slurry pipelines with heterogeneous size distribution. *Powder Technology*, *39*(2), 159-176.

Rouse, H. (1937). Modern conceptions of the mechanics or fluid turbulence. *Transactions of the American Society of Civil Engineers*, *102*(1), 463-505.

Sarkar, S., & Lakshmanan, B. (1991). Application of a Reynolds stress turbulence model to the compressible shear layer. *AIAA journal*, *29*(5), 743-749.

Schaeffer, D. G. (1987). Instability in the evolution equations describing incompressible granular flow. *Journal of differential equations*, *66*(1), 19-50.

Seshadri, V. (1982). Basic process design for a slurry pipeline. *Proceedings of The Short Term Course on Design of Pipelines for Transporting Liquid and Solid Materials*.

Seshadri, V., Malhotra, R. C., & Sundar, K. S. (1982). Concentration and size distribution of solids in a slurry pipeline. In *Proc. 11th Natl. Conf. on FMFP, BHEL Hyderabad, India*.

Shook, C. A., & Daniel, S. M. (1965). Flow of suspensions of solids in pipelines: Part I. Flow with a stable stationary deposit. *The Canadian Journal of Chemical Engineering*, *43*(2), 56-61.

Shook, C. A., & Daniel, S. M. (1965). Flow of suspensions of solids in pipelines: Part I. Flow with a stable stationary deposit. *The Canadian Journal of Chemical Engineering*, *43*(2), 56-61.

Skudarnov, P. V., Lin, C. X., & Ebadian, M. A. (2004). Double-species slurry flow in a horizontal pipeline. *Journal of fluids engineering*, *126*(1), 125-132.

Soliman, R., & Collier, P. (1990). Pressure drop in slurry lines. *Hydrocarbon Processing*, *69*(11), Hydrocarbon Processing, 1990, Vol.69 (11).

Sundqvist, Å., Sellgren, A., & Addie, G. (1996). Slurry pipeline friction losses for coarse and high density industrial products. *Powder technology*, *89*(1), 19-28.

Syamlal, M., Rogers, W., & O'Brien, T. J. (1993). MFIX documentation: Theory guide. *National Energy Technology Laboratory, Department of Energy, Technical Note DOE/METC-95/1013 and NTIS/DE95000031*.

Thomas, D. G. (1965). Transport characteristics of suspension: VIII. A note on the viscosity of Newtonian suspensions of uniform spherical particles. *Journal of Colloid Science*, *20*(3), 267-277.

Vasquez, S. A., & Ivanov, V. A. (2000, June). A phase coupled method for solving multiphase problems on unstructured meshes. In *Proceedings of ASME FEDSM'00: ASME 2000 fluids engineering division summer meeting, Boston* (pp. 1-6).

Vlasak, P., Kysela, B., & Chara, Z. (2012). Flow structure of coarse-grained slurry in a horizontal pipe. *Journal of Hydrology and Hydromechanics*, *60*(2), 115-124.

Vocaldo, J. J., & Charles, M. E. (1972, September). Prediction of pressure gradient for the horizontal turbulent flow of slurries. In *2nd International Conference on the Hydraulic Transport of Solids in Pipes, Coventry, UK, Paper* (No. C1, pp. 1-12).

Wasp, E. J., & Aude, T. C. (1970). Deposition velocities, transition velocities, and spatial distribution of solids in slurry pipelines. In *Presented at the 1st International British Hydromechanics Research Association Hydraulic Transport of Solids in Pipes Conference, War Wickshire Univ, Conventry, England, Sept. 1-4, 1970*. (No. H4 Proceeding).

Wasp, E. J., Kenny, J. P., & Gandhi, R. L. (1977). Solid--liquid flow: slurry pipeline transportation. [Pumps, valves, mechanical equipment, economics]. *Ser. Bulk Mater. Handl; (United States)*, *1*(4).

Weiss, J. M., Maruszewski, J. P., & Smith, W. A. (1999). Implicit solution of preconditioned Navier-Stokes equations using algebraic multigrid. *AIAA journal*, *37*(1), 29-36.

Wilson, K. C. (1976, May). A unified physically-based analysis of solid-liquid pipeline flow. In *Proc. Hydrotransport* (Vol. 4, pp. A1-1).

Wilson, K. C., Clift, R., & Sellgren, A. (2002). Operating points for pipelines carrying concentrated heterogeneous slurries. *Powder technology*, *123*(1), 19-24.

International Conference on Petroleum Engineering 2016 (ICPE-2016)
Bangladesh University of Engineering & Technology (BUET)
Dhaka-1000, Bangladesh

ICPE (2016-030)

Seismic Attributes Analysis and Evaluation of Prospective Hydrocarbon Zones by Seismic Inversion in the Surma Basin, Bangladesh

Md Shofiqul Islam[1)*], Shefa Ul Karim[2)], Mohammad Moinul Hossain[3)] and Iqbal Hossain[1)]

1) Dept. of Petroleum and Mining Engineering, Shahjalal University of Science and Technology, Sylhet3114, Bangladesh

2) Petroleum Geophysics Program, Department of Geological Sciences, Chiang Mai University , T. Suthep, A. Muang, Chiang Mai Thailand, 50200

3) Geophysical Division, Bangladesh Petroleum Exploration and Production Company, Dhaka, Bangladesh

ABSTRACT

Reservoir characterization plays an important role in different parts of an industrial project which gives insight into rock and fluid properties to optimize the choice of drilling locations and reduce risk and uncertainty. This article has made comparative studies among different seismic attributes and delineated potential reservoir zones by post stack seismic inversion analysis for further production in a specific gas field of Surma Basin. The first step towards a successful hydrocarbon discovery is a good subsurface image of seismic data. But resolution problems seismic data does not give the most clearly view of subsurface and can be misled under certain condition. Model Based Post-stack inversion technique was used to create pseudo logs at each seismic trace at the well location to constitute high resolution inverted acoustic impedance (AI) models. A High co-relation coefficient value (0.91) in inversion quality control analysis proved that result is more consistent with well log study. All of potential hydrocarbon zones at Well #X show relatively low AI values from 18856-22243(ft/s) (g/cc) in inverted section which are as same as the calculated AI. On the contrary, shale zones show high Impedance from 27519 to 33152 (ft/s) (g/cc). The impedance value at 1660-1980 ms representing alternating sequence of shale and sand typical characteristics of lower Bokabil and upper Bhuban Formation. By considering the impedance values in inversion section some locations are marked as potential gas bearing zones which are more prospective for optimizing the gas recovery from this field by placing additional wells.

Keywords: Seismic attributes, Wavelet, Acoustic Impedance, Seismic Inversion, Reservoir

* Corresponding Author address
Email: sho_fiq@yahoo.com

1. INTRODUCTION

Reservoir characterization plays an important role in different parts of an industrial project which gives insight into rock and fluid properties to optimize the choice of drilling locations and reduce risk and uncertainty [1]. Perception of reservoir characterization requires integrated analysis and understanding of the available data, such as seismic data and well log data. In any seismic reservoir characterization studies, the first step towards a successful hydrocarbon discovery is the mastering of a good subsurface image of seismic data. Seismic data is the output of a convolution operation that produces a band-limited trace [2]. Band limited nature of the seismic data and lack of low frequencies prevents the transformed impedance trace from gaining the basic impedance. An attempt to recover this resolution is usually made by Seismic Inversion.

Seismic inversion is a technique that has been used to transform the spiked seismic reflectivity at geological boundaries into meaningful petrophysical properties (impedances) and play an important role in reservoir characterization [3]. Since, well log present accurate petrophysical properties of subsurface, but has spatial limit due to limited number of well. On the contrary, seismic data being most continuous information available (lower vertical resolution) [4]. The inversion algorithm transforms the reflection amplitudes into AI, which is the product of density and P-wave velocity. In well-log measurements, both of these properties can be measured, and therefore impedance logs can be obtained and directly compared to the seismic AI. Through the process of seismic inversion, we can transform seismic sections to AI sections which represent the lithological properties of the rather than the interface properties. Therefore, transformation to AI simplifies is an optimal way to get a better subsurface image and crucial for seismic interpretation and reservoir characterization [5, 6].

The seismic reflection characteristics and other instantaneous attributes have been studied to make a comparative analysis and identify distinguishable hydrocarbon zone. Finally, Model based post-stack seismic inversion analysis is used to enhance better understanding of subsurface geology of the study area and identified some gas bearing potential zones and possible well locations for further development.

2. GEOLOGY AND STRATIGRAPHY

The study area is situated in the transition zone between the central Surma Basin and the folded belt in the east and is closest to the eastern margin of the central Surma Basin and is separated in the north from Kailashtila Anticline, in the east from Harargaj Anticline and in the south from Batchia Anticline. This structure appeared as a reversibly faulted asymmetrical anticline with NNE- SSW trending axis [7, 8]. Structural and combination traps of Miocene age occur along stratigraphic boundaries, in sandstone-filled channel deposits, and in sandstone beds sealed laterally by shale-filled channels; these comprise major traps in the eastern part of the basin [9].

The Surma Basin contains a great thickness of Tertiary sedimentary strata and lithologies consist of deltaic, estuarine, and shallow-marine sandstones, siltstones, and shales that contain abundant plant-derived organic matter. The variety of sediment facies indicates a range of depositional environment during Neogene time [10]. Thermal maturation is sufficient to generate natural gas and liquids throughout

much of the area [9]. Fenchuganj gas fields' geology is similar to that of other fields situated in Surma Basin. The sediments of Fenchuganj structure consist of alternate shale and sandstone in varying proportion of Oligocene to Recent age [11]. The reservoirs have been found in the Miocene sediments and Potential source rocks include shales and carbonaceous shales of Eocene, Oligocene, and Miocene age [8, 12].

3. METHODOLOGY

Basically the seismic inversion method is a process of transforming seismic amplitude value to impedance value by using seismic data as input and well data as control [13]. Post-stack seismic inversion method use stacked (zero-offset) seismic data to produce images of the AI in depth or time. The fundamental concept of seismic exploration is measure reflection coefficient. Equation (1) can be used as a simplified model for the reflection found on a stacked seismic section. Actually the recorded seismic trace is the convolution of the reflectivity with a band limited seismic wavelet plus some additive noise (Equation 2) [14]. Lindseth (1988) inverts the Equation (1) to iteratively obtain the acoustic impedance in the next layer.

$$r_i = \frac{Z_{i+1} - Z_i}{Z_{i+1} + Z_i} \qquad (1)$$

Where, r_i reflection coefficient and $Z =$ AI

$$S_t = w_t * r_t + n_t \qquad (2)$$

Where S_t seismic trace, w_t seismic wavelet, r_t, (*) denoting convolution, and nt noise component.

$$Z_{i+1} = Z_i \left[\frac{1 + r_i}{1 - r_i}\right] \qquad (3)$$

Applying of Equation (3) to a seismic trace can effectively transform the seismic reflection data to P-impedance. In this method, the impedance for the nth layer can be calculated as follows [15].

$$Z_n = Z_1 * \prod \left(\frac{1 + r_i}{1 + r_i}\right) \qquad (4)$$

But the most severe drawback is remove the low frequency component of the reflectivity and treat the trace as a set of reflection coefficient, which means that it can never be exactly recovered Eq. (2). To resolve this problem an update approach to inversion is Model Based inversion [14, 16]. The main steps in the inversion procedure include the data preparation and data input into the software, calibration by tying well logs to the seismic data, estimation of the wavelet, generation of a low-resolution initial model, inversion analysis and inversion.

3.1. Well to seismic tie:

In well to seismic tie a synthetic trace was generated to correlate with recorded seismic trace. Since the well logs are in depth domain while seismic data is in the time domain, a check shot data was applied before correlation to convert well data into time domain [17]. Steps common to the most good tie processing include [18]:

1. Calculate vertical reflection times and coefficients from sonic and density log.
2. Convert reflectivity from depth to time.
3. Convolve the reflection coefficient series with the wavelet.
4. Match the synthetic with the observed seismic trace.
5. Update the time depth curve.

Synthetic seismic trace can be recomputed using different wavelets and filters to improve the correlation coefficient. Through a trial-and-error process determines at what point the artificial trace "best fits" the seismic data [19].

3.2. Wavelet Extraction:

A seismic wavelet is the source signature and a good wavelet is the core of inversion [20]. In frequency domain wavelet extraction consists of determining the amplitude spectrum and phase spectrum. The amplitude spectrum is determined from the autocorrelation function of the data, under the usual assumption of "random" (or "white") reflectivity [6]. The phase spectrum is more difficult to determine. Since Wavelets can and do change from trace to trace and as a function of travel-time, extraction process should be determining a large set of wavelets for each seismic section. More meaningful and practical solution is to extract a single average wavelet for the entire section [21].

3.3. Initial Model:

Initial model provides the low and high-frequency components missing from the seismic data, which were used to reduce the non-uniqueness of the solution [5, 13]. Low frequency cutoff point, several band-pass filters were applied to the seismic data to the best estimate of the missing frequency range. The spatial interpolation method used in the H-R software utilizes inverse-distance weighting [22].

3.4. Inversion Analysis:

The Inversion QC (quality control) analysis on selected well location means testing a range of inversion parameters quickly and comparing different parameters before performing the actual inversion. When the parameter analysis is satisfactory, Strata calculates a single global scale, and that the inversion results will be applied to the whole seismic volume.

3.4. Model Based Inversion:

Model Based inversion is a recent approach to inversion, which is based on the convolution model Eq. (2) [14]. If the noise is uncorrelated with the seismic signal, we can solve the reflectivity satisfying this equation Eq. (2). This is a non-linear and band-limited equation and solved iteratively [6, 22, and 23]. Theory of model based inversion is as follows. The reflectivity approximation is given by re-expressing equation 1 as:

$$r_i \approx \frac{1}{2}[\Delta \ln Z_{i+1} - \ln Z_i] \qquad (5)$$

For N samples reflectivity, Equ. (3) can be written in matrix form as:

$$\begin{bmatrix} r_1 \\ r_2 \\ \vdots \\ r_N \end{bmatrix} = \frac{1}{2}\begin{bmatrix} -1 & 1 & 0 & \cdots \\ 0 & -1 & 1 & \ddots \\ 0 & 0 & -1 & \ddots \\ \vdots & \ddots & \ddots & \ddots \end{bmatrix}\begin{bmatrix} \mathrm{L}_1 \\ \mathrm{L}_2 \\ \vdots \\ \mathrm{L}_\mathrm{N} \end{bmatrix} \qquad (6)$$

Where, $\mathrm{L_i} = \ln Z_i$

Equation (7) is seismic trace as the convolution of the seismic wavelet with the earth's reflectivity.

$$\begin{bmatrix} S_1 \\ S_2 \\ \vdots \\ S_N \end{bmatrix} = \begin{bmatrix} w_1 & 0 & 0 & \cdots \\ w_2 & w_1 & 0 & \ddots \\ w_3 & w_2 & w_1 & \ddots \\ \vdots & \ddots & \ddots & \ddots \end{bmatrix}\begin{bmatrix} r_1 \\ r_2 \\ \vdots \\ r_N \end{bmatrix} \qquad (7)$$

Where, S_i of the seismic trace and w_j extracted seismic wavelet. Combining Eq. (4) and (5) gives us the forward model which relates the seismic trace to the logarithm of P-impedance:

$$\mathrm{S} = (1/2)\mathrm{WDL} \qquad (8)$$

Where, W is the wavelet matrix given in equation (7) and D is the derivative matrix given in Eq. (6).

If Eq. (7) is inverted using a standard matrix inversion technique there are two problems; costly and unable to recover low frequency data. An alternate strategy is to build an initial guess impedance model and then modified iteratively to give the best fit to seismic data [14].

4. RESULT AND DISCUSSION

In this study, log data of well FG #X and post-stack 2D seismic section SBL #A shown in Figure 2 are used to evaluate the potential for middle to deep zone in the study area. This study focuses on SBL #A, because it is located over the most productive part of study area and well FG #X is situated on this line. The post-stack seismic section illustrates a typical cross section of an anticline (Figure 2). Low amplitude may be indicated the potential zones and high amplitude in shale sequence. The flank portion of the seismic section shows an alternative of two major reflection patterns probably representing alternating sequence of shale and sand typical characteristics of Surma Group of sediments represented by Bokabil and Bhuban Formation. The middle right of this seismic section is seismically blind zone due to a fault.

Seismic attributes is a quantity extracted or derived from seismic data that can be analyzed to enhance information that might be more subtle in a conventional seismic image, leading to a better interpretation of the data [24]. The seismic reflection characteristics and other instantaneous attributes have been studied to identify distinguishable hydrocarbon zones, evaluate reservoir. The instantaneous frequency attributes of seismic section show in Figure (2). Frequency attributes can help to identify the high frequency sand-shale sequence, a low frequency anomaly with flat spot may indicate hydrocarbon saturated zone at the middle part of structure. Figure (3) is the instantaneous amplitude attributes. The bright spots are found in middle to lower left zone and lower right zone are possible hydrocarbon accumulated zones. Sequence boundaries are very clear in this figure. Figure (4) is the energy attribute of SBL #A, this is used to map the strongest direct hydrocarbon indicator. The yellow color indicates high energy portion that might relate with strong lithological variation and possible indicator of hydrocarbon saturated zone. In the middle to lower left zone and lower right zone bright spots are interesting for possible hydrocarbon saturated.

Due to data resolution problems attribute analysis does not give the most clearly view of subsurface and can be misled under certain condition. To make better understanding of subsurface geology model based inversion has been applied. As first step of inversion well to seismic tie shows in Figure (5). The well to seismic tie has long been considered an art for geophysical interpreters [18]. The synthetic trace using full wavelet (estimated by using log and seismic data) gives a high correlation level with composite trace where the current correlation coefficient is 0.905. Because of band limited nature of seismic data, the lowest and

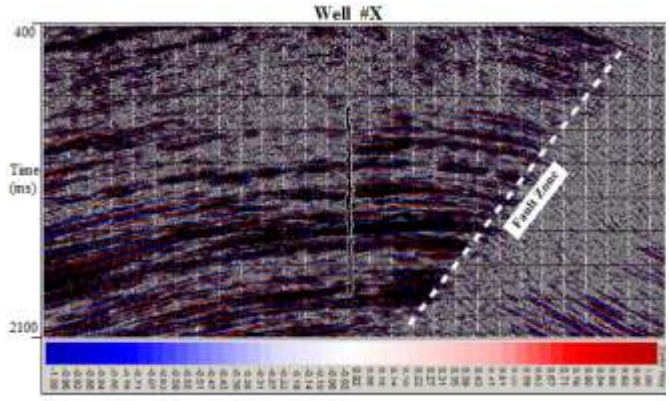

Figure 1: Zero offset seismic section of line SBL #A with P-wave curve from well FG #X. The scale of legend varies from -1.00 to 1.00 where red color shows positive amplitudes and a blue color represents negative amplitudes.

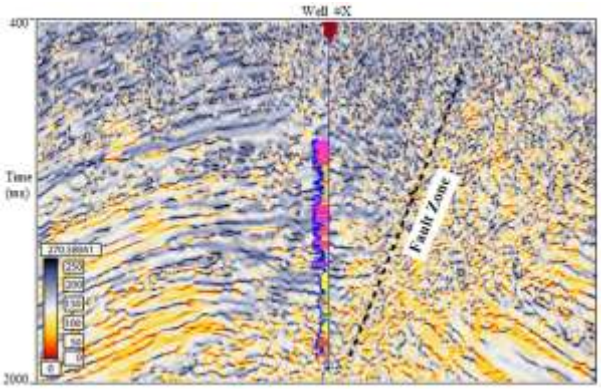

Figure 2: Instantaneous frequency attributes of seismic section with well FG #X. The scale of legend varies from 270.58041 to 0 for black to red color. The middle right zone of this section shows lower frequency which is fractured zone.

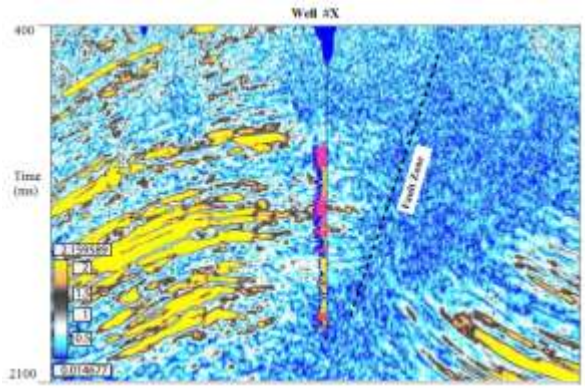

Figure 3: Instantaneous amplitude attributes of seismic section with well FG #X. The scale of legend varies from 2.159585 to 0.014677. The bright spots are found in middle to lower left zone and lower right zone.

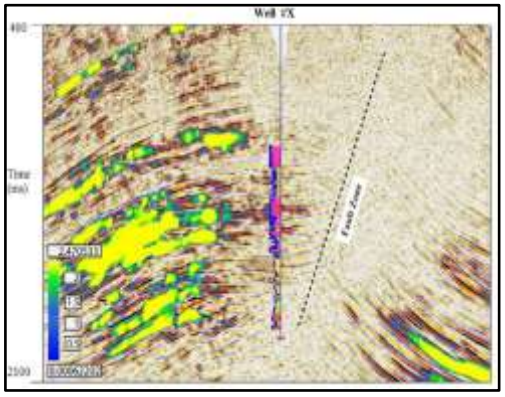

Figure 4: Energy attributes of seismic section with well FG #X. The scale of legend varies from 2.470533 to 0.00062202. Bright spots are interesting for possible hydrocarbon saturated zone.

the highest frequencies were missed [20]. To supply the low frequency component missing from the seismic trace an initial model was built by interpolating the AI from targeted well location shown in Figure (5). After building initial model, Model Based inversion analysis has carried out (Figure 6). The original well log used in inversion ended at the time level 900ms and below 2000ms in Figure (7). Inversion analysis means testing a range of inversion parameters quickly and comparing among different parameters before performing the actual inversion [25]. A visual comparison of real seismic data and inverted synthetic trace in well location shows a good correlation coefficient of 0.867 (Figure 7). The analysis of the inversion product has proved that the result is consistent with the actual gas presence observed from the existing well in the study area.

Figure (8) represents a cross section of the Model Based post-stack inversion result. All of predicted gas bearing zones in the log section of well FG #X shows low impedance value in the inverted section with impedance value are nearly 18856 to 22243 (ft/s)* (g/cc). Lower impedance value takes place in sand zones, but the amount of lowering depends upon the fluid content of sand. In hydrocarbon bearing sand, lowering of impedance will be high if compared to that of water bearing sand [26]. The calculated value of AI through log data at potential reservoir zones are almost same as the extracted value from inverted section (Table 1). At inverted section low acoustic impedance zones at time nearly 1100 ms, 1250 ms, 1300 ms and 1430 ms are marked as potential reservoir lacations (Figure 8). On the other hand, at time near 1280 ms, 1400 ms and 1600 ms, with higher impedance, indicate the overlaying shale layers. Variation in AI values on inverted section at a time 1660-1980 ms represents an image of the thin sand and thick shale layer alteration of Upper Bhuban formation. Through the observation of relatively lower impedance values in the inverted section three prospect well locations PW-1, PW-2 and PW-3 are estimated (proposed).

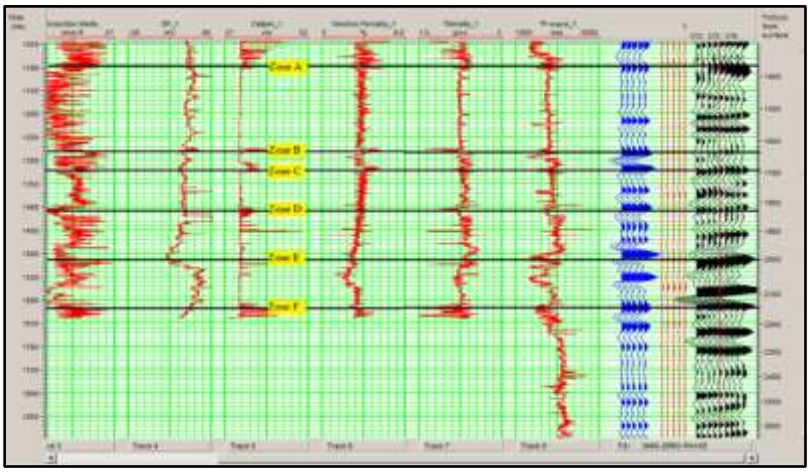

Figure 5: Correlation window by using the Full wavelet. The blue trace represents the synthetic trace and the black traces represents original seismic trace. Zone (A, B, C, D, E, F and G) marked as interpreted reservoir zones based on logging data of well FG #X.

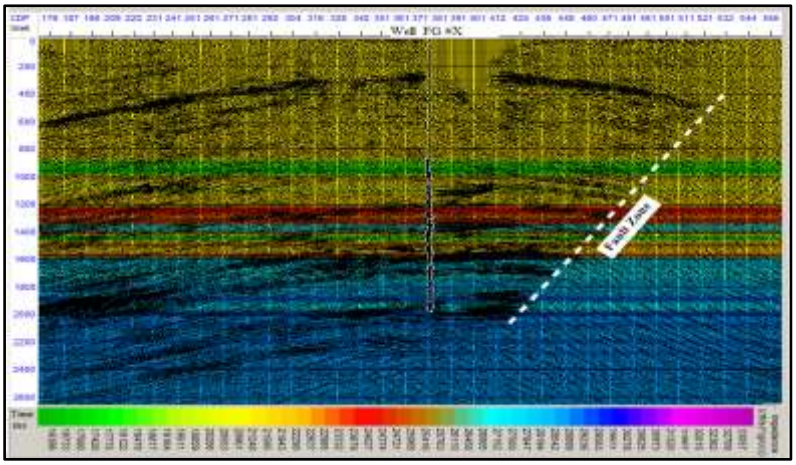

Figure 6: This low frequency background impedance model (Initial model).

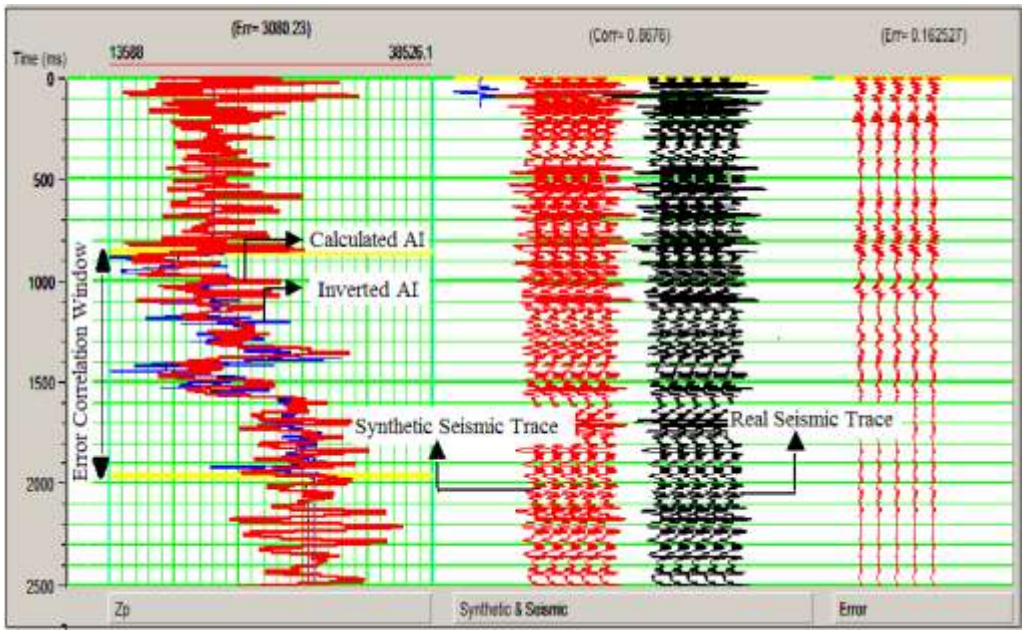

Figure 7: Inversion analysis window at the well FG#X. Time limit from 900 ms to 2000 ms with error calculation and the impedance misfit was minimized during the inversion.

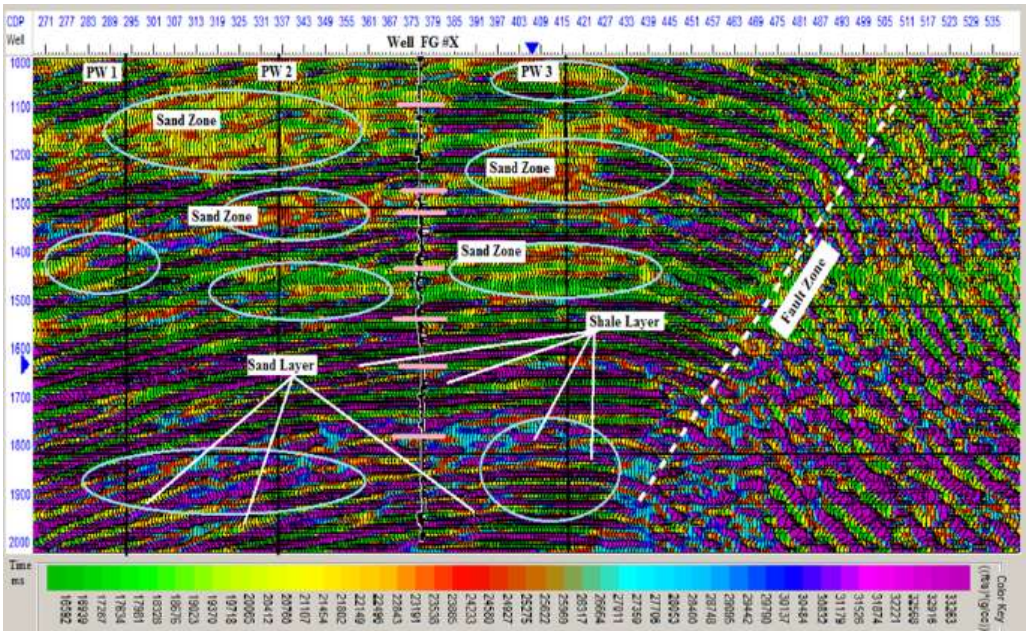

Figure 8: Model Based Post-stack seismic inverted section. PW 1, PW 2 and PW 3 are prospect wells. Baffling impedance amplitudes at right portion of this section indicate the fault effected part (fractured zone) of the structure.

Table 3: Calculated and extracted AI value at delineate reservoir zone through log interpretation

Depth (m)	Time (ms)	Lithology	Remark	Average density (g/cc)	Vp (from log data) (ft/s)	Calculated AI (ft/s)* (g/cc)	AI from Inverted volume (ft/s)* (g/cc)
1350-1375	1074-1095	Sand	Zone A	2.27	8446	19172	19480
1375-1655	1095-1287	Shale	-	2.39	13123	31363	32619
1655-1680	1287-1306	Sand	Zone B	2.3	9194	21146	21935
1680-1693	1306-1320	Shale	-	2.4	13393	32143	33075
1693-1705	1320-1331	Sand	Zone C	2.325	9842	22882	21687
1705-1815	1331-1405	Shale	-	2.4	12467	29920	28922
1815-1850	1405-1432	Sand	Zone D	2.25	8202	18454	18856
1850-2020	1432-1531	Shale	-	2.394	14017	33556	33152
2020-2080	1531-1576	Sand	Zone E	2.247	8773	19713	19176
2080-2148	1576-1632	Shale	-	2.38	13939	33174	32860
2148-2154	1632-1636	Sand	Zone F	2.314	9352	21640	22243
2154-2206	1636-1687	Shale	-	2.405	11826	28441	27519

5. CONCLUSION

The seismic data (seismic line 14_FG-10) has used in this study to find the fault, fractured zones and evaluate lithology. Some seismic attributes analysis windows are used to identify the potential zone. Sand-shale dominated banded sequence is clearly identified by seismic attribute analysis. In addition, fault line and fractured zones are also fairly identified through the attributes. To get more clearly subsurface image inversion analysis has been done. The synthetic trace using Full Wavelet gives a high correlation coefficient about 0.905. The inversion analysis result at well FG#X with an error of 0.1625 gives a good correlation (0.9867) between the inversion trace and the original trace. All of the predicted gas bearing zones in the well FG #X show the low impedance values in inverted section and those are almost same as the calculated AI value from logging data. This promising result is a proof of concept that seismic inversion can be used as one of the tool to approach the hydrocarbon or reservoir distribution prediction. Zones of the low acoustic impedance at near times 1100 ms, 1250 ms, 1300ms and 1430 ms, are marked as potential sand zones. Furthermore, the impedance value in inverted section from 1660ms to

1980ms represents an image of alteration of thin sand and a thick shale layer of Upper Bhuban formation. Considering the AI value three prospect well locations (PW-1, PW-2 and PW-3) are marked, which are more prospective for optimizing the gas recovery from this field.

6. ACKNOWLEDGEMENT

Authors are grateful to BAPEX (Bangladesh Petroleum Exploration and Production Company) authority, especially Geological and Geophysical Division for allowing us to collect the necessary data and use their softwares for this study.

REFERENCES

1. Torres, C., and Sen, M., (2004). Integrated Approach for the Petrophysical Interpretation of Post- and Pre-stack 3D Seismic Data, Well Log and Core Data, Geological Information and Production Data via Bayesian Stochastic Inversion; Third Annual Report, Institute of Geophysics, Texas.
2. Yilmaz, O., (2001). Seismic data analysis Society of exploration geophysicists 74170-2740.
3. Lindseth, R.O., (1979). Synthetic sonic logs-a process for stratigraphic interpretation, **44** (1), 3-26.
4. Sen, M.K., (2006). Seismic Inversion (Society of Petroleum Engineers: USA).
5. Russell, B., and Hampson, D., (1991), A Comparison of Post-stack Seismic Inversion, 61th Annual International Meeting, SEG 876-878.
6. Swisi, A., (2009). Post- and Pre-stack Attribute Analysis and Inversion of Blackfoot 3D Seismic Data Set", M.Sc. Thesis, University of Saskatchewan, Saskatoon.
7. Hiller, K., and Elahi, M., 1(984). Structural development and hydrocarbon entrapment in the Surma Basin, Bangladesh (northwest Indo-Burman fold belt), Singapore Fifth Offshore Southwest Conference, Singapore.
8. Islam, S.M.A., Islam, M.S., and Hossain, M.M., (2014). Investigation of fluid properties and their effect on seismic response, A case study of Fenchuganj Gas Field, Surma Basin, Bangladesh, Int. J. Oil Gas Coal Engg, **2** (3), 36-54
9. Geological Survey Bulletin (2001), U.S Geological Survey –Petrobangla cooperative assessment of undiscovered natural gas resources of Bangladesh. U.S. 2208-A: 119.
10. Evans, P., (1964). The tectonic framework of Assam, Journal Geological Society of India, **5,** 80–96.
11. Immam, B., (2013). Energy Resources of Bangladesh Published by University Grant Commission of Bangladesh, 2nd Edition.
12. Mannan, M.A., (2002). "Stratigraphic evolution and geochemistry of the Neogene Surma Group, Surma Basin, Sylhet, Bangladesh PhD Dissertation, Department of Geology, University of Oulu.
13. Sukmono, S., (2002). An Introduction to Seismic Reservoir Analysis, in Seismic Inversion and AVO Analysis for Reservoar Characterization Geophysical Engineering, ITB, Bandung.
14. Russell, B., Hampson, D., and Bankhead, B., (2006) An Inversion Primer CSEG Recorder, 31.

15. Pendrel, J., (2001). Seismic inversion the best tool for reservoir characterization, CSEG Recorder, **26** (1), 18-24
16. Lee, K., Yoo, D.G., McMechan, G.A., Hwang, N., and Lee, G.H., (2013). A Two-Dimensional Post-Stack Seismic Inversion for Acoustic Impedance of Gas and Hydrate Bearing Deep-Water Sediments Within the Continental Slope of the Ulleung Basin, East Sea, Korea Terr. Atmos. Ocean. Sci., **24** (3) 295-310.
17. Karbalaali, H., Shadizadeh, S.R., and Riahi, M.A., (2013). Delineating Hydrocarbon Bearing Zones Using Elastic Impedance Inversion: A Persian Gulf Example Iranian Journal of Oil & Gas Science and Technology, **2** (2), 8-19.
18. Munoz, A., Hale, D., "Automatically tying well logs to seismic data", Center for Wave Phenomena, Colorado School of Mines, Golden, CO80401, USA, p. 253-260.
19. Nawaz, U.S., (2013). Acoustic and Elastic Impedance Models of Gullfaks Field by Post-Stack Seismic Inversion M.Sc. Thesis, Norwegian University of Science and Technology.
20. Jain, C., (2013). Effect of Seismic Wavelet Phase on Post Stack Inversion 10th Biennial International Conference & Exposition, Kochi, P -410.
21. Russell, H., (1999). Theory of the STRATA Program Hampson-Russell, CGG Veritas.
22. Russell, H., (2007). STRATA guide, Hampson-Russell, CGG Veritas.
23. Veeken, P.C.H., and Silva, M.D., (2004). Seismic inversion methods and some of their constraints, EAGE, **22,** 47-70.
24. Sheriff, R.E., Geldart, L.P., (1995). Exploration Seismology, 2nd Edition: Cambridge University Press, New York, USA, p. 592.
25. Hidayat, L., (2009). Prediction of Gas Distribution Using Seismic Simultaneous Inversion Method, M.Sc. Thesis, University of Indonesia, Jakarta.
26. Dubey, A.k., (2012). Reservoir Characterization using AVO and Seismic Inversion Techniques, 9th biennial int. conf. & on exposition petroleum geophysics, p-205.

International Conference on Petroleum Engineering 2016 (ICPE-2016)
Bangladesh University of Engineering & Technology (BUET)
Dhaka-1000, Bangladesh

ICPE (2016–034)

Estimation of Downhole Cuttings Concentration: A Comparative Study of Two Empirical Models Using Experimental Data

Dipankar Chowdhury* *& *Pål Skalle
Department of Petroleum Engineering and Applied Geophysics, Norwegian University of Science and Technology, Trondheim, Norway

ABSTRACT

Estimation of downhole cuttings concentration is a challenging task. Many different factors influence cuttings accumulation downhole such as RPM, ROP, eccentricity, hole inclination and change in fluid viscosity in radial direction. Therefore, different empirical models are developed by different researchers based on experimental data. In the current article, a model developed by Ahmed et al. (2010) and another by Rubiandini (1999) are studied using the experimental data published by Ahmed et al.

Ahmed's model was developed using dimensional analysis, while Rubiandini extended the empirical cuttings slip velocity model of Larsen et al. (1997) to cover the entire hole inclination angle range from 0 to 90^{o} using experimental data of Larsen et al. and Peden et al. (1990). Larsen's cuttings concentration estimation model (incorporating viscosity correction factor) is combined with Rudiandini's critical mud velocity model in the current work to estimate cuttings concentration using critical mud velocity approach.

For the experimental data published by Ahmed et al. (2010), Rubiandini's model provided cuttings concentration estimates with comparable accuracy to Ahmed's model for medium and large annulli while Ahmed's model outperforms Rubiandini's model for small annulus. However, Ahmed's model is found to be inapplicable for vertical wells and for non-rotating drillstring cases (turbo-drilling) while Rubiandini's model can provide negative cuttings concentration if critical mud velocity is less than applied pump rate.

Keywords: Cuttings concentration, empirical models, annulus size

INTRODUCTION

With the recent downturn in the global hydrocarbon market, reduction in operational cost gets higher focus than ever. Operators are focusing on drilling wells at reduced cost by minimizing NPT. Hole problems and equipment failure (drillstring and tool) are considered two main causes of NPT (Mitchell, Lake, & Engineers, 2006). Hole problems (pack-off and lost circulation), addressed by hydraulics measurement, are associated

* Corresponding Author address
Email: dipankar.chowdhury@ntnu.no

with and influenced by downhole cuttings accumulation. ECD is directly affected by amount of cuttings downhole as shown analytically by EXLOG (Whittaker, 1985). Mechanical hole failure is often combined with inadequate hole cleaning ability and is believed to cause 5-10% of drilling costs in exploration and production (Fjaer, Horsrud, Raaen, Risnes, & Holt, 1992). Hence, monitoring of change in downhole cuttings concentration while drilling is of utmost importance to reduce drilling cost and avoid expensive stuck pipe incidents.

A number of parameters influence cuttings transportation and hence affect cuttings concentration downhole. In the order of decreasing influence and decreasing ease of control at the field, these parameters can be arranged as – flow rate, hole size and hole angle, drillpipe eccentricity, fluid rheology, mud weight, ROP, cuttings density, drillpipe rotation, hole cleaning pills and cuttings size (Mohammadsalehi & Malekzadeh, 2011). In addition, the flow of cuttings in the annulus is subject to many forces in existence such as those of gravity, buoyancy, drag, intertia, friction and inter-particle contact (Azar & Samuel, 2007). All these parameters and forces make analytical description of cuttings transport a daunting task. Hence empirical correlations developed using experimental data are considered a practical approach (Whittaker, 1985).
In this paper, a comparative study of two emprical models is presented using the experimental data published by Ahmed et al. (Ahamed, Sagheer, & Takach, 2010). The first model was developed by Ahmed et al. using dimensional analysis and experiments performed in the 85' long low-pressure ambient temperature flow loop developed at the University of Tulsa. The second model was developed by Rubiandini (Rubiandini, 1999) using experimental data of Peden et al. (Peden, Ford, & Oyeneyin, 1990). Rubiandini extended the model published by Larsen et al. (Larsen, Pilehvari, & Azar, 1997) to cover the entire hole inclination angle range from 0 to 90^o. Hereon, the two models are named respectively after their developers in this paper i.e. the model developed by Ahmed et al. is named as 'Ahmed model' and that by Rubiandini as 'Rubiandini model'.

EMPIRICAL MODELS & EXPERIMENTAL DATA

Both Ahmed and Rubiandini models are based on simplifying assumptions and experimental observations.

Ahmed Model

Ahmed et al. used the following correlation to estimate cuttings concentration:

$$C_c = (1 - \emptyset)A_C$$

The dimensionless parameter A_c accounts for the severity of annular blockage due to the formation of the cuttings bed. It is determined using dimensional analysis. Using the experimental data obtained with a concentric drillpipe, the following equation of A_c was developed by Ahmed et al.:

$$A_c = A_o \theta^{A_1} {S_t}^{A_2} Re^{A_3} {C_d}^{A_4}$$

Where $A_o = 2.55 \times 10^8$, $A_1 = 1.94$, $A_2 = -0.842$, $A3 = -2.22$, $A_4 = 0.174$ (determined using experimental data conducted with no variation of eccentricity)
Close observation of the above model reveals that A_c increases with increasing hole inclination angle, but decreases with increasing RPM, increasing flow rate and decreasing ROP. This supports the intuitive understanding of cuttings transportation. C_c is proportionally related to A_c as considered by Ahmed et al.
The model has two principal limitations. Firstly, the model is not applicable for vertical wells. For vertical wells, Θ is zero rendering A_c to be zero. This means C_c will be zero according to Ahmed's model for vertical wells under all drilling conditions. Secondly, the model cannot be used for turbo-drilling condition where the drill string does not rotate. In turbo-drilling, the formation is drilled by pumping mud through a stationary drill string to turn a turbine attached to the drill bit. Under turbo-drilling condition, S_t becomes zero since drillpipe

RPM is zero. This means A_c is zero, which in turn means C_c is zero under turbo-drilling condition. The model also does not consider eccentricity.

Rubiandini Model

Rubiandini considered drillstring rotation in his model which was ignored by Larsen et al. (1997). He ignored eccentricity like Ahmed et al. He used Moore's slip velocity formulation for vertical well to develop a new set of equations for estimating critical mud velocity. He incorporated correction factors for angle of inclination, drillstring rotation and mud weight in his model of cuttings slip velocity by dimensionless plotting of slip velocity (obtained from Peden's and Larsen's experiments) against angle of inclination.

Unlike Ahmed, Rubiandini used the concept of critical mud velocity in his model. It is assumed that no cuttings bed is formed as long as the mud flow rate is at and above the critical value. Cuttings bed formation is observed for inclination angles above 10^o (Iyoho, 1980).

Rubiandini developed the following set of equations valid for $0^o - 90^o$ deviation angles:

General formulation: $$v_{crit} = v_{cut} + (1 + C_{inc}\, C_{mud}\, C_{RPM})v_{sv}$$

$\theta \leq 45^o$: $$v_{crit} = v_{cut} + \left\{1 + \frac{\theta(600 - RPM)(3+\gamma_m)}{202500}\right\} v_{sv}$$

$\theta > 45^o$: $$v_{crit} = v_{cut} + \left\{1 + \frac{(600 - RPM)(3+\gamma_m)}{4500}\right\} v_{sv}$$

Cuttings velocity: $$v_{cut} = \frac{ROP}{36\left[1-\left(\frac{d}{D}\right)^2\right]C_{cut}}$$

Cuttings concentration at v_{crit}: $$C_{cut} = 2\ (\Theta < 55^o)$$
$$= \left(0.64 + \frac{18.16}{ROP}\right)\ (\Theta > 55^o)$$

For vertical wells and turbo-drilling condition (RPM=0), Rubiandini's model turns into Moore's slip velocity model. The model shows critical mud velocity is independent of hole inclination angle above 45^o which is not intuitive. The model is reported to over-predict critical mud velocities in comparison with typical field values (Ranjbar, 2010).

In order to determine cuttings concentration, the approach laid out by Larsen et al. incorporating correction factor for mud viscosity is used in this paper. The equation for cuttings concentration involves determination of critical mud flow rate calculated using critical mud velocity derived from Rubiandini's model-

$$C_c = 100\left(1 - \frac{Q_{pump}}{Q_{crit}}\right)(1 - \emptyset)(0.97 - 0.00231\mu_a)$$

This approach can produce negative Cc if Q_{crit} is smaller than Q_{pump}. One such situation was encountered in the current work.

Experimental data

The experimental data used in the current study is collected from the experiment performed by Ahmed et al. (2010) without any mechanical cleaning device in the test string. They used 1.25 lbm/bbl Poly Anionic Cellulose suspension in their experiments, which was a Power Law fluid (n=0.69 and K=0.45 lbfsn/100ft^2). The 85' long test section consisted of a transparent acrylic pipe (simulating a wellbore) having an ID of 8" and an aluminium drill pipe which was concentric with the annulus at the ends and eccentric in the test section due to sagging under its own weight (Fig. 1). All experiments were repeated three times to ensure result reliability. 3.35

Figure 1: Inside of the 85' long test section (Sagheer, 2009)

mm river gravels with 2.6 sg and 40% porosity was used as cuttings in the experiment. An auger was used to inject cuttings into the mud stream to simulate three different ROP – 40, 60 and 80 ft/hr. Three different annulus sizes were used – 4.5"x8", 3.5"x8" and 3.0"x8". Mud flow rates used in the experiment were 300, 400 and 550 gpm. Hole inclination angle was varied between 40^o, 65^o and 90^o. The drill pipe was rotated at 90, 110 and 140 rpm during the experiment. No variation in eccentricity was done during the test. Cuttings bed height in the test section was measured using a travelling camera system.

ANALYSIS OF EXPERIMENTAL DATA

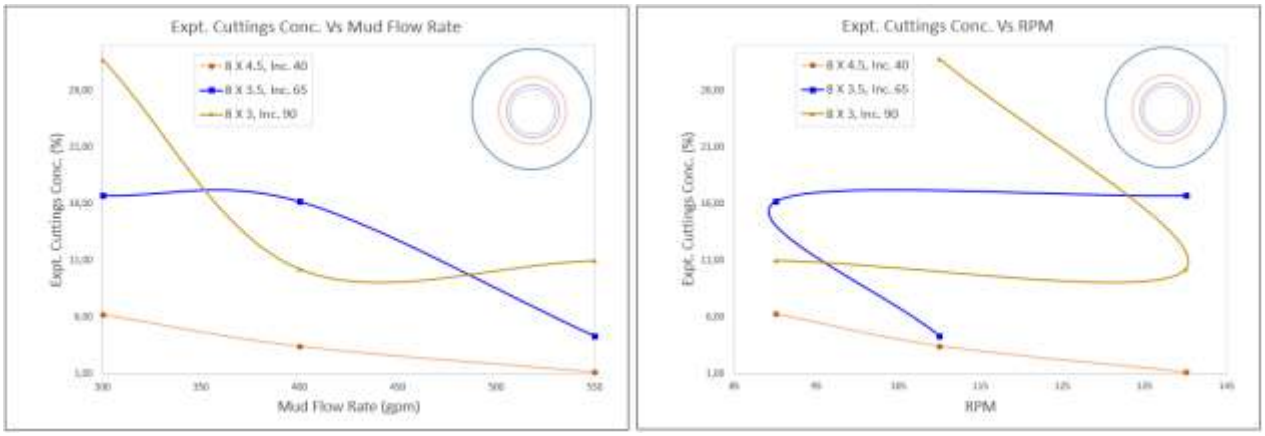

Figure 2: Change in cuttings concentration with mud flow rate and drill pipe rotation

Three different annulus sizes were used for three different hole inclination angles. Hole inclination angle was increased from 40^o through 65^o to 90^o as the annulus size was increased from 8"x4.5" through 8"x3.5" to 8"x3". For the smallest annulus size, both flow rate and RPM were increased from smallest through medium to largest values during the experiment resulting in reduced cuttings concentration with increased mud flow rate and drill pipe rotation (Fig. 2). However, mud flow rate and RPM values were combined differently for other two annulus

sizes. But overall a reduction in cuttings concentration with increased mud flow rate was observed for all the annulus sizes. However, cuttings concentration maintained a positive relationship with ROP for all the test conditions.

Iyoho reported that cuttings bed formation is negligible for $\Theta \leq 10^o$ (1980). He observed steady cuttings bed for $\Theta > 10^o$ even at mud velocities as high as 1.22 m/s. Ahmed et al. observed cuttings bed at the three inclination angles used in the experiment. All of them were much larger than 10^o.

COMPARISON OF MODELS

The two models will be compared separately for the three different annulus sizes used in the experiment performed by Ahmed et al.

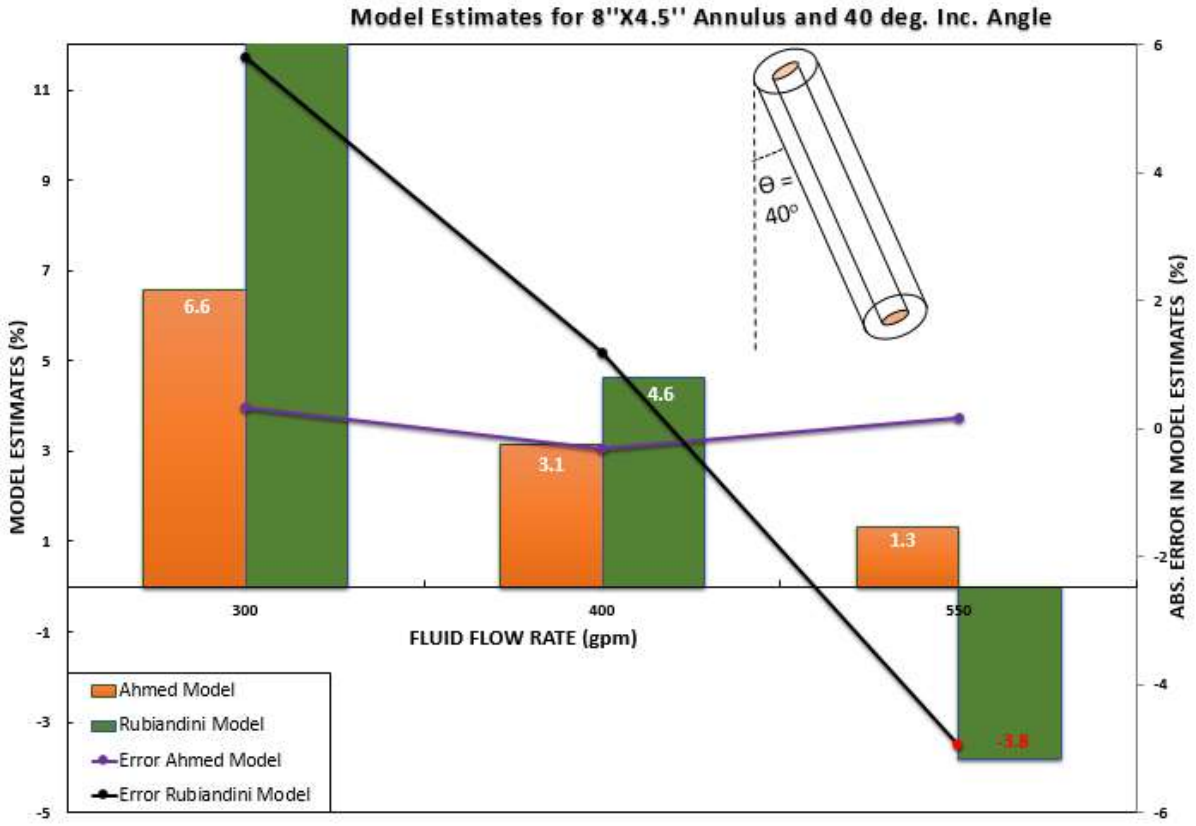

Figure 3: Ahmed's and Rubiandini's model comparison for 8" x 4.5" and 40^o inc. angle

For the smallest annulus size and lowest inclination angle, Ahmed's model outperformed Rubiandini's model (Fig. 3). The combined chart shown in Fig. 3 presents model estimates for the three different flow rates used along with absolute eror in each estimation. Ahmed's model produces estimates with approx. 0 absolute error while Rudiandini's model provides estimates with absolute error ranging between 1 and 6. Close examination of the diagram reveals further that Rubiandini's model does not predict formation of any cuttings bed for the

test where highest flow rate and RPM were used. This leads to estimation of negative cuttings concentration by the model (marked by red text in Fig. 3).

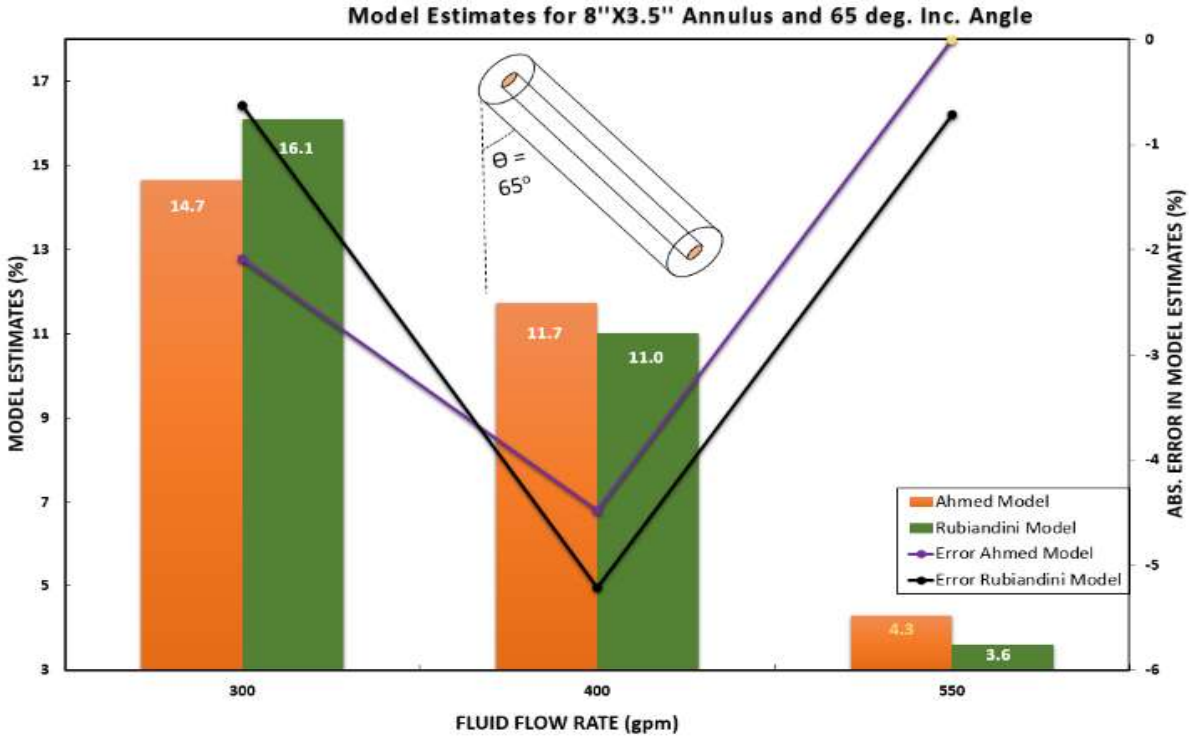

Figure 4: Ahmed's and Rubiandini's model comparison for 8" x 3.5" and 65^o inc. angle

For the medium annulus size and deviated hole condition used in the experiment, the two models are found quite comparable to each other in estimating cuttings concentration (Fig. 4). Ahmed's model produced an estimate with approx.0 absolute error for the highest flow rate used in the test. Both models under-predict the observed cuttings concentration for the three flow rates used in this test condition (represented by negative absolute error). To be noted that Rubiandini's model is not affected by variation of inclination angle above 45^o. Given that test fluid density was kept constant, it is only RPM affecting the critical mud velocity calculated by Rubiandini's model. Close observation reveals that Rubiandini's model provides good estimates at higher RPM values coupled with high or low flow rates compared to the low RPM value coupled with medium flow rate under the given test condition. To be noted that both the models underpredicted C_c for the three flow rates.

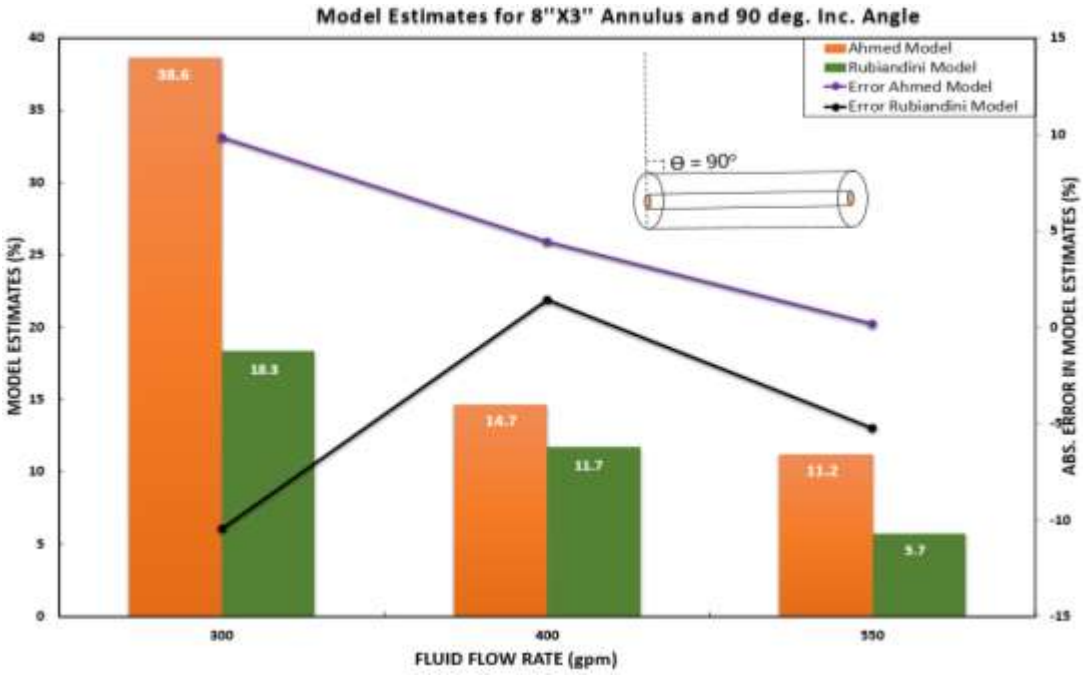

Figure 5: Ahmed's and Rubiandini's model comparison for 8" x 3" and 90^o inc. angle

For the largest annulus size, a horizontal well condition was used in the experiment conducted by Ahmed et al. None of the models can provide good estimates for low fluid flow rate. With increase in flow rate, the estimates provided by the two models improved (Fig. 5). While Ahmed's model over-predicted C_c for all the three flow rates, Rubiandini's model under-predicted C_c for low and high flow rates.

CONCLUSION & FURTHER RECOMMENDATIONS

The comparison is conducted using a limited set of data. Both models are emiprical. So both are highly influenced by the experimental conditions used for developing them. The constants used in Ahmed's model are experimentally determined and this model does not incorporate any correction factor.

While Ahmed's model was developed using dimensionless approach, Rubiandini's model was built on the concept of critical mud velocity. As long as the flow rate is at and above the critical value, no cuttings bed is assumed to form. Both these models consider drill pipe rotation. However, Ahmed's model is inapplicable to turbo-drilling condition and 0^o inclination angle.

Annulus size and inclination angle were found to influence the estimates provided by the two models. Ahmed's model provided very good estimates for the small annulus size used in the experiment. The two models provided comparable estimates for the two other test conditions- namely deviated well with medium annulus and horizontal well with large annulus.
It is recommended to test the two models against further field and laboratory data to evaluate the accuracy produced by them. Due to the complicacy involved in cuttings transport, it is a daunting task to develop analytical models taking all the different factors influencing cuttings transport. Hence finding out empirical model that can provide acceptable accuracy under different drilling and well conditions will be a fruitful work.

NOMENCLATURE

$A_o - A_4$	constants used in Ahmed model, dimensionless
A_c	ratio of cuttings bed to annulus cross-sectional area, dimensionless
C_c	cuttings concentration, dimensionless
C_{cut}	cuttings concentration at critical mud velocity, %
C_d	delivery concentration, dimensionless
C_{inc}	correction factor for inclination, dimensionless
C_{mud}	correction factor for mud weight, dimensionless
C_{RPM}	correction factor for drillstring rotation, dimensionless
d	drillpipe outer diameter, m
D	annulus internal diameter, m
n	fluid behavior index
K	fluid consistency index ($Pa.s^n$)
Q_{pump}	pump flow rate, m^3/s
Q_{crit}	critical flow rate, m^3/s
Re	Reynolds number, dimensionless
RPM	drillstring rotation
ROP	rate of penetration, m/min
S_t	Strouhal number
V_{cut}	cuttings velocity or cuttings transport velocity, m/s
v_{crit}	mud critical velocity, m/s
v_{sv}	Moore's cuttings slip velocity for vertical wells, m/s
γ_m	mud weight, kg/m^3
Θ	inclination angle, radians
μ_a	apparent viscosity, Pas
$\emptyset$	porosity, dimensionless

REFERENCES

Ahamed, R., Sagheer, M., & Takach, N. (2010). Experimental studies on the effect of mechanical cleaning devices on annular cuttings concentration and application for optimizing ERD systems. SPE, 134269.

Azar, J. J., & Samuel, G. R. (2007). Drilling engineering: PennWell Books.

Fjaer, E., Horsrud, P., Raaen, A., Risnes, R., & Holt, R. (1992). Petroleum related rock mechanics (Vol. 33): Elsevier.

Iyoho, A. (1980). Drilling-Cutting Transport by Non-Newtonian Drilling Fluids Through Indined, Eccentric Annuli, The Universihy of Tulsa. Ph. D. Thesis.

Larsen, T., Pilehvari, A., & Azar, J. (1997). Development of a new cuttings-transport model for high-angle wellbores including horizontal wells. SPE Drilling & Completion, 12(02), 129-136.

Mitchell, R. F., Lake, L. W., & Engineers, U. S. o. P. (2006). Petroleum engineering handbook. Vol. 2. Drilling engineering (Vol. II): SPE.

Mohammadsalehi, M., & Malekzadeh, N. (2011). Optimization of hole cleaning and cutting removal in vertical, deviated and horizontal wells. Paper presented at the SPE Asia Pacific Oil and Gas Conference and Exhibition.

Peden, J., Ford, J., & Oyeneyin, M. (1990). Comprehensive experimental investigation of drilled cuttings transport in inclined wells including the effects of rotation and eccentricity. Paper presented at the European Petroleum Conference.

Ranjbar, R. (2010). Cuttings transport in inclined and horizontal wellbore. (MSc), University of Stavanger, Stavanger.

Rubiandini, R. (1999). Equation for estimating mud minimum rate for cuttings transport in an inclined-until-horizontal well. Paper presented at the SPE/IADC Middle East Drilling Technology Conference.
Sagheer, M. (2009). Study of Effect of Down-Hole Mechanical Cleaning Devices (MCDs) on Cuttings Transport. (MSc), The University of Tulsa.

Whittaker, A. (1985). Theory and applications of drilling fluid hydraulics: IHRDC Press,Boston, MA; None.

International Conference on Petroleum Engineering 2016 (ICPE-2016)
Bangladesh University of Engineering & Technology (BUET)
Dhaka-1000, Bangladesh

ICPE –2016-036

Drilling Challenges: A case study of Rashidpur field

Hasan Mahmud*[1], Shahriar Mahmud[2] , Evana Tinny[3]
Sylhet Gas Fields Limited, Bangladesh [1,3]
Petroleum and Mineral Resources Engineering Department, Bangladesh University of Engineering and Technology, Bangladesh[2]

ABSTRACT

The study focuses on the problems encountered during drilling of three recent wells in Rashidpur Gas Field. The field is located in the Northeast part of Bangladesh and was discovered by Shell in 1960.

Geologically, the field is in the south central part of the Surma basin and has asymmetrical anticline structure. The main reservoir sands of this field are Tipam, Boka Bil and Bhuban formations. Boka bil formation (1036-2710m) contains alternation of sandstone, siltstone and clay layers. A total of eleven wells have been drilled so far in this field since the discovery. During the drilling, several problems were encountered by thick shale sequence of this Boka bil formation.

Recently, three wells namely Rashidpur-9, 10 & 12 were drilled in this structure. From these, Rashidpur-10 Well was drilled to 3055 m (MD) in June 2016. Rashidpur-12 was spudded-in on July 09, 2016 and drilled to 3135 m directionally by august, 2016. The remaining Rashidpur- 09 well was drilled to 3308 m vertically in October 2016.

Rashidpur-10 well was planned to be drilled vertically. However due to poor control of wellbore path, the hole became directional with maximum 17.5 degree inclination. Besides, wellbore instability became a major concern during drilling operation. The main problem encountered during drilling these three wells were mud loss, caving, washout, damage of the rig's control system, wireline tool stuck, gas influx, foaming, bad cement job, frequent tight spots and over pull during wiper trip etc.

This study analyses the challenges that were encountered during the drilling of these three wells to find out the root causes and possible preventive/remedial actions have been suggested as lessons learned for future drilling campaigns.

Key words: **Drilling Challenges, hole deviation, wellbore instability, possible preventive.**

INTRODUCTION

The Rashidpur gas field is one of the onshore gas fields in Bangladesh. The field is located in the Surma Basin, which is a Miocene gas producing province in the North Eastern part of Bangladesh about 84 miles

*Assistant Manager, Rashidpur Gas Field, Sreemongal, Sylhet.
Email: hmplus02@gmail.com

north east of Dhaka and 44 miles southeast from Sylhet. It lies between Shillong Plateau in the North and the Tripura High in the South. The field was discovered by Pakistan Shell Oil Company (PSOC) with well RP-1 which was drilled in 1960, and is now operated by Sylhet Gas Fields Limited (SGFL).

Currently there are seven wells penetrating the Rashidpur structure all together. RP-2 was drilled subsequently in 1961 to evaluate and deepen the RP-1 well. RP-3 andRP-4 wells were drilled in 1989 development drilling campaign and were completed as producers. RP-1 and RP-2 wells were also worked-over and completed as producers during these campaign period. RP-5, RP-6 and RP-7 wells were drilled during another development drilling campaign in 1999.

BAPEX acquired 325 square kilometer 3D Seismic data over Rashidpur Structure during 2010-'11.With the new prospects revealed by 3D seismic, proposal has been put forward to drill more development wells in Rashidpur Gas Field. Based on the 3D seismic result, decision came to drill three more wells namely RP-9, RP-10 & RP-12 in this structure. These wells drilled as an Exploratory/Appraisal cum development well according to the development program. Drilling main target for Rashidpur Well #9 is to appraise the Upper Marine Shale (UMS) Sand prospect.RP-10 was designed as an exploratory well targeting the Lower Gas Sand (LGS) NW prospect. RP-12 was also designed as exploratory well targeting the PGS NE-S, MGS NE-S and the LGS mid-N prospect.[1]

Rashidpur 10 spudded on 17 May 2016 targeting to drill vertically up to 2900 m .Tight spot, caving, hole deviation, failed to pass logging tools, top drive problem etc were the main challenges on the way of smooth well drilling. Drilling of RP-12 well commenced on July09, 2016 to reach the target depth of 3100 m TVD directionally. Problems encounters to drill the well were mud loss, random tight spot, pack-off annulus etc.Rashidpur-9 well was spudded on august 10, 2016 to drill up to 3500 m vertically. During the drilling, tight spot & caving were observed but not significant as earlier two well. Gas influx, foaming & wireline tool stuck were also observed during drilling.[2]

DRILLING OPERATION

The architecture of these three wells are 30" extended hole guide × 20" surface casing × 13-3/8" Conductor casing ×9-5/8" Intermediate casing × 7" liner. Well construction of RP-10 is shown in figure-1.

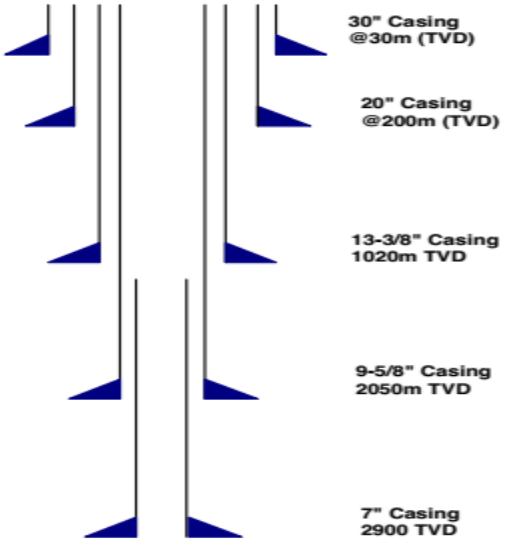

Figure-1: proposed well construction of RP-10.

Rashidpur-10: Rashidpur-10 well is an appraisal well that was drilled in June, 2016. The operational sequence of this well is as follows:

1. Preparation of the site, drilling water well to 30 m , installing 30" casing.
2. Drilled 30-201 m with Low Gel Polymer Mud, run 20" casing, cementing , WOC.
3. Rig Up and nipple up Wellhead, BOP, Ran 17.5" Bit & BHA tagged cement top at 198 m MW 1.08 SG. Drilled out cement,and 3 m of new formation to 204 m. Performed FIT and EMW 1.38SG,andpressure tested casing. Converted mud to Low gel KCL polymer mud on the flywhiledrillingandcontinueddrilling from 204 m to 1206 m (Interval TD) with final MW 1.09 SG. Carried out Wiper trip without any complications. 9 m3 Hi-Viscous pill was pumped andcirculated for better hole cleaning. Performed Wirelinelogging. Ran 13-3/8" Casing, Cementing, WOC.
4. N/Down BOP 20-3/4". N/Up13 5/8" BOP, Ran 12.25" Bit & BHA , tagged cement top at 1189 m, Drilled out cementand new formation to 1209 m. Performed FIT , EMW 1.43 SG, and pressuretested casing. Converted mud to KCL polymer + GEM CP +CLAYSEAL PLUS mud on the fly while drillingand continued drilling from 1209 m to 1504 m (Interval TD) with MW 1.15 SG. Wiper trip was carried out notabe tight pulls. POOH BHA, inspect BHA, L/Out bottom(above motor) stabilizer- 12 ¼".
5. Drilling from 1504 m to 2053 m (Interval TD) with final MW 1.15 SG. Circulated for hole clean until shakers were clean, Wiper trip was carried out with tight pulls noted .Maximum 15 ton over pull was observed. Tight spots cleared by reaming.Hgh Vis pill was circulatedfor hole cleaning and final circulation carriedout until shakers were clean. POOH with no tight pulls. Performed Wire line logging, Observed held up atdepth 1650m, tool encountered washout greater than 22" (caliper arms completely extended).Run #1 was attempted a second time with centralizers attached, but faced thesame held up at 1650 m. Pull Outfor this run was also smooth with no tight pulls. Once the second run tool configuration was on the surfacesevere weather lightning struck the rig causing electrical damage to the top drive system which resulted 5days without being able to circulate the entire mud system.
6. RIH to bottom, while circulating at bottomcaving's were observed and increased MW from 1.16 SG to 1.18 SG, still caving's were observed furthincreased the MW from 1.18 SG to 1.20 SG to 1.26 SG to 1.32 SG to1.36 SG andalso increased inhibition in mud to stabilize the hole. Run wireline tool but again held up at 1650. Wireline logging from 1200-1650 m. RIH with MWD tool, an inclination of 17.83 degrees was found. The kick off point was 1650 m. Lowered 9 5/8"casing to bottom, cementing, WOC.
7. Ran 8.5" Bit & BHA to bottom and drilled 3 m of new formation to 2053 m. Reduced MWfrom 1.36 SG to1.18 SG. Performed FIT, EMW 1.61 SG,and pressure tested casing. Continued drilling from 2053m to 3046 m, in this interval two wiper trips and one short trip was carried out without any complications . POOH for coring and corewas taken from depth 3046m to 3055m. Performed Wirelinelogging . RIH liner keeping the shoe at 3054.43m and 7" liner cementation job was performed [2].

Rashidpur-12: Rashidpur-12 well was drilled directionally to 3200 m MD (TVD 3164 m) in August, 2016. The operational sequence of this well is as follows:

1. Preparation of the site, drilling water well to 30 m , installing 30" casing.
2. Drilled 26 " hole form 30 to 202 m with Low Gel Polymer Mud, circulation, wiper trip, run 20 " casing, cementing , WOC.
3. Nipple up Wellhead, BOP, Ran 17.5" Bit & BHA tagged cement top at 198 m, drilled out cement, shoe, drilled 202-207 m, perform FIT, Drilled 207-737 m, monitor mud loss(12 m3/hr at 723 m. From 722 m to 738 m added BARACARB-5,STEELSEAL-400,BAROFIBRE, and Bentonite as background LCM to the active system to help stop thelosses but it was not successful and observed 20 m3 downhole losses. Prepared 10 m3 LCM pill and Spotted at 738 m. Wait on pill soaking 5.5 hrs. Afterpill soaking observed 1.2 bbl. loss in trip tank in 5.5 hrs. After pill soaking circulated at casing shoe andObserved mud tank levels were stable. Cut back mud weight to 1.08 SG.
4. Drilled 737-1182m . LCM was added in the mud during drilling the well. Performed wiper trip two times & obtain overpull up to max. 10 t,wireline logging, Circulate and cleaned the well with high vispill . Ran 13-3/8" casing, cementing unit failure, Pumped 569bbl lead slurry from total volume 803,4 bbl. Tail cement can't pumped, WOC, conduct CCL/GR log, top cement at 593m, performed top job of cement through the annulus.
5. Set BOP for 12-1/4 " drilling, drill out cement, shoe and drilled to 1185m by12-1/4 " directional BHA, performed FIT. Drilled 1187-2248 m , Circulate hole, got over pull 10-15t when wiper trip and pull out , treat the mud with lubricant, meanwhile weight up the MW to max.1.26sg, ran wireline log, run 9-5/8 " casing to 2245m, cementing, WOC.
6. Completed BOP testing, Ran in with 8.5" Bit and BHA, tagged cement top at 2230 m. Drilled through cement and fresh formation to 2253 m. Conducted FIT to EMW of 1.81 SG. Ran CBL, Resumed drilling by directional BHA to 2672m, random overpull& tight spot observed during wiper trip, Observed tight spot at 2556m (15ton over pull). Attemptedto ream, unable to circulate/rotate, drill string had packed off, SPP increased to 2000psi. Ran in one stand to 2592m establishcirculation, ream stand pumped Hi vis sweep ($5m^3$).Reamed stand, circulate with both the pumps. Ream out of hole to 2508m, working BHA over tight spots at 2552m (10ton) and 2535m (15ton) .Continuedrilling 8.5" section to 3191 m MD. Wiper trip & faced overpull, coring from 3191-3200, cleaned the hole, ran wireline log, cement plug 2200-2300m , performed DST, not susscessful,Nipple down BOP and Niple Up X-mas tree, rig down. [2]

Rashidpur-09: Rashidpur-9 well is appraisal cum development well that was started to be drilled on August 10, 2016 and completed on November 14, 2016. The operational sequence of this well is as follows:

1. Preparation of the site, drilling water well to 30 m , installing 30" casing.

2. Driling 20-206 m by 26" bit with bentonite spud mud, wiper trip, circulationg hole, run 20" casing, cementing , WOC.
3. RIH 17-1/2 " BHA, pressure test BOP's , Drill out cement, casing shoe, drill 206-209, performed FIT, drilled 209-1204 m with Low Gel KCl Polymer mud, run wireline log, run 13-3/8 " casing, cementing. WOC.
4. Set BOP for 12-½ " hole, RIH 12-1/2 " BHA, pressure test BOP's , Drill out cement, casing shoe, drill 1204-1207 m, performed FIT, drilled 1207-2508 m with Low Gel KCl Polymer mud. While drilling observed caving. Performed wifer trip three times, observe cavings, drag,overpull up to maximum 25 t. To overcome cavings problem, the mud weight was increased gradually from 1.10 to1.36 SG. Run wireline log, RIH 9-5/8 casing, cementing, WOC.
5. N/D BOP, N/U BOP & flow line, conduct P/T of BOP rams, Drill out cement, float collars, shoe, drill 2508-2512 m,perform FIT , run CBL, Drill 2512-2945 m with KCL-Polymer plus-borehid mud. Gradually increase MW to 1.26. Drill 2945-3300 m by rotary BHA to drill through possible high pressure zone. During wiper trip, several tight spot, dragwith max. 20 t was faced. During circulation max. 8.85 % gas show was observed. Caving also observed while circulating. Gradually increase MW. To 1.45 SG. Core was taken from 3300-3309m,wiper trip, clean the hole.
6. Ran wireline log. During Ist run pull out, logging cable was stuck at 3041 m. cut the cable, perform fishing. Wiper trip, meet tight spots, observe caving, drag at 3306, reaming, add LCM, spot high viscus sweep.
7. Wireline logging, tool held-up at many depth, observed many tight points, wiper trip, run 7" liner, cementing, WOC.
8. RIH DST/TCP string, drop the bar for perforation 3225-3245 m, no indication of perforation, attemped to fish the bar, not successful, RIH bailer, bailer could not pass 3150 m depth, then two attempt to run bailer but can pass to maximum 3179 m.POOH DST/TCP string. Gun fired 100%&perforation was confirmed at 3225-3245 m by CCL/GR correlation. RIH DST again, result is not satisfactory. Set packer at 3200, 2360 & 1450 m, sqeezecement , Made perforation at 1316.5-1327 m. Perform successful DST. RIH completion string, set production packer at 1280 m. Nipple down BOP and Niple Up X-mas tree. Ran production test & complete the well, rig down. [2]

CHALLENGES

Tight spot: While drilling RP-10 about 20 tight spots were observed with in 1400 m-2053m. due to shale swelling and poor hole cleaning. The shale absorbed water from mud, expanded and squeezed during setting process of hole. Poor inhibition could not build adequate filter cake and prevent shale swelling. In RP-12 and RP-09 tight spots were not observed as frequent as RP-12. But in RP-09 low concentration of filtration control agent in gel polymer caused high fluid loss and resulted in thick filter cake thus was spoiling the hole conditions. Figure -2 shows two 18MT & 17MT overpull while pull out in 1725m & 1690m depth respectively in Real time log of RP-10 well drilling. [3,4,5,6]

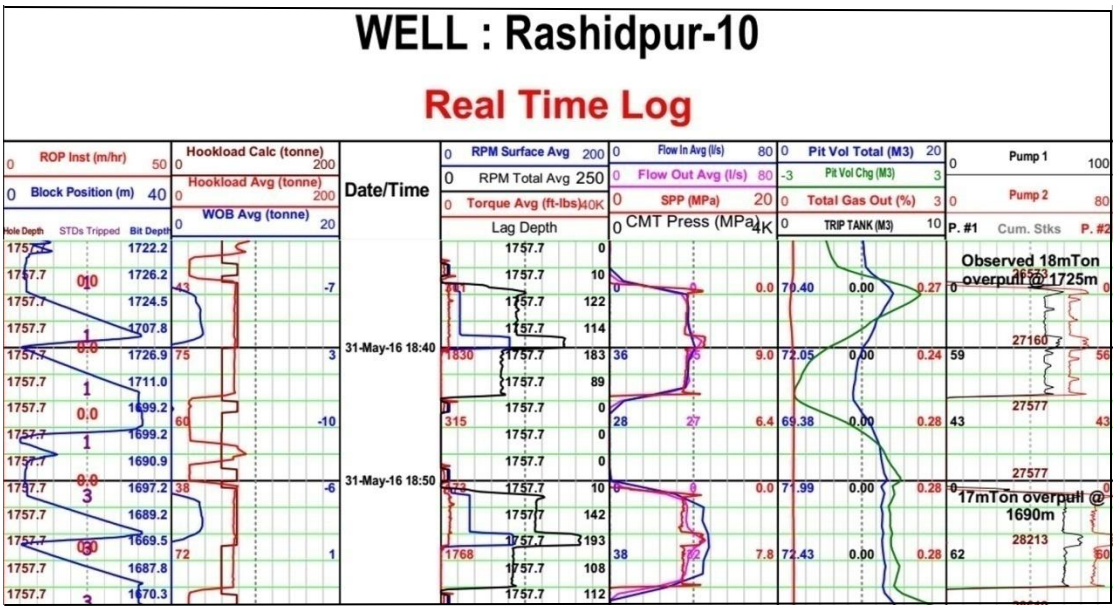

Figure 2: Tight spot indication in Real time log

Actions: Mud weight increased, hi-vis pill pumped and maintained inhibitors concentration with clayseal plus mud system to prevent tight spots. Treated with higher dosage of filtration control agent in RP-09 hole improvement.[5]

Wireline logging operation problem & stuck: In RP-10 wellbore exposed long time to formation because of bad weather promoted to shale swelling and filled the hole. So, wireline logging tools could not pass after 1650m. But in RP-09 while running logging tool excessive mud weight created differential pressure over logging cable and got stuck. As failure to unlatch the tool, fishing assembly was done.

Actions: Wiper tripped with reaming up and down, pumped hi-vis pill to make the hole clean and then logging done in RP-10.[3,5]

Cavings: The soft shale section penetrated by the borehole of well and resulted cavings in both RP-10 and RP-09. About 20-30% of cavings was laminar type form.

Figure 3: Sample of cavings.

Actions: Mud weight and mud inhibition increased to stabilize the hole. [3,5,6]

Washout: Washout problem noticed only in RP-10 as a result of cavings. The hole enlargement at a depth 1650m which was greater than 22", also caused an inclination of 17.83 degrees.

Actions: Mud weight and mud inhibition increased.

Mud loss: Due to unconsolidated sand formation mud loss up to 12m3 observed while drilling up to 1182 m in RP-12.

Actions: Treated mud with Lost Circulation Material (LCM), reduced mud weight.

Hole deviation: RP-10 well was planned to be drilled vertically. But unfortunately, the hole became directional with maximum 17.5 degree inclination in between 1550-2053 m drilling. While drilling through the shale zone, frequent tight spot was encountered & thus the BHA was changed & lay out bottom stabilizer after drilling 1550m. This might be the main reason for this deviation. Figure-4 shows that 9 5/8 casing was set with a maximum 17.83 degree inclination in RP-10 well.

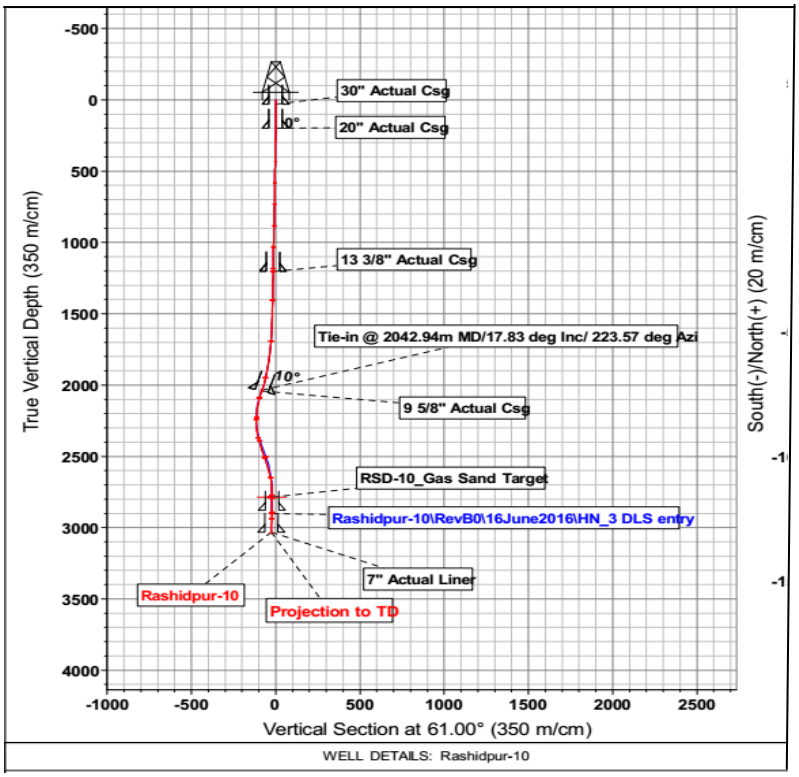

Figure-4: MWD survey of RP-10

Actions: MWD tool was used to make the direction back to the horizontal.

Pack-off of annulus: Inadequate inhibitors concentration at a depth 2672m resulted the pack-off of annulus.

Actions: Fluid system treated with GEM-CP for clay inhibition and TORQ-TRIM for lubricity. MW increased, high vis pill used to hole clean, Baro-Trol was also added to aid wellbore stability.[4,7]

Gas influx: In RP-09 due to presence of nearby gas zone from 3150 to 3242 m gas influx observed.

Actions: Ran the degasser during drilling and circulation, increased mud density.

Foaming on the shakers: Bicarbonate contamination from formation while drilling RP-09 resulted in foaming on the shale shakers.

Actions: Added defoamer to de - foam system[5]

DISCUSSION

The lithology of Rashidpur-09, 10 & 12 Wells were more or less same but challenges were different. Proper mud system is very important to keep the wellbore stable. The predicted mud weight of three wells were same (1.04 – 1.09) SG. But the range of mud weight needed to use in RP 09 was larger than other two wells.(RP 10 1.03 – 1.14sg ; RP 12 1.04 – 1.20sg ; RP 09 1.03 – 1.45sg.) But the tight spot and cavings problems in RP 09 were overcome from the lessons of RP 10 & RP12. Adequate monitoring, actions and decisions ended these wells without any big hazard.

RECOMMANDATION

From the above discussion following recommendations can be given :

- Using adequate mud system with proper mud weight and inhibition in swelling shales.
- High mud weight could be as harmful as low mud weight. Living with a manageable amount of cavings requires extra steps in hole cleaning and solids control.
- Qualty number of wiper trip even in controlled wellbore condition. But minimize reaming to reduce impact onhole surface.
- Proper selection of stabilizer in the BHA to contol hole deviation for horizontal well.
- Minimize period of hole exposoure to formation.
- If drilling stop for any equipmental problem or connection period and string stay in hole circulation must be continued to keep the string free.

REFERENCES

[1] BAPEX, .2012. Rashidpur 3D Interpretation Report. Prepared for Sylhet Gas Fields Limited

[2] GAZPROM, .2016 . Daily Drilling Reports of Rashidpur 10, 12 & 09 well. Prepared for Sylhet Gas Fields Limited.

[3] Halliburton Baroid Bangladesh, .2016. Final Well Recap of Rashidpur -10. Prepared for Sylhet Gas Fields Limited.

[4] Halliburton Baroid Bangladesh, .2016. Final Well Recap of Rashidpur -12. Prepared for Sylhet Gas Fields Limited.

[5] Halliburton Baroid Bangladesh, .2016. Final Well Recap of Rashidpur -09. Prepared for Sylhet Gas Fields Limited.

[6] K.K. Borah and S.K. Mishra, .2009. Deep drilling Challenges in Oil's Assam Field- a Case Study. SPE/IADC 125337.

[7] JerryTobing and Erwindo Tanjung, .2013. Drilling Challenge of Unstable Hole Condition in kilo Field: A Case Study in Southeast Asia. SPE 165338.

International Conference on Petroleum Engineering 2016 (ICPE-2016)
Bangladesh University of Engineering & Technology (BUET)
Dhaka-1000, Bangladesh

ICPE (2016-044)

A Review of Mud Loss While Drilling through Naturally Fractured Reservoirs

Faysal Ahammad[1*], Shahriar Mahmud[1]
[1]Department of Petroleum and Mineral Resources Engineering, Bangladesh University of Engineering and Technology, Dhaka, Bangladesh

ABSTRACT

Drilling through a reservoir with pre-existed fractures sometimes called as naturally fractured reservoir presents many complex challenges. The most common of them is the loss of drilling mud through those fractures which is generally known as lost circulation. As drilling fluid contributes on an average 10% of the total drilling cost, it is of utmost importance to comprehend this phenomenon better and to find an efficient way to minimize this loss. Apart from the financial implications the Lost Circulation phenomenon can also cause subsequent Well Kick, damaging Reservoir property damage etc. With an aim to reducing or if possible ceasing that fluid loss to make the drilling operation more cost-effective, many researchers have tried to investigate lost circulation through experimental observations and numerical modeling. But very few of those work made an effort to model the drilling fluid flow in natural fractures. Pioneering work on that issue considered the drilling mud as Newtonian fluid. Later, more advance models were developed by Scientists and Engineers regarding the fluid as Non-Newtonian.
This paper gives a summary of those various models on fluid flow in fractures to grasp the underlying mechanism of lost circulation better and to determine the factors which intrigues that phenomenon. The results described in this paper would provide better understanding and enable a drilling engineer to initiate a treatment to mitigate lost circulation instantaneously.

Keywords: Naturally fractured reservoirs, lost circulation, Newtonian and Non-Newtonian fluid

* Corresponding Author address
Email: faysalbd@gmail.com

INTRODUCTION

Naturally fractured formations are common around the world (Reiss, 1980; Van Golf-Racht, 1982; Nelson, 1985). The fracture system (Figure 1) within the formation is a complex matrix of inter-connecting and non-connecting fractures (Jones et al., 1988). The area of an individual fracture plane can be varied from a few square inches to several hundred square feet (Parker, 1942; Kelly &Clinton, 1960; Hodgson, 1961). Moreover, a wide range in the spacing of the fractures can be found (Kelly &Clinton, 1960; Parker, 1942). However, fracture spacing of several feet are common (Asfari and Witherspoon, 1973). These fractures are not uniform with parallel walls, but are two dimensional complex networks of variable aperture (Tsang, 1984; Brown and Scholz, 1985; Wang and Narasimhan, 1985; Brown and Kranz, 1986; Schrauf and Evans, 1986; Pyrak Nolte et al., 1988; Morrow et al., 1989). At much lower pressure gradient, viscous and pressure forces become important in fracture flow than in flow through rock matrix. And pressure gradients vary from tens of psi/ft to a fraction of 1 psi/ft far from the wellbore into the formation (Rossen and Kumar, 1992).

Presence of fractures (Figure 1) can provide adequate productivity to make a marginally economic reservoir into a commercially productive one. However, while presence of natural fractures is a favorable condition for a reservoir to be highly productive, it can also be a potential source of disaster during drilling operation. In particular, fracture can increase the fluid transmitting capability of a reservoir significantly; therefore, any abrupt change in hydrostatic pressure in the wellbore due to the flow of drilling fluid in fractures can give rise to critical well-control issues. If during drilling, a high pressure fractured zone is encountered, formation fluid will flow into the wellbore which may result in a well control scenario. In contrast, if a low pressure fractured zone is encountered; costly drilling fluid will rapidly flow into the fracture which will reduce the hydrostatic pressure in the wellbore, therefore, posing a risk of sudden flow of formation fluid in the wellbore from the formation above that may ended in a blowout.

During overbalance drilling partial or complete loss of drilling fluid into the fractures is called lost circulation. It is one of the major events that increase Non Productive Time (NPT) in drilling industry. In addition to increasing overall cost of drilling fluid, lost circulation may result in some negative consequences such as stuck pipe, reduced drilling rate, induced kick and the loss of entire well or wellbore (Feng et al. 2016). According to the published data, in Gulf of Mexico 12% of the NPT is caused by lost circulation (Wang et al. 2007), and 10% to 20% of the drilling cost of high-temperature and high-pressure wells is related to lost circulation (Cook et al. 2011).There are various reasons that can cause lost circulation. Complete mud losses occur in heavily fractured formation while partial losses with mud gains occur when a fracture of limited extension is encountered if the pumps are shut down and the circulation is stopped. In non-fractured shale formation, lost circulation has been attributed to the borehole wall deformation (Gill 1989).

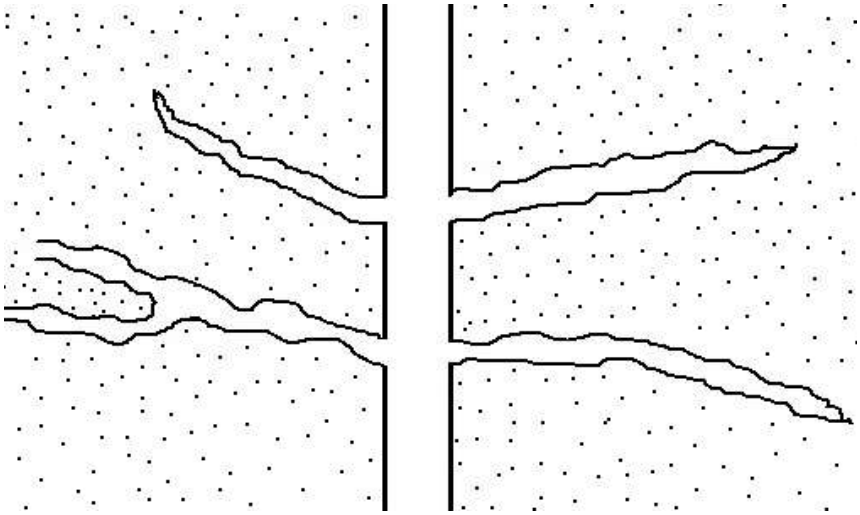

Figure 1: Natural Fractures

As loss of drilling mud i.e. lost circulation is a common event in overbalanced drilling, therefore, it is very crucial to know about the behavior and flow pattern of the drilling mud inside fracture to facilitate a proper treatment scheme instantaneously. Modeling drilling fluid flow through naturally occurred fracture has been a topic of research since the 1990's (e.g. Liétard et al. 1996, Sanfillippo et al. 1997; Maglione et al. 1997; Lavrov and Tronvoll 2004; Majidi et al. 2008; Lavrov 2013 etc.). The purpose of this article is to provide a summary of the existing knowledge on drilling fluid flow in fractured media, and to identify the areas of further research to improve the comprehension.

In the following sections of this paper, existing experimental and theoretical knowledge on fluid flow in fractures is reviewed in section 2. And directions to further research are discussed in section 3.

FLUID FLOW THROUGH FRACTURES

Drilling mud is continuously circulated into the wellbore to transport cuttings on the surface, cooling the bit and balance between hydrostatic pressure in the wellbore and formation pressure. The loss of drilling mud is a common scenario while drilling through naturally fractured formations. Apart from that, drilling mud also got lost into the formation through pores and induced fractures. The distinction between different types of fluid loss can be made by observing the mud losses in the mud tank. For natural fractures, there is a rapid initial loss of drilling mud which declines with time; whereas for mud loss through pores, the loss rate increases gradually as the flow of drilling mud increases (Dyke et al. 1995). During overbalance drilling, when a fracture is encountered, drilling mud will flow naturally into the fracture due to existing pressure gradient between the wellbore and the fracture.

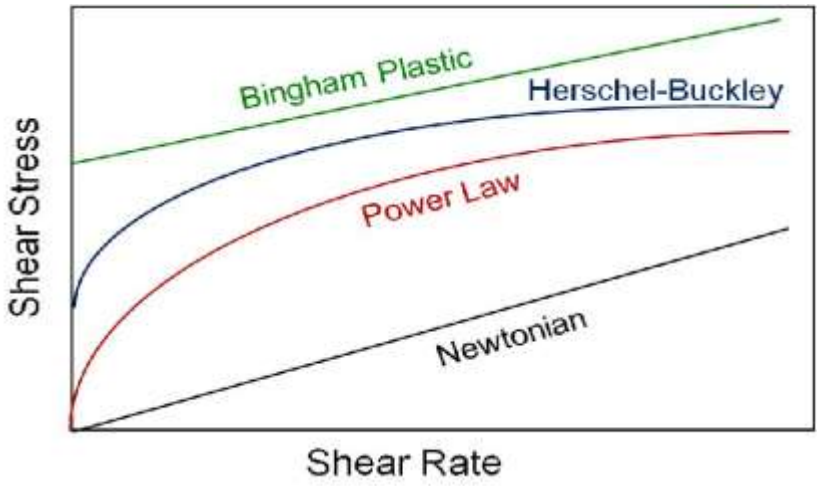

Figure 2: Newtonian and Non-Newtonian Rheological Models

Till now, many authors have tried to understand the behavior of drilling mud inside fractures characterizing the mud as Newtonian and Non-newtonian fluid (Figure 2). The summary of those works given below:

2.1. Newtonian Fluid:

Newtonian fluid is any fluid that follows Newton's law of viscosity which states that applied stresses is proportional to shear rate (Figure 2):

$$\tau = \mu\gamma \qquad (1)$$

Where τ is the shear stress, μ is the viscosity and γ is the shear rate

The flow of Newtonian fluid in fractures is well researched. There have been numerous works done on Newtonian fluid flow inside fractures. Initially, fluid flow in fractures was understood using parallel plate model (Huitt, 1955; Snow, 1965). Considering this model, Wtherspoon et al. (1980) developed the classical cubic law equation for steady state isothermal, laminar flow between two smooth walled parallel plates:

$$Q = 5.11 \times 10^{6}\left[\frac{W\Delta Pb^{3}}{L\mu}\right] \qquad (2)$$

Where Q = flow rate (bbl/day), W = Width of the fracture face (ft), ΔP = Pressure differential (psi), b = fracture aperture (in), L = length of fracture (ft), μ = fuid viscosity (cp)

Later, Jones et al. (1988) applied Bernoulli's equation for flow in pipes to natural fractures and build an equation for single phase laminar and turbulent flow calculations. The equation is:

$$Q = 5.06 \times 10^4 W[\frac{\Delta P b^3}{fL\rho}]^{0.5} \quad (3)$$

Where f = friction factor, ρ = fluid density lb/cu ft

Assuming laminar flow of Newtonian fluid flowing radially into highly conductive circular fractures, Sanfillippo et al. (1997) developed a model to estimate width of the fracture and to describe how drilling fluids fill natural fractures during drilling operation. The model is based on radial diffusivity equation:

$$\frac{\partial^2 p}{\partial r^2} + \frac{1}{r}\frac{\partial p}{\partial r} = \frac{\emptyset_{frac}\,\mu_{mud}\,C_{mud}}{k_{frac}}\frac{\partial p}{\partial t} \quad (4)$$

Poiseuille's law is valid for this model. Therefore, the fracture width (w) is linked with fracture permeability (k) by the following equation:

$$k = \frac{w^2}{12} \quad (5)$$

Solving radial diffusivity equation assuming constant terminal pressure boundary condition and substituting equation (5) into it yields:

$$a\frac{\frac{w^2 t}{12\mu_{mud}\,\emptyset_{frac}\,C_{mud}\,r_w^2}}{\ln\frac{w^2 t}{12\mu_{mud}\,\emptyset_{frac}\,C_{mud}\,r_w^2}} - \frac{V(t)}{2\pi\emptyset_{frac}\,C_{mud}\,r_w^2 w\Delta P} = 0 \quad (6)$$

Where a is a constant equal to 2.01, ΔP is the overbalance pressure, $w$is the width of the fracture, t is the time, μ_{mud} is the mud Newtonian viscosity,$\emptyset_{frac}$ is the fractureporosity, C_{mud} is the mud compressibility, $r_w$is the wellbore radius, and V(t) is the cumulative volume of mud lost in the fracture at time t.

Apart from theoretical works, many authors had carried out experiments (Jones et al., 1988) and simulation to comprehend the flow Newtonian fluid inside fractures (Asfari and Witherspoon, 1973; Douglas et al., 1987; Yang et al., 1989; Sarkar et al., 2002; Cardenas et al., 2007; Koyama et al., 2008)

2.2. Bingham Plastic Fluid:

Bingham plastic fluid is defined as the fluid that follows the Bingham plastic model (**Figure 2**) which can be expressed mathematically by the following equation:

$$\tau = \tau_y + \mu_p \gamma \quad (7)$$

Where τ = shear stress, τ_y = yield stress, μ_p = plastic viscosity

Liétard et al. (1996, 1999) developed a model based on Darcy's law to describe the flow of Bingham plastic fluid inside fractures. They assumed the flow regime is laminar and drilling mud is flowing radially into a smooth walled fracture of constant aperture for a constant drilling overbalance pressure. The flow behavior of drilling fluid inside fractures can be known by solving the following equation describing local pressure drop due to laminar flow of Bingham plastic fluid in a slot of constant width (w):

$$\frac{dp}{dr} = 12\mu_p \frac{V(r,t)}{w^2} + \frac{3\tau_y}{w} \quad (8)$$

Where p is pressure, μ_p is plastic viscosity τ_y is the yield stress of the drilling fluid, and V(r, t) is fluid velocity for radial flow, equal to:

$$V(r,t) = \frac{1}{2\pi r w}\frac{dV_m}{dt} \quad (9)$$

Then, the amount of mud loss V_m can be evaluated by integrating equation (9):

$$V_m(t) = \pi w\left[r_i^2(t) - r_w^2\right] \quad (10)$$

Where r_i is the invasion radius at time t

Substituting equation (9) and (10) into equation (8) yields:

$$\frac{dt_d}{dr_d} = \frac{4r_d \ln r_d}{1 - \alpha(r_d - 1)} \quad (11)$$

Where dimensionless radius, $r_d = \frac{r(t)}{r_w}$; dimensionless time, $t_d = \frac{w^2}{r_w^2}\frac{\Delta P}{3\mu_p}t$ and mud invasion factor, $\alpha = \frac{3r_w}{w}\frac{\tau_y}{\Delta P}$ and ΔP is the constant overbalance pressure.

Several authors worked on Liétard model to solve equation (11) analytically and estimate fracture width without using type curves. Firstly, Sawaryn (2001) found an analytical equation (11):

$$t_d = \frac{4r_{dmax}\ \ln(r_{dmax})}{\alpha}\left[\{\ln\left(\frac{r_{dmax}-1}{r_{dmax}-r_d}\right)-\frac{r_d-1}{r_{dmax}}\}\right. \\ +\frac{4r_{dmax}}{\alpha}\sum_{n=2}^{\infty}\frac{1}{n}\left(\frac{1}{r_{dmax}}\right)^n\{\ln(r_{dmax})+\frac{1}{n}\}-r_d^n\{\ln\left(\frac{r_{dmax}}{r_d}\right) \\ \left.+\frac{1}{n}\}\right] \tag{12}$$

Later, Civan& Rasmussen (2002) also provided an analytical solution of equation (11):

$$t_d = 4r_{dmax}\ (r_{dmax}-1)\left[-\ln r_d\{\frac{r_d}{r_{dmax}}+\ln(1-\frac{r_d}{r_{dmax}})\}+\sum_{n=2}^{\infty}\frac{1}{n^2}\{\left(\frac{1}{r_{dmax}}\right)^n \right. \\ \left.-\left(\frac{r_d}{r_{dmax}}\right)^n\}\right] \tag{13}$$

Further improvement was done by Huang et al. (2011) who eradicated the necessity of type curve matching by deriving a cubic equation to determine fracture width (w) using known values of wellbore radius (r_w), overpressure ratio ($\frac{\Delta P}{\tau_y}$), and the maximum mud-loss volume (v_{max}):

$$\text{Fracture width, } w = \left[\frac{\frac{9v_{max}}{\pi}}{\left(\frac{\Delta P}{\tau_y}\right)^2}\right]^{\frac{1}{3}} \tag{14}$$

In contrast to the model proposed by Lietard et al. (1996, 1999) model, Maglione et al. (1997, 2000) studied the flow of Bingham plastic fluid inside fractures based on radial diffusivity equation. Assuming drilling mud behaves as Bingham plastic fluid and flowing radially into the fracture of constant width; thus solving the radial diffusivity equation under steady state conditions the bottomhole drilling overpressure ΔP can be expressed as:

$$\Delta P(t) = \frac{6Q_{loss}\,\mu_p}{\pi w^3}\ln\frac{\left(\frac{V(t)}{\pi w^2}+r_w^2\right)^{\frac{1}{2}}}{r_w^2} \tag{15}$$

Where Q_{loss} represents mud loss rate as recorded by the flowmeter, r_w is the wellbore radius, μ_p is the plastic viscosity of the drilling mud and $V(t)$ is the cumulative mud loss into the fracture at any time t.

In addition, Amadei & Savage (2001) derived a time dependent solution for Bingham plastic fluid flowing into the fracture with an empirical correction for fracture roughness. Mitsoulis & Huilgol (2004)

numerically investigated the flow of Bingham plastic fluid inside fracture with abruptly changing aperture.

2.3. Power Law Fluid:

Power law fluid is the fluid that follows the power law model (**Figure 2**):

$$\tau = K\left|\frac{\partial V}{\partial Z}\right|^{n-1}\frac{\partial V}{\partial Z} \tag{16}$$

Where n is the flow behavior index, K is the consistency index and $\frac{\partial V}{\partial Z}$ is the shear rate

At n<1 the fluid shear thinning and at n>1 the fluid has the shear thickening behavior. This model is not applicable at low shear rates as viscosity would become infinite at $\frac{\partial V}{\partial Z}$ = 0. In that situation it is more realistic to consider the fluid as carreau or cross fluid.

Assuming the drilling mud as power law fluid, Lavrov (2004, 2014) proposed a model to describe the flow drilling mud inside fractures. In their model, they assume that fracture is already filled with a fluid and defined fracture width as:

$$w = w_0 + \frac{P}{K_n} \tag{17}$$

Where, P is the local fluid pressure inside fracture; K_n is the proportionality co-efficient between fracture width increment and fluid pressure increment and w_0 is the fracture width when the fluid pressure inside the fracture is zero.
Considering stated assumptions, they developed a differential equation of drilling mud flowing into a deformable horizontal fracture of finite length:

$$\frac{\partial w}{\partial t} - \frac{n w^{\frac{2n+1}{n}}}{(2n+1)2^{\frac{n+1}{n}}K^{\frac{1}{n}}}\frac{1}{r}\frac{\partial P}{\partial r}\left(\frac{\partial P}{\partial r}\right)^{\frac{1-n}{n}} - \frac{n}{(2n+1)2^{\frac{n+1}{n}}K^{\frac{1}{n}}}\frac{\partial}{\partial r}\left[w^{\frac{2n+1}{n}}\frac{\partial P}{\partial r}\left(\frac{\partial P}{\partial r}\right)^{\frac{1-n}{n}}\right] = 0 \tag{18}$$

Only few experiments on power law fluid have been done so far. Auradou et al. (2008, 2010) carried out experiments assuming the fluid as Carreau fluid and flowing between two parallel rough surfaces. On the other hand, Di Federico (1997) and Lavrov (2013) numerically investigated the Power law fluid flow inside rough fractures and found out that the ratio of the equivalent fracture width to the actual fracture width increases with increasing roughness and flow behavior index.

2.4. Yield Power Law Fluid:

A Yield power law fluid also called as Herschel-Bulkley fluid (**Figure 2**) can be described mathematically as follows:

$$\tau = \tau_0 + k\gamma^n \tag{19}$$

Where τ = shear stress, τ_0 = yield stress, k = consistency index, n = flow behavior index and γ = shear rate

Literature review suggests that less research has been done on fracture flow of Yield Power Law (YPL) fluid. Majidi et al. (2008) developed a model by characterizing the drilling fluid as YPL fluid to more accurately predict the behavior of drilling fluids inside fracture. Like Liétard et al. (1999), they also provided type curve describing mud loss volume vs. time to determine the fracture width and predict the maximum volume of mud loss based on:

$$\frac{dr_d}{dt_d} = \frac{[1-\alpha(r_d-1)]^{\frac{1}{m}}}{2^{\frac{m+1}{m}} r_d \left(\frac{{r_d}^{1-m}-1}{1-m}\right)^{\frac{1}{m}}} \tag{20}$$

Where m = flow behavior index; K = consistency index; dimensionless radius, $r_d = \frac{r(t)}{r_w}$; dimensionless time, $t_d = \frac{m}{2m+1}\left(\frac{w}{r_w}\right)^{\frac{m+1}{m}}\left(\frac{\Delta P}{K}\right)^{\frac{1}{m}} t$ and dimensionless mud invasion factor, $\alpha = \frac{2m+1}{m+1}\frac{2r_w}{w}\frac{\tau_y}{\Delta P}$

CONCLUSION

Different research works on fluid flow inside fractures have been discussed in this paper. A model should possess the ability of predicting real scenario of drilling mud flow inside fractures to be proved useful. Drilling mud is generally of Non-Newtonian type that exhibit shear thinning and shear thickening behavior. When circulation stops, due to drilling fluids shear thickening behavior, it will remain as thick gel in the wellbore until sufficient pressure is applied to overcome its yield stress. This property can play an important role in the lost circulation treatment. As drilling fluid follows Yield Power Law (YPL) model, the model proposed by Majidi et al. can more accurately explain the lost circulation phenomenon. One drawback of this model that the fracture wall permeability and roughness isn't included in the model. In addition, drilling fluid properties (i.e. flow behavior index, consistency index and yield stress) are measured at surface conditions, whereas these properties significantly vary under bottomhole conditions. By incorporating these factors, a more robust model can be built to accurately explain the lost circulation phenomenon and enable a drilling engineer to treat lost circulation effectively.

REFERENCES

Dyke, C. G., Wu, B., & Tayler, D. M. (1995). Advances in Characterizing Natural- Fracture Permeability from Mud-Log Data. SPE 25022-PA, SPE Formation Evaluation.

Sanfillippo, F., Brignoli, M., Santarelli, F. J., & Bezzola C. (1997). Characterization of Conductive Fractures while Drilling. Paper SPE 38177, SPE European Formation Damage Conference held in The Hague, Netherlands, 2-3 June 1997.

Lietard, O., Unwin, T., Guillot, D., & Hodder, M. (1996). Fracture Width LWD and Drilling Mud/LCM Selection Guidelines in Naturally Fractured Reservoirs. Paper SPE 36832 presented at the 1996 European Petroleum Conference, Milan, Italy, (Oct. 22-24), 181.

Lietard, O., Unwin, T., Guillot, D., & Hodder, M. (1999). Fracture Width Logging While Drilling and Drilling Mud/Loss-Circulation-Material Selection Guidelines in Naturally Fractured Reservoirs. SPE Drilling & Completion, Vol. 14, No. 3, September 1999.

Sawaryn, S.J. (2001). Discussion of Fracture Width Logging While Drilling and Drilling Mud/Loss-Circulation-Material Selection Guidelines in Naturally Fractured Reservoirs. SPEDC 268, December 2001.

Civan, F., & Rasmussen, M. L. (2000). Further Discussion of Fracture Width Logging while Drilling Mud/Loss Circulation Material Selection Guidelines in Naturally Fractured Reservoirs. SPE 81590-DS, SPE Drilling and Completion 17 (4): 249-250, 2000.

Huang, J., Griffiths, D. V., & Wong, S. W. (2011). Characterizing Natural Fracture Permeability from Mud Loss Data. SPE 139592-PA, SPE Journal, March 2011.

Verga, F. M., Carugo, C., Chelini, V., Maglione, R., & De Bacco, G. (2000). Detection and Characterization of Fractures in Naturally Fractured Reservoirs. Paper SPE 63266, SPE Annual Technical Conference and Exhibition held in Dallas, Texas, USA, 1–4 October 2000.

Maglione, R., & Marsala, A. (1997). Drilling mud losses: problem analysis. AGIP Internal Report, 1997.

Lavrov A. & Tronvoll J. (2004). Modeling Mud Loss in Fractured Formation. Paper SPE-88700-MS presented at the 11th Abu Dhabi International Petroleum Exhibition and Conference held in Abu Dhabi, U.A.E., 10-13 October 2004

Lavrov A. (2014). Radial Flow of Non-Newtonian Power-Law Fluid in a Rough-Walled Fracture: Effect of Fluid Rheology. Springer, Transport Porous Media 105:559–570, DOI: 10.1007/s11242-014-0384-6, 2014.

Majidi, R., Miska, S. Z., & Thompson, L. G. (2008). Quantitative Analysis of Mud Losses in Naturally Fractured Reservoirs: The Effect of Rheology. SPE 114130, SPE Western Regional and Pacific Section AAPG Joint Meeting held in Bakersfield, California, U.S.A., 31 March- 2 April 2008.

Bourgoyne Jr, A. T., Millheim, K. K., Chenevert, M. E., & Young Jr, F. S. (1991). Applied Drilling Engineering. 2nd printing; SPE: Richardson, TX, 1991; pp 131-135.

Amadei, B & Savage, W. Z. (2001). An analytical solution for transient flow of Bingham viscoplastic materials in rock fractures. Int J Rock Mech Min Sci 38: 285-296.

Auradou, H., Boschan, A., Chertcoff, R., D' Angelo, M. V., Hulin, J. P., & Ippolito, I. (2010). Miscible transfer of solute in different model fractures: From random to multiscale wall roughness. ComptesRendus Geoscience 342: 644-652, 2010.

Auradou, H., Boschan, A., Chetcoff, R., Gabbanelli, S., Hulin, J. P., & Ipoolito, I. (2008). Enhancement of velocity contrasts by shear-thinning solutions flowing in a rough fracture. J Non-Newtonian Fluid Mech 153: 53-61, 2008.

Cardenas, M. B., Slottke, D. T., Ketcham, R. A., & Sharp, J. M. Jr. (2007). Navier-Stokes flow and transport simulation using real fractures shows heavy tailing due eddies. Geophys. Res. Letts. 34, L14404, doi: 10.1029/2007GL030545, 2007.

Di Federico, V. (1997). Estimates of equivalent aperture for non-Newtonian flow in a rough-walled fracture. Int. J. Rock Mech Min Sci 34: 1133-1137, 1997.

Koyama, T., Neretnieks, I., & Jing, L. (2008). A numerical study on differences in using Navier-Stokes and Reynolds equations for modeling the fluid flow and particle transport in single rock fractures with shear. Int. J. Rock Mech Min Sci 45: 1082-1101, 2008.

Lavrov A. (2013). Numerical modeling of steady-state flow of a non-Newtonian power-law fluid in a rough-walled fracture. Computers and Geotechnics 50: 101-109, 2013.

Mitsoulis, E., & Huilgol, R. R. (2004). Entry flows of Bingham plastics in expansions. J. Non-Newtonian Fluid Mech 122: 45-54, 2004.

Brown, S. R., Kranz, R. L., & Bonner, B. P. (1986). Correlation between the surfaces of natural rock joints. Geophys. Res. Letters (1986) 13, 1430.

Rossen, W. R., & Kumar, A. T. A. (1992). Single and two phase flow in natural fractures. Paper SPE 24915 presented at the 67th annual Technical Conference and Exhibition of the Society of Petroleum Engineers held in Washington, DC, USA, October 4-7, 1992.

Brown, S. R., & Scholz, C. H. (1985). Broad bandwith study of the topography of natural rock surfaces. J. Geophys. Res. (1985) 90, 12575.

Jones, T. A., Wooten, S. O., & Kaluza, T. J. (1988). Single phase flow through natural fractures. Paper SPE 18175 presented at the 1988 Annual meeting of the SPE, New Orleans, LA, Sept. 23-26.

Morrow, N. R., Brower, K. R., & Buckley J. S. (1989). Fluid flow in healed tectonic fractures. Paper SPE 19096 presented at the 1989 SPE gas technology symposium, Dallas, TX, June 7-9.

Reiss, L. (1980). The reservoir engineering aspects of fractured formations. Gulf Publishing Company, Houston, 1980.

Pyrak-Nolte, L., Cook, N. G. W., & Nolte, D. D. (1988). Fluid percolation through single fractures. Geophys. Res. Lett. (1988) 15, 1247.

Tsang, Y. W. (1984). The effect of tortuosity on fluid flow through a single fracture. Water Resour. Res (1984) 20, 1209.

Van Golf-Racht, T. (1982). Fundamentals of fractured reservoir engineering. Elsevier Scientific Publishing, New York, 1982.

Schrauf, T. W., & Evans, D. D. (1986). Laboratory studies of gas flow through a single natural fracture. Water Resour. Res.(1986) 22, 1038.

Wang, J. S. Y., & Narasimhan, T. N. (1985). Hydraulic mechanisms governing fluid flow in a partially saturated fractured, porous medium. Water Resour. Res. (1985) 21, 1861.

Asfari, A., & Witherspoon, P. A. (1973). Numerical simulation of naturally fractured reservoirs. SPE paper 4290 presented at the 3rd Numerical Simulation of Reservoir Perforation Conference of the SPE, held in Houston, TX, Jan 10-12, 1973.

Kelley, V.C., & Clinton, N. J. (1960). Fracture systems and tectonic elements of the Colorado plateau. U. of New Mexico Publ. Geol. #6, U. of New Mexico Press, Albuquerque, N. Mex., 1960.

Parker, J. M. (1942). Regional systematic jointing in slightly deformed sedimentary rocks. Bull., Geol. Soc. Am. (March, 1942), Vol. 53, p. 381.

Hodgson, R. A. (1961). Regional study of jointing in Comb-Novajo Mountain Area, Arizona and Utah. Bull., AAPG (1961), Vol. 45, No. 1, p. 1.

Huitt, J. L. (1955). Fluid flow in simulated fractures. Amer. Inst. Chem. Eng. Journal, vol. 2, pp. 259-264, 1955.

Sarkar, S., Toksoz, M. N., & Burns, D. R. (2002). Fluid flow simulation in fractured reservoirs. Report, Annual Consortium Meeting, MIT Earth Resources Laboratory, 2002.

Snow, D. T. (1965). A parallel plate model of fractured permeable media. Ph.D. Dissertation, University of California.

Witherspoon, P. A., Wamg, J. S. Y., Iwai, K., & Gale, J. E. (1980). Validity of cubic law for fluid flow in a deformable rock fracture. Water Resour. Res. 16, 1016-1024, 1980.

Nelson, R. A. (1985). Geological Analysis of naturally fractured reservoirs. Gulf Publishing Co., Houston, 1985.

Douglas, J. Jr., Paes Leme, P. J., Arbogast, T., & Schmitt, T. (1987). Simulation of flow in naturally fractured reservoirs. Paper SPE 16019 presented at the 9th SPE Symposium on Reservoir Simulation held in San Antonio, TX, USA. February 1-4, 1987.

Yang, G., Cook, N. G. W., & Myer, L. R. (1989). Network modeling of flow in natural fractures. Rock mechanics as a guide for efficient utilization of natural resources, Khair (ed.), Rooterdam, ISBN 90 6191 8715, 1989.

International Conference on Petroleum Engineering 2016 (ICPE-2016)
Bangladesh University of Engineering & Technology (BUET)
Dhaka-1000, Bangladesh

ICPE (2016– 052)

Distribution of Heavy Metals in the Surface Water and Bed Sediments of Sundarbans Region

M. Z. H. Khan, M. R. Hasan*, F. K. Tarek, S. Paul, M. A. Bhuiyan
Dept. of Chemical Engineering, Jessore University of Science and Technology, Jessore 7408, Bangladesh.

ABSTRACT

The concentrations of major (Si, Al, Ca, Fe, K) and minor (Mn, Ni, Pb, U, Zn, Co, Cr, As, Cu, Rb, Sr, Zr,) elements in the surficial water and bed sediments were studied in an attempt to establish their concentration in the Shella River near Sundarban coast. It was revealed that the majority of the trace elements have been introduced into the Bengal marine from the riverine inflows. The concentration of heavy metals was measured using Atomic Absorption Spectroscopy (AAS) and ED-XRF instruments. The heavy metal concentrations in the river sediments were remarkably high, but varied among sampling points, and the concentrations in water were mainly within the permissible limits. Attention should be paid to mitigate element mobilization from sediments as their effects may become significant during seasons and years of low water flow in the river. Constant monitoring of the water quality is needed to record any alteration in the quality and mitigate outbreak of health disorders and the detrimental impacts on the aquatic ecosystem.

Keywords: Pollution, Shella River, Sundarbans coast, sediment, water, heavy metals, environment.

* Corresponding Author address
Email: zaved.khan@yahoo.com

INTRODUCTION

In recent years, the pollution of the aquatic environment with heavy metals has become a worldwide problem. Toxic pollutants, such as heavy metals originating from direct atmospheric deposition, geologic weathering, or through the discharge of industrial waste products deposited in marine sediments as a sink. Due to their potential toxic effect and ability to bioaccumulation in aquatic ecosystems [Rainbow, 2007; Wang and Rainbow, 2008], the investigation of distribution and pollution degree of heavy metals in coastal area has attracted more public concerns recently [Christophoridis et al., 2009; Larrose et al., 2010; Feng et al., 2011].

The potential sources of heavy metal pollution in the aquatic environment are industrial wastes and mining [Liu et al., 2011]. Metals like arsenic, cadmium, chromium, mercury, nickel and lead in marine environment are often considered indicators of anthropogenic influence and are themselves of potential risk to the natural environment [Sundaray et al., 2011]. Several researchers have demonstrated that marine sediment is highly polluted by heavy metals; therefore, the evaluation of metal distribution in surface sediment is useful to assess pollution in the marine environment [Varol, 2011; Gao and Chen, 2012]. Therefore, it is important to assess and track the abundance of these heavy metals in coastal ecosystem [Yang et al., 2012].

Southern part of Bangladesh is situated at the coast of Bay of Bangle. World's greatest mangrove forest is situated at this part. So far, there are limited or no work focused on heavy metals investigation near this coastal area.

MATERIALS AND METHODS

2.1 Sample preparation

Ten surface sediment samples were collected during winter season. Anti-rust scoop was used to collect the sediment samples by scooping up 10 cm of the bed sediment from 10 m away from the coastal bank and sediments were naturally dried at room temperature (25°C ± 2) in the laboratory prior to analysis. The sampling bottles were pre-conditioned with 5% nitric acid and later rinsed thoroughly with distilled de-ionized water. Before sampling was done, the polyethylene sampling bottles were rinsed at least three times. Sediment samples were collected using grab sampler from two sites. Samples were transported to the laboratory and once air-dried; sediment samples were powdered and passed through 160 µm sieve. After packing in polyethylene bags the samples were stored below -20°C prior to analysis. Sediments samples were weighed placed into the digestion bombs with 10 mL of HNO3/HCl (1:3 v/v) and digested in a microwave digestion system. Sediments analysis was carried out according to the standard procedure described earlier.

2.2 Instrumentation

The elements determinations were performed by means of a SHIMADZU AAS-7000 (Flame Atomic Absorption spectrometer) (for Al,Fe,Ba,Mn,Cu,Ni,Zn,V,Cu,Pb), The Thermo Scientific ARL QUANT'X EDXRF Spectrometer analyzer were used for determining m/m % for a wide band metals.

RESULTS AND DISCUSSION

3.1 Heavy metals concentration in sediment

Of the elements of study, the concentration of six heavy metals K, Cu, Zn, Fe, Cr, and Mn in sediment from Shela River and Sundarban region, Bangladesh and comparison with different Sediment Quality Guidelines (SQG) are given in Table 2. It exposed that the ranking sequence of mean concentrations of traced heavy metals in sediment were Mn > K > Fe > Zn > Cu > Cr (mg/kg) gradually.

3.2 Sediment quality assessment

To evaluate the status of heavy metals in sediment, we used four approaches, Geo-Accumulation Index, Enrichment Factor, Contamination Factor, and Pollution Load Index.

3.2.1 Geo-Accumulation Index (I_{geo})

The geo-accumulation index (I_{geo}) has been widely studied to assist the pollution status of sediment. I_{geo} was calculated using following formula:

$$I_{geo} = \log (C_n / 1.5 \times B_n)$$

Where C_n is the analyzed concentration of the metal (n) in sediments and B_n is the geological background of the metal (n). Others reported on mean shale concentration of various metals which is used as background concentration throughout the study and factor 1.5 is bring in to comprise possible variation of the background values due to lithogenic effect. Some researchers proposed seven domination of the I_{geo} which are given in Table 1. Based on Muller formula, the calculated values of I_{geo} of heavy metals in sediment are given in Table 3. The I_{geo} values indicated that the sediments of Shela River and Sundarban region are unpolluted for all metals in all sample.

3.2.2 Contamination Factor (CF)

Calculated Contamination Factor is used to express the contamination quality of sediment. To calculate the CF, Hakanson (1980) have been proposed the following formula

CF = Concentration of measured metal / Background Concentration of the same metal

We are used mean shale concentration of various metals as background concentration throughout the study from reference [Wang and Rainbow, 2008]. Considering calculated CF, low contaminations were found for all samples that means CF < 1. The CF values for all analyzed metals are given in Table 4. The Mean CF for all metals were found 0.00014491mg/kg for K, 0.00170222mg/kg for Cr, 0.008961846 for Mn, 5.8475E-05 for Fe, 0.007593704 for Cu, and 0.005219474 for Zn. The comprising sequence of mean CF if all metals is Mn > Cu > Zn > Cr > K > Fe.

3.2.3 Pollution Load Index

According to particular sample, PLI is used to express the pollution effect of sediment. PLI value for a particular site is calculated by the following formula:

$$PLI = \sqrt[n]{CF_1 \times CF_2 \times CF_3 \ldots \times CF_n}$$

Where, CF and n are indicate the contamination factor of metals and the number of metals. The PLI provides assessing a site quality. Tomlinson (1980) proposed three domination of the PLI which are given in Table 1. The PLI values for all sites are lower than 1 which assign to all sites not polluted. The PLI values for all sites are given in Figure 1.

Table 1 Categories of sediment quality according to Geo Accumulation Index (Muller 1969), Contamination Factor (Hakanson 1980), Pollution Load Index (Tomlinson 1980), and Enrichment Factor (Sinex and Helz 1981)

Values	Class	Sediment Quality
I_{geo} Values		
$I_{geo} \leq 0$	0	Unpolluted
I_{geo} = 0-1	1	From unpolluted to moderately polluted
I_{geo} = 1-2	2	Moderately polluted
I_{geo} = 2-3	3	From moderately to strongly polluted
I_{geo} = 3-4	4	Strongly polluted
I_{geo} = 4-5	5	From strongly to extremely polluted
$I_{geo} > 6$	6	Extremely
CF values		
CF < 1	1	Low CF
1≤ CF < 3	2	Moderate CF
3≤ CF < 6	3	Considerable CF
CF ≥ 6	4	Very high CF
PLI values		
PLI < 1	1	Perfection
PLI = 1	2	Pollutant are present in baseline level
PLI > 1	3	pollutant

Table 1 Concentration (mg/kg) of heavy metals in sediments and comperes with different sediment quality guidelines

Sample ID	K	Fe	Cu	Zn	Cr	Mn
S-1	2.471	BDL	0.3812	0.7125	0.155	4.92
S-2	BDL	BDL	0.2725	BDL	0.1505	6.39
S-3	1.985	BDL	0.7529	0.9163	0.2594	4.49
S-4	2.473	BDL	0.5114	BDL	0.2062	11.83
S-5	3.5	BDL	0.3275	BDL	0.1606	6.6003
S-6	BDL	BDL	0.5	BDL	0.3455	2.8688
S-7	7.613	BDL	0.2275	BDL	0.1353	11.38
S-9	7.129	BDL	0.3876	BDL	0.23	4
S-10	6.398	BDL	0.2525	BDL	0.1555	11.235
S-11	6.977	BDL	0.3826	0.83	0.01	8.111
S-12	BDL	BDL	0.48	BDL	0.23	9.21
S-13	BDL	BDL	0.644	BDL	0.16	11.65
S-14	BDL	0.3	0.3826	1.07	0.1606	8.44
S-15	BDL	0.5	0.325	0.34	0.1606	8.44
S-16	BDL	1	0.2099	0.82	0.1403	7.5
S-17	BDL	4	0.2375	0.288	0.1429	7.24
S-18	BDL	8	0.1749	0.7887	0.1353	6.82
S-19	BDL	BDL	0.2825	0.866	0.0947	5.82
S-20	BDL	BDL	0.3125	0.934	0.1429	8.64
S-21	BDL	BDL	0.26	0.89	0.1707	7.64
S-22	BDL	BDL	0.35	0.87	0.1459	8.03
S-23	BDL	BDL	0.26	0.83	0.1074	7.48
S-24	BDL	BDL	0.3551	0.97	0.1277	7.34
S-25	BDL	BDL	0.23	0.74	0.09	6.94
S-26	BDL	BDL	0.3651	0.82	0.08	8.22
S-27	BDL	BDL	0.4939	1.04	0.2	8.32
S-28	BDL	BDL	0.3388	BDL	0.13	10.7
S-29	BDL	BDL	0.54	0.95	0.158	9
WHO(2004)	-	-	25	123	25	-
USEPA(1999)	-	30	16	110	25	30
CCME(1999)	-	-	35.7	123	37.3	-

Among the analyzed sediment samples, Mn was traced in amount compassing from 1.6544-11.83mg/kg, K from 1.985-7.613mg/kg, Fe from 0.3-8mg/kg, Zn from 0.2-1.07mg/kg, Cu from 0.014-0.7529mg/kg and Cr from 0.01- .3455mg/kg. The result revealed that the mean concentration of Mn (7.617mg/kg) was higher than other metals. The mean concentration of heavy metals in the sediment were compared with WHO (2004), USEPA (1999) and CCME (1999) sediment quality guidelines. It was found that the mean concentrations of Mn and Fe in sediment lower than the USEPA (1999) sediment quality guidelines. Also it were found that the mean concentrations of Cr, Cu, and Zn lower than WHO (2004), USEPA (1999) and CCME (1999) sediment quality guidelines.

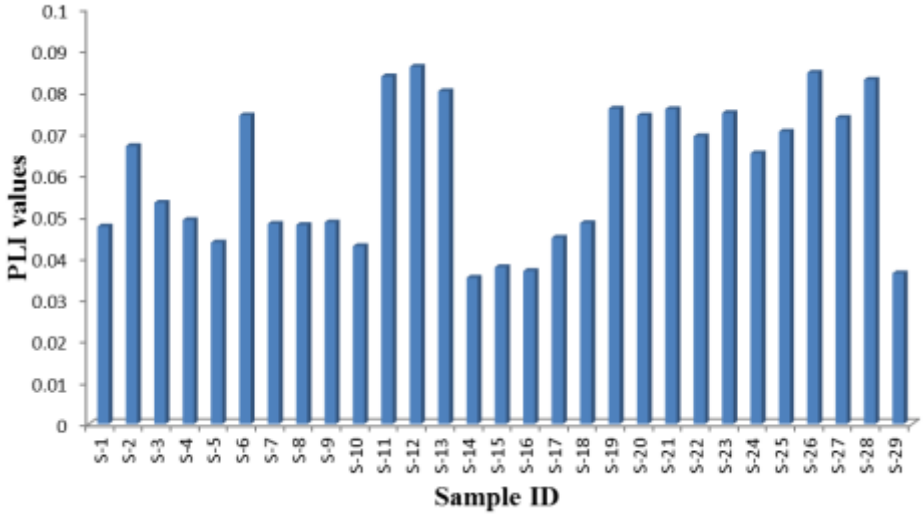

Figure 1: PLI values of sediment from Shela River and Sundarban region

Generally, the element mobilization in the sediment environment is dependent on physiochemical changes in the water at the sediment-water interface. The precipitation of heavy metal elements in the form of insoluble hydroxides, oxides and carbonates might be the result of alkaline pH. The minor elements such as Cr, Cu and Co have interacted with organic matter in the aqueous phase and settled resulting in a high concentration of these elements in the sediment.

CONCLUSION

The results of this finding present a valuable baseline data on the heavy metals in the water, sediments from Shela River near Sundarban region. It was observed that the concentrations of heavy metals recorded in the water samples were below the WHO & FEPA recommended limits. However, the fact that some level of bioaccumulations was found in the sediment samples from Shela River is a cause for constant monitoring of the water because the surrounding villagers depend on the water downstream for domestic and agricultural purposes.

REFERENCES

Christophoridis, C., Dedepsidis, D., Fytianos, K. (2009). Occurrence and distribution of selected heavy metals in the surface sediments of Thermaikos Gulf, N. Greece. Assessment using pollution indicator. Journal of Hazardous Materials 168, 1082-1091.

Feng, H., Jiang, H., Gao, W., Weinstein, M.P., Zhang, Q., Zhang, W., Yu, L., Yuan D., Tao, J. (2011). Metal contamination in sediments of the western Bohai Bay and adjacent estuaries, China. Journal of Environmental Management 92, 1185– 1197.

Gao, X., Chen, C.-T.A., (2012). Heavy metal pollution status in surface sediments of the coastal Bohai Bay. Water Research 46, 1901–1911.

Hakanson, L., (1980). An ecological risk index for aquatic pollution control a sedimentological approach. Water Res. 14, 975-1001.

Larrose, A., Coynel, A., Schäfer, J., Blanc, G., Massé, L., Maneux, E. (2010). Assessing the current state of the Gironde Estuary by mapping priority contaminant distribution and risk potential in surface sediment. Applied Geochemistry 25, 1912-1923.

Liu, S., Shi, X., Liu, Y., Zhu, Z., Yang, G., Zhu, A., Gao, J., (2011). Concentration distribution and assessment of heavy metals in sediments of mud area from inner continental shelf of the East China Sea. Environmental Earth Sciences 64, 567–579.

Muller, G., (1969). Index of geoaccumulation in sediments of the Rhine river. Geol. J., 2, 109-118.
Rainbow P.S. (2007). Trace metal bioaccumulation: Models, metabolic availability and toxicity. Environment International 33, 576-582.

Sundaray, S.K., Nayak, B.B., Lin, S., Bhatta, D., (2011). Geochemical speciation and risk assessment of heavy metals in the river estuarine sediments – a case study: Mahanadi basin, India. Journal of Hazardous Materials, 186, 1837–1846.

Tomlinson, D.L., Wilson J.G., Harris C.R., Jeffney D.W., (1980). Problems in the assessment of heavy metal levels in estuaries and the formation of a pollution index. Helgol. Meeresunters. 33, 566-572.
Turekian, K.K. and Wedepohl K.H., (1961). Distribution of the elements in some major units of the earth's crust. Am. Geol. Soc. Bull., 72, 175-192.

Varol, M. (2011). Assessment of heavy metal contamination in sediments of the Tigris River (Turkey) using pollution indices and multivariate statistical techniques. Journal of Hazardous Materials 195, 355-364.

Wang, W.-X., Rainbow, P.S., (2008). Comparative approaches to understand metal bioaccumulation in aquatic animals. Comparative biochemistry and physiology Part C: toxicology and amp. Pharmacology 148, 315–323.

Yang, Y., Chen, F., Zhang, L., Liu, J., Wu, S., Kang, M., (2012). Comprehensive assessment of heavy metal contamination in sediment of the Pearl River Estuary and adjacent shelf. Marine Pollution Bulletin 64, 1947–1955.

International Conference on Petroleum Engineering 2016 (ICPE-2016)
Bangladesh University of Engineering & Technology (BUET)
Dhaka-1000, Bangladesh

ICPE (2016-053)

Design, Development and Validation of an Experimental Managed Pressure Drilling Setup

Al Amin, Dan Chen, Syed Imtiaz*, Aziz Rahman, Faisal Khan
Department of Process Engineering
Memorial University of Newfoundland
St. John's, NL A1C 5S7, Canada

ABSTRACT

In this paper, we present the design, development and validation of a lab scale managed pressure drilling (MPD) experimental setup. This scaled-down experimental setup was built to study the hydrodynamics of MPD operation. A brief overview of the design and development stages of the experimental setup is provided, followed by simulation of different real life scenario and comparison of the experimental frictional loss with various empirical friction loss models. The setup is a 4.7 m tall concentric flow loop where the inner pipe simulates the drill string and outer annulus represents the casing in a drilling operation. The system is equipped with a progressive cavity pump which can drive water from 20 LPM to 170 LPM and maximum pressure rating is 100 psi. Reynold's number and 'pressure drop per unit length' were matched with a real life drilling system to replicate similar hydrodynamic characteristics. However, the flow loop is limited to static drill string. The system can simulate hydrodynamic changes in a MPD system in a variety of operational scenarios including drill pipe extensions, pressure tapping, drill mud loss, and gas kick. The setup is used for validating theoretical frictional pressure drop model. We validated two theoretical models, the Darcy-Weisbach friction model and the frictional pressure drop model of commercial software, OLGA. The estimated pressure drop using Darcy-Weisbach friction model agrees within 7% of the experimental values, whereas the OLGA based simulation results give 12% average error.

Keywords: frictional pressure drop, drilling, Reynold's number, influx, annular flow

* Corresponding Author address
Email: simtiaz@mun.ca

INTRODUCTION

The concept of MPD was formally introduced in the late 60s in the Abnormal Pressure symposiums at Louisiana State University as in (Rehm et al., 2013). According to International Association of Drilling Contractors (IADC), MPD is a condition based adaptive technique which maintains the downhole pressure conditions in conjugation to the annular pressure profile by using components such as back pressure control, bottom hole annular pump or mechanical devices. The overall objective of this technique is to maintain the downhole pressure within available pressure window provided by pore pressure and fracture pressure. In 2008, Stamnes et al. developed an observer which is able to estimate the bottom hole pressure by estimating the hydrodynamic properties. Mass balance in drill string and the annulus control volumes are used to estimate the pressure conditions. The hydrodynamic flow is obtained from the momentum balance involving friction and flow parameters. Following the mass and momentum balance an observer is developed which can estimate the bottom hole pressure. Kaasa et al. (2012) presented a simplified hydraulic model for aiding the design and modeling procedure of a drilling system. The main objective of this research was to eliminate the complexity involved in the flow phenomena and use simple set of equation to capture the dynamics of the drilling system to predict the downhole pressure efficiently. Chin (2012) reviewed the equations involved in a Newtonian and non-Newtonian fluid flow conditions. Based on the condition, the flow and pressure values are evaluated from the equations available in the literature ranging from momentum equation to partial differential equations.

Reitsma (2010) presented a modified Dynamic Annular Pressure Control (DAPC) which can identify the influx situations based on the choke position and prediction of unexpected flow. The system was tested in PERTT facility installed in Lousiana State university. In 2010, Godhavn et al. developed a PID controller with high integral gains based on first order transfer function models derived from ordinary differential equations. While performing drill pipe extensions, this controller is able to track the choke pressure. The main objective of the controller is to drive the bottom hole pressure to a set point value. In 2011, Zhou et al. proposed a switch control method for kick attenuation. The study presented a controller which switches between pressure control and flow control. During normal operation, the control tracks BHP and maintain it between pressure window. Whenever a kick is detected, it switches to flow control mode which enables the controller to drive kick out of the system. The quest for ideal flow dynamics of the wellbore drilling system is still underway due to nonlinear behavior of the system and lack of precise technology for measurement. Our objective is to design and develop a scaled down concentric pipe flow loop with similar hydrodynamic properties as of a typical wellbore system. The developed system can be used to replicate different operational scenarios including drill pipe extension, pressure tapping, drill mud loss and gas kick. Hence we demonstrate the design methodology of developing an MPD experimental setup and the results from different operational scenarios.

SYSTEM DESCRIPTION

A typical MPD system generally consists of the components as shown in Figure 1. Initially, a mud pump is used to circulate the mud with q_p volumetric flow rate at pressure p_p. The drilling mud is pumped through the drill string to the down hole region and circulated back to the surface through the annulus. A choke is placed at the exit region to control the volumetric outflow q_c to maintain the pressure p_{bh} in the downhole region. The choke opening imposes a back pressure p_c to increase or decrease the bottom hole pressure. For simplicity, the hydrodynamic model we considered is based on Kaasa et al. (2012).

$$\dot{p}_p = \frac{\beta_d}{V_d}\,(q_p - q_{bit}) \tag{1}$$

$$\dot{p}_c = \frac{\beta_a}{V_a}\,(q_{bit} - q_c + q_k) \tag{2}$$

$$q_k = K_{pi}\,(p_{res} - p_{bh}) \tag{3}$$

$$\dot{q}_{bit} = \frac{1}{M}\,(p_p - p_c - p_{fd} - p_{fa} - (\rho_a - \rho_d)gh_t) \tag{4}$$

$$p_{bh} = p_p - p_{fd} + \rho_d g h_t \tag{5}$$

$$p_{bh} = p_c + p_{fa} + \rho_a g h_t \tag{6}$$

$$p_{st} = \rho g\, h_t \tag{7}$$

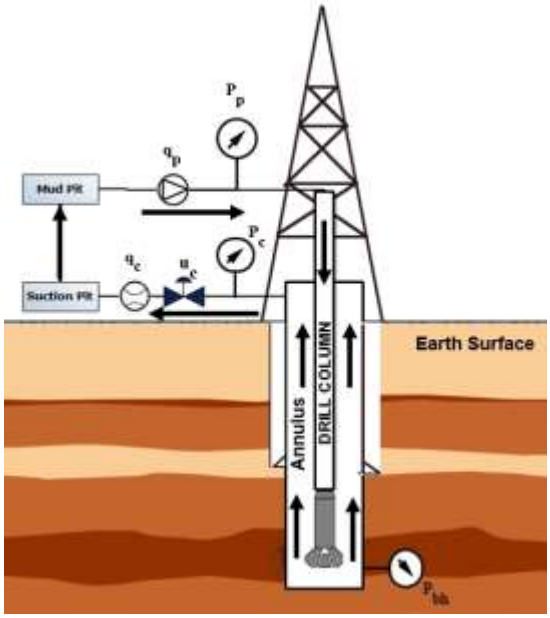

Figure 1. Schematic of a typical MPD setup

Bottom hole pressure can be calculated by summation of choke pressure, annulus frictional pressure drop and hydrostatic pressure in the annulus as shown in equation 5. p_{fd} and p_{fa} are frictional pressure drop in the drill string and annulus control volume. p_{st} is the hydrostatic pressure offered by drilling mud. q_k is the influx flow rate obtained from the interaction between reservoir pressure p_{res} and bottom hole pressure p_{bh} multiplied with a tuning constant K_{pi}. M is a constant based on the volume of drill string V_d, volume of annulus V_a, bulk modulus of drill string β_d and bulk modulus of annulus β_a. For simplicity, the back

pressure pump component is avoided in the mathematical model. However, in this paper, our main focus will be on the normal flow condition in drilling system only.

During mud circulation using the pump, the friction with pipe or casing surface leads to a frictional pressure loss. The magnitude of pressure loss varies based on the velocity of mud water. It can be obtained by Darcy-Weisbach equation from Moody (1944).

$$h_f = f\frac{L}{D}\frac{V^2}{2g} \tag{8}$$

$$\Delta P_{overall} = \rho g h_f + \rho g k\frac{v^2}{2g} \tag{9}$$

h_f is the head loss associated with velocity of fluid *V*. Length *L* and Diameter *D* is the geometric properties of the flow path. f is the friction factor based on the type of flow regimes. The flow regimes are obtained based on the fluid's physical properties such as density ρ, viscosity μ and the velocity *V* through the region having equivalent diameter *D*. For simplicity, Reynold's number above 2100 is considered as turbulent flow. For turbulent flow, the friction factor is obtained by solving Colebrook equation from Colebrook (1938). This equation primarily requires Reynold's number and pipe roughness for solving the equation.

$$Re = \frac{\rho v D}{\mu} \tag{9}$$

$$\frac{1}{\sqrt{f}} = -2\log_{10}\left(\frac{\frac{\epsilon}{D}}{3.7} + \frac{2.51}{Re\sqrt{f}}\right) \tag{10}$$

DESIGN METHODOLOGY

Typically, an MPD system needs to ensure the bottom hole pressure is maintained within the prescribed pressure window. Here we present a novel design of the flow loop that was developed on the basis of similarity analysis. The first objective is to design based on the geometric similarity, i.e. model should be an exact geometrical replica of the prototype. Secondly, dynamics of the model and actual system should be similar. It can be achieved by matching dimensionless groups. Reynolds number is used to perform similarity analysis. The field data was collected from the thesis work of Birkeland (2009).

Selection of pipe diameter

Initially, a fluid type is selected with desired hydrodynamic properties. Based on the Reynolds number offered by the particular type of fluid a diameter for drill string is chosen between 0.5 to 5 inches. This establishes the velocity diameter profiles as shown in Figure 2. Based on the diameter and Reynolds number the frictional pressure drop is evaluated. For annulus pipe, the equivalent diameter $(D_{eq} = D_{ai} - D_{do})$ in the range from 0.5 to 5 inches was chosen. Then, the Reynolds number was matched to obtain the velocity-diameter profile. The frictional pressure drop for the annulus pipe was evaluated after the pipe

selection. Finally, the design parameters were checked to make sure the values are feasible to build up the flow loop. The specifications of the designed flow loop pipe and annulus are shown in Table 1.

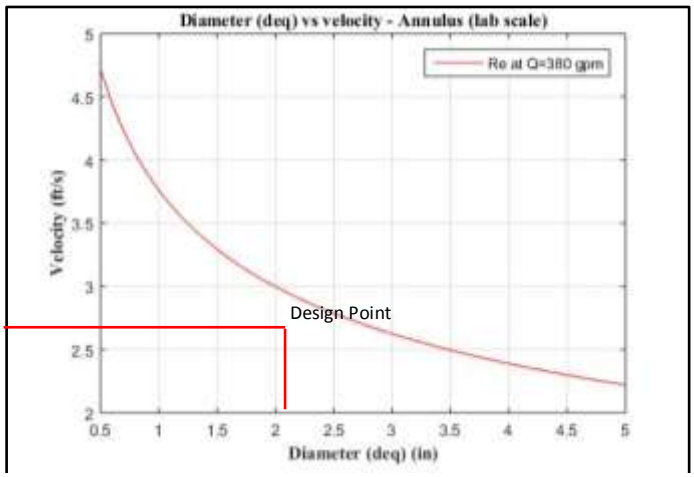

Figure 2 Diameter vs velocity profile for annulus

Table 1 Dimension of designed drill string and annulus pipe

	Length (in)	Inner diameter (in)	Pipe thickness (in)	Pipe Schedule	Material
Pipe	187	1.9	0.2	80	Black PVC Plastic
Annulus	175	2.9	0.3	80	Clear PVC Plastic

Assumptions

For initial experiments, only normal water is chosen as the primary drilling fluid. Besides this, the rate of penetration and the rotation of the drill string is considered zero as our main objective is to investigate the flow behavior at a static position of the drill string at a particular depth. The reservoir fluid is considered to be air. The air will be injected at a particular pressure to replicate the influx situations. Due to the smaller height of flow loop the inlet and outlet flow is considered constant. The choke is used for pressure regulation purpose.

Setup Description

A cylindrical tank of 600 l capacity having diameter 0.5 m and height 0.8 m is chosen. In order to drive the drilling fluid at varying pressure and flow rates, a screw type progressive cavity pump is chosen. The installed pump has 145 psi maximum discharge pressure and 60 gpm maximum flow rate. It is equipped with a Variable Frequency Drive (VFD) to control the rotation of the screw in the pump to obtain the desired flow rate and pressure during the experiment. The remaining components such as flow meter, pressure sensors and control valves were designed based on the dimension of the piping system. A SolidWorks CAD design was prepared to create the virtual model of the flow loop. All the sensors and actuators were placed in the respective positions as shown in Figure 3. The manufacturer provided

datasheet were used to determine the exact model of the equipment required for the installation. Table 2 show the types of sensors and actuators used in the flow loop along with their nomenclature.

Table 2 Component types along with nomenclature

Component Nomenclature	Type
PT	Pressure transmitter
FM	Flow meter
AF	Air flow meter
CV	Control valve
MV	Manual Valve
PCV	Progressive Cavity Pump
NRV	Non Return Valve

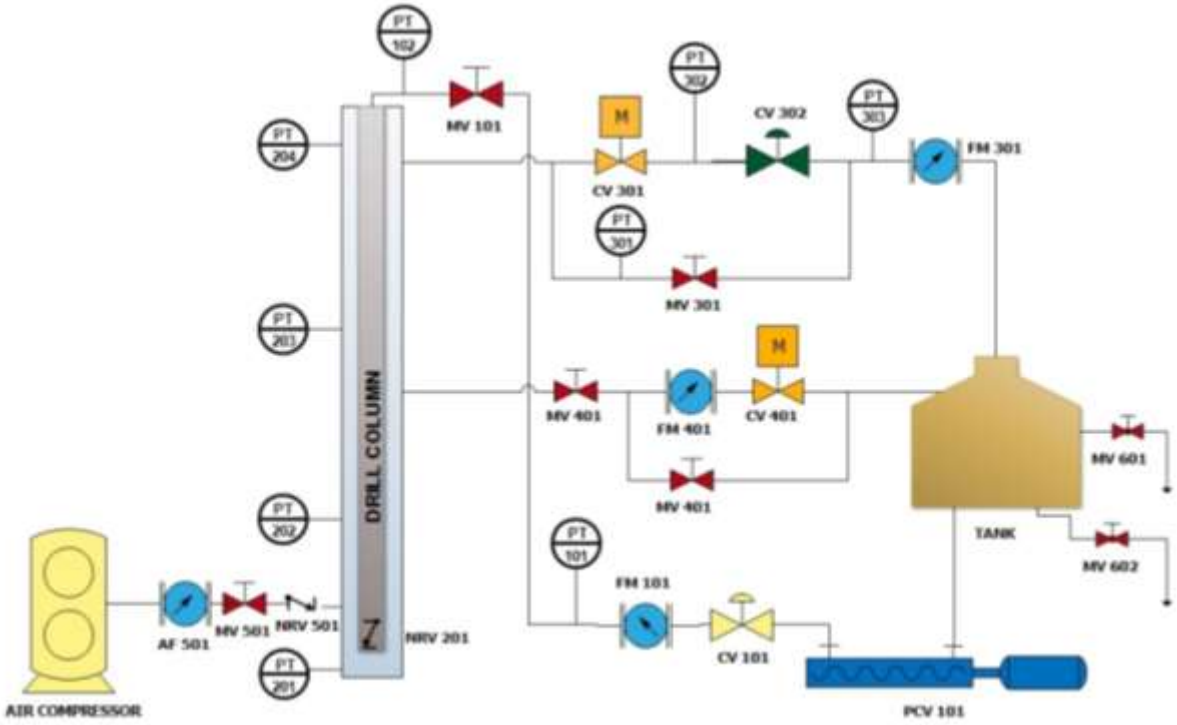

Figure 3 Process connection diagram of experimental setup

EXPERIMENTAL SETUP

The developed experimental setup is a lab scale replica of an actual MPD wellbore system. It is designed and installed in process engineering department at Memorial University of Newfoundland. The drill string pipe is a regular PVC pipe installed vertically. In the annulus region, a clear PVC pipe is placed concentric to the drill string pipe. The drilling fluid is pumped using a progressive cavity pump. For simplicity normal water and air is considered while experimenting. There are multiple 90^{o} bends and check valves at different points which induce frictional pressure drop to the drilling fluid being circulated throughout the system. The flow loop is equipped with multiple pressure transmitter which provides the pressure reading at the point of interest. During operation, the choke can be manipulated at different opening position to control the upstream and downstream pressure as desired. The sensors and actuators used in the flow loop is listed in Table 3.

Table 3 Sensors and Actuators used in the system

Component	Component type	Equipment
Flowmeter	Sensor	Rosemount 8711 Krohne Optiflux 3000 Omega FLR 6725D
Pressure Transmitter	Sensor	WIKA P31 Rosemount 2088
Control Valve	Actuator	Baumann 25000 and Fisher DCV 2000 Apollo and PMV Positioner

In order to simulate the reservoir conditions and observe the influx behavior, an air compressor is used to provide a gas kick. This feature will enable to validate mathematical models relating gas influx situations in a wellbore drilling operation. For measuring the amount of air injected into the system an air flow meter is also used to estimate the influx volume.

PHYSICAL CONNECTIVITY AND DATA ACQUISITION SYSTEM

All the sensors and actuator used in the system are rated to be operated on 4-20 mA current input and output respectively. Advantech data acquisition system is used as a communication interface between MPD plant and computer. ADAM 5000 TCP/IP is the backbone of overall communication operation. Four network cards had been used for measurement and control purposes. The communication between Matlab and the ADAM DAQ hardware is performed using OPC server. In the OPC browser, all available OPC server in the client is displayed. Matlab OPC toolbox is used to control the inflow and outflow of data from sensors and actuators. All the sensors and actuators were pre-calibrated when purchased from the supplier. So, while interfacing the system with the DAQ, the maximum and minimum range were matched with 4-20 mA current input and output for the sensors and actuators. The schematic of MPD communication system is shown in Figure 4.

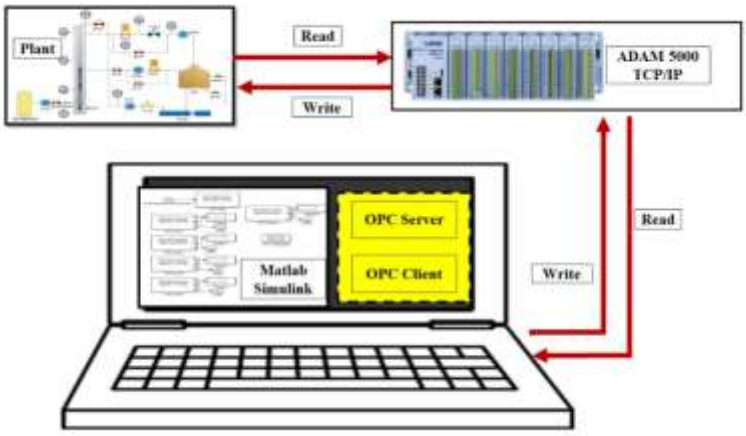

Figure 4 MPD communication system

EXPERIMENTAL RESULTS

Two different types of experiments were conducted to observe the behavior of the flow loop in conjugation to the actual theoretical model. Kaasa model and Darcy-Weisbach friction model was considered as the theoretical models for validating the results of the flow loop. The experiments were performed for water flow rate between 60 lpm and 160 lpm. The choke opening is manipulated between 40% and 100%. No influx, influx and pipe extension scenarios are primarily investigated in these experiments. On the other hand, the OLGA simulation was set up using the exact geometric properties of the developed experimental setup using water as the primary drilling fluid. The simulation results are compared in Figure 7.

No Influx scenarios

In this experiment, the flow loop was operated for a time span of 6 minutes where the inlet water flow rate was changed by 20 lpm at every minute starting from 60 lpm. No additional fluid was used in the experiment. The ultimate objective of this experiment is to observe the pressure and flow response in the inlet, bottom hole and outlet region. According to Figure 5, it is observed that the inlet and outlet flow rate are almost equal. Whenever the inlet flow rate was changed the outlet flow rate changed in equal magnitude at 100% choke opening position. The majority of the loss were associated with a frictional pressure drop across non-return valves and control valves. The overall frictional pressure drop is the summation of major loss and minor loss. For the designed experimental setup, the sum of minor loss friction coefficient (k) is considered to be 24 which includes a 90-degree elbow, 180^0 flow reversal and non-return valve. Figure 6 presents the pressure response corresponding to particular flow.

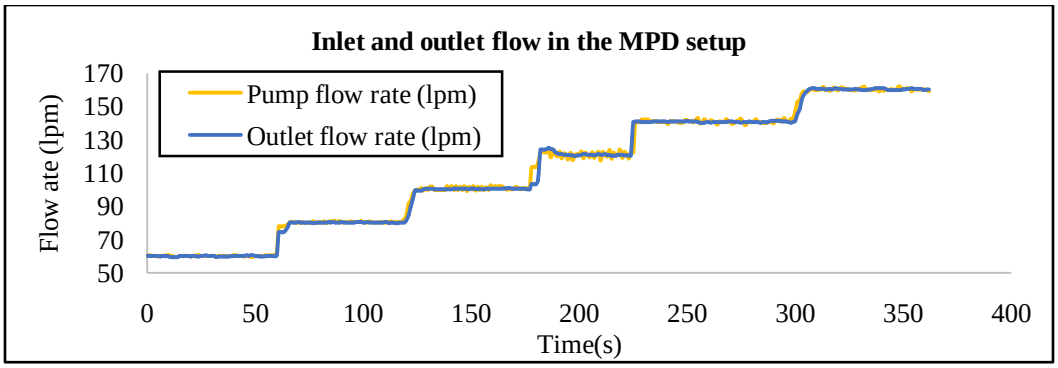

Figure 5 Inlet and outlet flow behavior in the experimental setup

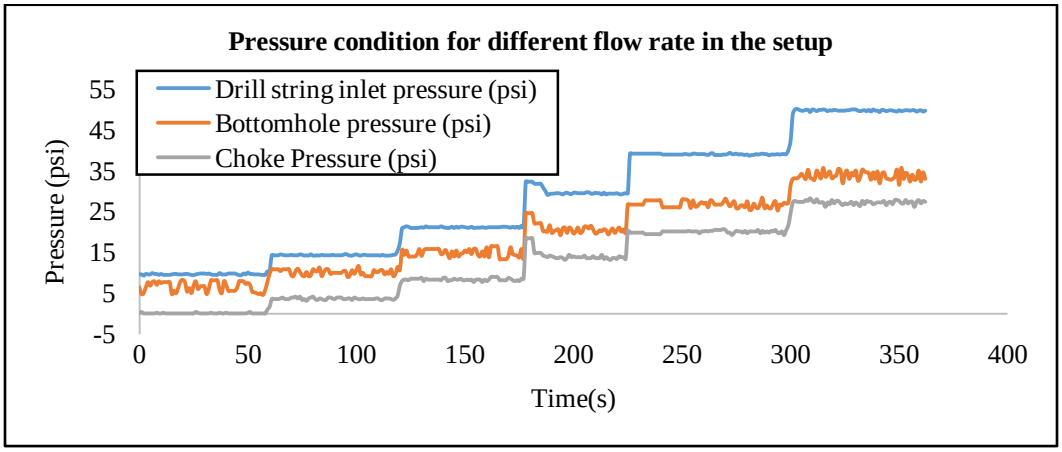

Figure 6 Pressure response at different flow rates in MPD setup

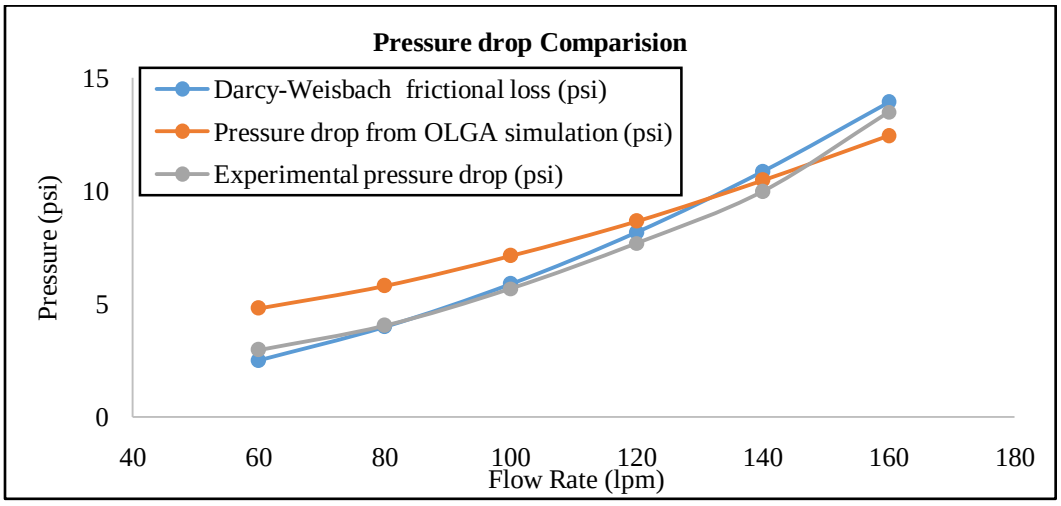

Figure 7 Pressure drop comparison

The validation of the experimental results was performed comparing the pressure drop values with the Darcy-Weisbach frictional loss and pressure drop from OLGA simulation. Figure 7 shows the comparison between the theoretical and experimental pressure drops at different flow rates. From Figure 7, it is evident that the flow loop follows the theoretical friction loss equations. It is found that the model is able to estimate the bottom hole pressure with an average error below 2%.

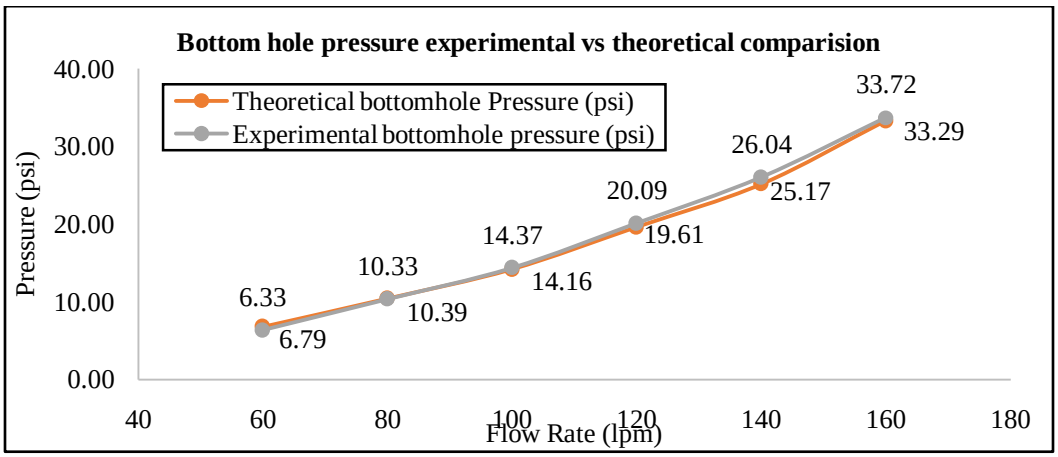

Figure 8 Bottom hole pressure estimation and comparison with experimental values

Influx situations

In this experiment, the flow rate was kept constant at a particular value. The goal of this experiment is to confirm the ability of the setup to generate influx scenarios and control it. The resulting flow behavior is monitored when the choke is manipulated from 100% to 40%. The air is injected into the system after 30 seconds from the start of the pump. After 1 minute from the air injection time, the choke opening starts to decrease by 5% in every 10 seconds. The influx situations are illustrated in Figs. 9 & 10 for different flow rate and choke openings. In all cases, the influx volume was 2.7 lps.

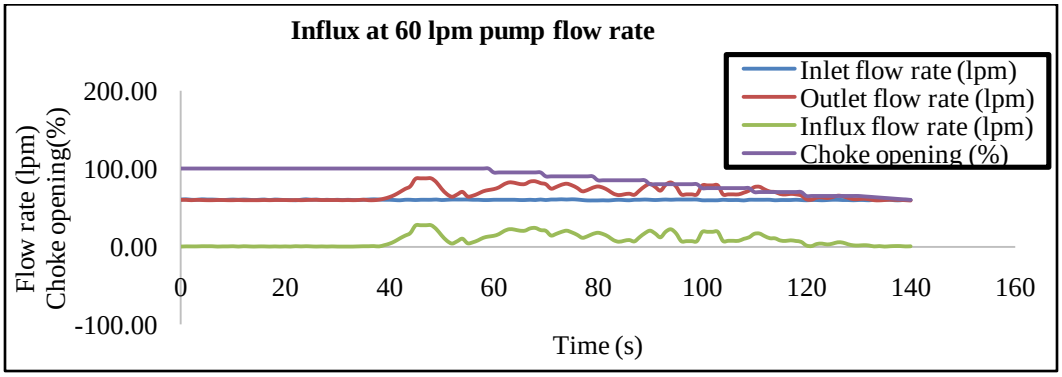

Figure 9 Influx at 60 lpm pump flow rate

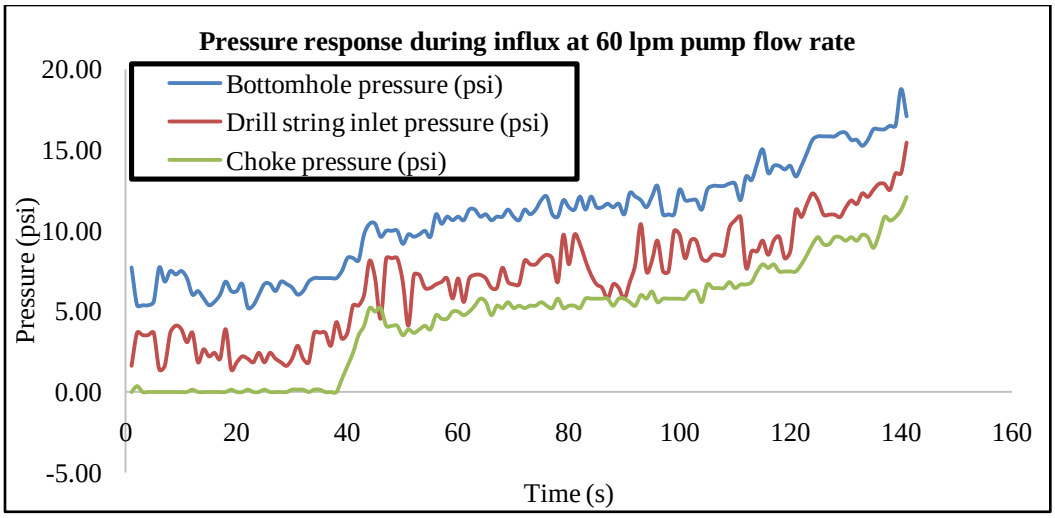

Figure 10 Pressure response during influx at 60 lpm pump flow rate

From Figs. 9 & 10 it can be concluded that the setup is able to generate influx situation maintaining the hydraulics of a drilling system. Moreover, the choke manipulation helps to maintain pressure in the overall system which controls the abnormal situation typically desired for a managed pressure drilling setup.

DISCUSSION

The pressure response of the overall system is dependent on the frictional pressure drop induced in the system. This loss is dependent on the velocity and type of fluid used in the operations. Even though water is used in our experiments for validating the model, non-Newtonian friction loss models can also be used when the fluid types are changed. With the assumption of minor loss coefficient to be 24 which is a constant for the experimental setup, the friction model was successful in predicting the bottom hole pressure in relation to the drill string inlet pressure. The developed experimental setup has the ability to observe the drilling parameters at different pump flow rates, influx condition and choke opening.

It is observed, in order to stop an influx situation, either the pump flow rate has to be increased or the choke opening has to be decreased. However, in our case, the pump flow rate is controlled by variable frequency drive linked with the pump which has to be changed manually. So, it is desired to change the system pressure by choke manipulation only.

CONCLUSIONS AND FUTURE WORKS

The developed experimental setup is capable of replicating the hydraulics of a typical managed pressure drilling system. The hydrodynamic behavior has been verified with both experimental and theoretical comparison. Future work will include the setups ability to respond to different control algorithms such as PID, MPC and NMPC control. These control algorithms will be used to device a model for safe operation which will help to get rid of problems associated in abnormal drilling conditions.

REFERENCES

Aadnoy, B.S. (2009). *Advanced drilling and well technology*. SPE. Advanced Drilling and Well Technology. *Society of Petroleum Engineers ISBN978-1-55563-145-1*.

Birkeland, T. (2009). Automated well control using MPD approach.

Chin, W. C. (2012). *Managed Pressure Drilling: Modeling, Strategy and Planning*. Gulf Professional Publishing.

Colebrook, C. (1938). Turbulent Flow in Pipes, and CF Colebrook and CM White, The Reduction of Carrying Capacity of Pipes with Age. *J. Inst. Civil Engrs*, *11*(133), 1939.

Godhavn, J., & Asa, S. (2010). Control Requirements for Automatic Managed Pressure Drilling System, (November 2009), 17–19.

Hannegan, D. M., & others. (2006). Case studies-offshore managed pressure drilling. In *SPE Annual Technical Conference and Exhibition*.

Hauge, E., Aamo, O. M., Godhavn, J. M., & Nygaard, G. (2013). A novel model-based scheme for kick and loss mitigation during drilling. *Journal of Process Control*, *23*(4), 463–472. http://doi.org/10.1016/j.jprocont.2013.01.006

Kaasa, G., & Stamnes, Ø. N. (2012). Simplified Hydraulics Model Used for Intelligent Estimation of Downhole Pressure for a Managed-Pressure-Drilling Control System. In *SPE/IADC Managed Pressure Drilling and Underbalanced Operations Conference & Exhibition, Denver*.

Moody, L. F. (1944). Friction factors for pipe flow. *Trans. Asme*, *66*(8), 671–684.

Nauduri, A. S. S., Medley, G. H., Schubert, J. J., & others. (2009). MPD: Beyond narrow pressure windows. In *IADC/SPE Managed Pressure Drilling and Underbalanced Operations Conference & Exhibition*. Society of Petroleum Engineers.

Nygaard, G., Vefring, E., Fjelde, K., Naevdal, G., Lorentzen, R., & Mylvaganam, S. (2007). Bottomhole Pressure Control During Drilling Operations in Gas-Dominant Wells. *SPE Journal*, *12*(1), 11–12. http://doi.org/10.2118/91578-PA

Rehm, Bill, Schubert, Jerome, Haghshenas, Arash, Paknejad, Amir Saman, & Hughes, J. (2013). *Managed Pressure Drilling*. Elsevier.

Reitsma, D. (2010). A simplified and highly effective method to identify influx and losses during Managed Pressure Drilling without the use of a Coriolis flow meter. In *SPE/IADC Managed Pressure Drilling and Underbalanced Operations Conference and Exhibition*. Society of Petroleum Engineers.

Scheid, C.M., Calçada, L.A., Braga, E.R., Paraiso, E.C.H., & Martins, A.L., 2011. Hydraulic study of drilling fluid flow in circular and annular tubes. *Brazilian Journal of Petroleum and Gas*, *5*(4).

Stamnes, O. N., Zhou, J., Kaasa, G.-O., & Aamo, O. M. (2008). Adaptive observer design for the bottomhole pressure of a managed pressure drilling system. In *Decision and Control, 2008. CDC*

2008. 47th IEEE Conference on (pp. 2961–2966).

Zhou, J., Stamnes, Ø.N., Aamo, O.M., & Kaasa, G.O. (2011). Switched control for pressure regulation and kick attenuation in a managed pressure drilling system. *IEEE Transactions on Control Systems Technology*, *19*(2), pp.337-350..

International Conference on Petroleum Engineering 2016 (ICPE-2016)
Bangladesh University of Engineering & Technology (BUET)
Dhaka-1000, Bangladesh

ICPE (2016-056)

Reservoir Rock Properties Analysis Using Core Data of Begumganj Gas field

B.M. Khasbur Rahman[1], Mohammad Islam Miah[2]
[1]Student, M.Sc., Department of Petroleum and Mineral Resource Engineering, Bangladesh University of Engineering and Technology
[2]Assistant Professor, Department of Petroleum and Mining Engineering, Chittagong University of Engineering and Technology

ABSTRACT

This research presents reservoir rock properties analysis using core data of Begumganj gas field well #3. Core analysis is to reduce uncertainty in reservoir evaluation by providing data representative of the reservoir at in situ conditions. The advances in core analysis techniques provide the premise to measure required petro-physical properties and to acquire simultaneously other reservoir rock dependent parameters. The quality and reliability of core data have become more important with the ever-increasing pressure to optimize field development. Basic (routine) core analysis involves the measurement of the most fundamental rock properties under near-ambient (atmospheric) conditions. Porosity (storage capacity for reservoir fluids), permeability (reservoir flow capacity), saturation (fluid type and content), and gross lithology all provide critical information in deciding whether a wellbore will be economic. It progresses through a phase of exploring alternate sources of information; well tests, logs, previous cores, and cuttings or sidewall cores. This core analysis research contains the results of a conventional core analysis program performed on core samples of the Begumganj well #3 (Core-1). The average sandstone of this core is 60% and shale is 40%. But whole core no.7 of upper portion has large amount of sandstone that is 70%.Among conclusive depth interval of the core, the porosity is moderate or fair, permeability is moderate. The average porosity of core is 14.3%. This porosity denoted that core is moderate or fair for reservoir rock. In individual analysis, sample no. 05, 06, 10 is better than other sample. Because of porosity of 05, 06, 10 are good category for reservoir rock. The average water saturation of the core-1 is 32%. That is why the amount of gas saturation is high. In individual analysis of core plug, sample no.3 has 54% water saturation that means it has large volume of water in the pore. Other core plug has low water saturation so that saturation of gas is high that is near by 67-68%. Cored interval image log of core-1 reveals both sandstone and shale bedding and core interval composite log of core-1 show moderate to good value of porosity and medium permeability. But, around at some lower part of the core may be dissolute. The formation resistivity factor verses cementation factor may be used in reservoir rock estimation and interpretation. Core analysis results are represented to moderate reservoir zone. These results are more reliable to use for further reservoir analysis and reserve estimation.

Keywords: Coring, Porosity, Permeability, KEYPHI instrument, Petrophysical properties, logging.

* Corresponding Author address
bm.khasbu2011@gmail.com

INTRODUCTION

Coring and core analysis form an integral part of formation evaluation and provide vital information unavailable from either log measurements or productivity tests. Core information includes detailed lithology, microscopic and macroscopic definition of the heterogeneity of the reservoir rock, capillary pressure data defining fluid distribution in the reservoir rock system, and the multiphase fluid flow properties of the reservoir rock, including directional flow properties of the system. The parameters that determine the behavior of the pore system are known as petrophysical properties and are porosity, permeability, saturation and capillarity. Porosity determines the storage capacity, while the permeability indicates the flow capacity of the rock for fluids. Saturation is used when more than one fluid is present and is defined as the fraction of the porosity that is occupied by a certain fluid such as oil, gas or water. Finally, capillarity determines the affinity between the reservoir fluids and the rock matrix and has therefore a strong influence on how much of the hydrocarbons that are stored in the pores can be produced.

In this research is the field of Begumganj well #3, an appraisal-cum-development well (Vertical), was spud on 27.07.2013 and drilled by GazProm. The drilled depth is 3565 meter. One core has taken from the depth of 2890.2-2897.2 meter. This core analysis research contains the results of a conventional core analysis program performed on core samples of the Begumganj well #3. The objectives of this research are given below:

- To determine the lithology of the core and it changes.
- To determine porosity and grain density, permeability of the core and observed how changes this value of parameters by depth.
- To determine fluid saturation in in-situ and surface condition (before extraction and after extraction of core plug).
- To measurement of rock resistivity.
- To determine formation factor (F), formation resistivity index (I), tortuosity, cementation factor (m), saturation exponent (n).

LOCATION OF THE STUDY AREA

State-run Petrobangla's exploration wing BAPEX (Bangladesh Petroleum Exploration and Production Company) has discovered a gas field in at Begumgonj in Noakhali. Begumganj Upazila (Noakhali district) with an area of 426.05 sq km, is bounded by Laksham upazila on the north, Noakhali sadar (old name Sudharam) upazila on the south [1]. Senbagh upozila is at the east, Lakshipur sadar and Chatkhil upozila on the west. The location of the Begumganj town is 22.944103N 91.100171E. Begumganj (town) stands 9 km to the north of Noakhali sadar [2], [3]. The location of Begumganj upozila is given in figure-1.

Figure-1: Location of begumganj upazila [4].

METHODOLOGY

The petrophysical parameters determination processes are followed by three stages: Procedures for Sampling, Routine Core Analysis and Special Core Analysis (of certain petrophysical parameters). Analysis and determine of this research are physical analysis by photography, lithology of the core, porosity and grain density, permeability of the core, fluid saturation in in-situ and surface condition (before extraction and after extraction of core plug), measurement of rock resistivity, formation factor (F), formation resistivity index (I), tortuosity, cementation factor (m), saturation exponent (n).

Photography and core preparation: The cores (1 meter each) should be clean and then keep into core photography system unit to examine hydrocarbon presence by (i) ultraviolet & (ii) white light color photography relationship. After this photography job, these cores are drilled in 2.54 cm (1") or in 3.81cm (1.5") diameter in cylindrical form with Automatic drill press fitted with diamond core bits (1" or 1.5"). For accommodating our laboratory equipment the samples (plugs) are cut by 1" or 3" length (maximum 2 plugs at every depth position point) [5], [6]. Their ends should be parallel to each other and vertical to the sample length axis.

Porosity and permeability: The KEYPHI instrument is a fully automated multi-samples porosimeter (and also permeameter) dedicated to measure the porosity & permeability to helium/nitrogen of plug sized core samples at multiple confining pressures ranging from 400 psi to 10,000 psi. The instrument is provided with a data acquisition & calculation computer station. Porosity & pore volume measurements are made using the Boyle's & Charles' law technique. Procedure to start sensor calibration: a) select transducer calibration tab panel b) select auto and 270 psi for P_{max}, & 10 psi for ΔP in configuration c) install standard volume $N^0>1$ d) confine e) connect at outlet instrument's pressure calibrator f) click on start calibration panel [10]. Procedure to start tank or volume calibration: a) click on clear calibration tank panel/button b) install standard $n^0 2$ c) select in the table the line $n^0 1$ d) confine e) click on start calibration button f) wait for availability of start calibration button g) vent the confining h) replace the standard by the next one h) select next line in the table i) repeat step d-I j) when last standard is finished, click on validate calibration tank button. Procedure to start measurement sample: a) in measure tab panel, fill the fields Name, Diameter, Length, Weight, Confining Pressure b) fill the Pore volume, if porosity option is not checked c) choose measures to do on the sample (porosity or porosity & permeability) by checking or not the porosity option d) install the sample e) click on start button f) wait for availability of start button g) go to the calculation tab panel to view results. To shutoff procedure, switch off the PoroPerm and unplug it from the main power [6].

Saturation: Weigh a clean, dry thimble. Use tongs to handle the thimble. Place the cylindrical core plug inside the thimble, and then quickly weigh the thimble & sample. Fill the extraction flask two-thirds full with toluene. Place the thimble with sample into the long neck flask. Tighten the ground joint fittings, but do not apply any lubricant for creating tighter joints [6], [7]. Start circulating cold water in the condenser. Turn on the heating jacket or plate and adjust the rate of boiling so that the reflux from the condenser is a few drops of solvent per second. The water circulation rate should be adjusted so that excessive cooling does not prevent the condenser solvent from reaching the core sample. Continue the extraction until the solvent is clear. Change solvent if necessary. Read the volume of collected water in the graduated tube. Turn off the heater & cooling water and place the sample into the oven (from 105^0C to 120^0C), until the sample weight does not change. The dried sample should be stored in desiccators. Obtain the weight of the thimble & the dry core. Calculate the loss in weight W_L, of the core sample due to the removal of oil & water [9], [10]. Measure the density of a separate sample of the oil. Calculate the oil, water & gas saturations after the V_p of the sample is determined.

Resistivity: At first, prepare a brine solution for an expected salinity or for brine system to core sample analysis. Saturate clean & dry core sample in this brine for 3 or 4 days using a covered glass vessel as the

saturating chamber. Before machine power switch turning, turn meter performance test switch (S_{w-4}) to 'test' position; then turn to resistance range selector switch (S_{w-1}) when X-1 on multiplier position and turn output control potentiometer (R_{-1}) & resistance reading potentiometer (R_{-2}) fully counterclockwise to zero. Turn power switch (S_{w-3}) to 'on' position. After 2 minutes warm-up, turn R_{-1} clockwise until potential reading meter (M_{-1}) reads exactly center scale, null position. Press potential matching switch S_{w-2} and adjust R_{-2} until M_{-1} reads exactly center scale. Repeat adjustment in R_{-2} as needed to cause M_{-1} to read the same with S_{w-2} in either position. Final resistance reading on R_{-2} times a multiplier (X-1) should be 510 ohms. Obtain a glass beaker thoroughly flushed with distilled water and then air dried. Pour sufficient brines in the glassware to completely cover the dip cell electrodes furnished using the same solution in which the core samples are saturating. Connect current (red) & potential (black) jumper leads of dip cell to test unit, grouped CA/PA & PB/CB respectively. Turn S_{w-4} to 'measure' position; turn S_{w-1} to X-100 on multiplier and turn R_{-1}& R_{-2} fully counterclockwise. Then turn S_{w-3} to on position. After 2 minutes warm-up, turn R_{-1} clockwise until M_{-1} reads approximately mid-scale, or turn range multiplier $S_{w-1}$to lower position until the first range is found where the mid-scale reading is possible. Press S_{w-2} and adjust R_{-2}until M_{-1} reads mid-scale as before. Repeat adjustment in R_{-2} as needed to cause M_{-1} to read the same null with S_{w-2} in either position. Multiply R_{-2} reading by S_{w-1} range multiplier to obtain brine resistance in ohms. Resistance of the brine multiplied by the dip cell constant gives resistivity in ohm-meters. Remove the 2 Bakelite retainer rings, from each side of the core holder. Remove the 2 chamois skin discs from these retainer rings and soak them in the brine in which the core samples are saturated. Remove chamois discs from the brine, squeezing out the excess water before placing over each brass plate electrode of the core holder. Install a Bakelite retainer ring over each chamois disc to hold it in place on the brass disc [6]. Remove the core from its brine container, wiping off all excess brine from the surface with the hand, and carefully place it between the 2 electrodes of the core holder. Connect core holder electrical leads to the resistivity measuring unit. Current leads CA & CB are attached to screws located on the rear of each core holder end plug and provide a current path across the entire end section of the sample. Voltage leads PA & PB are attached to each platinum wire installed in chamois retainer rings[8], [11]. Insure that CA/PA & PB/CB are used in pairs at each end of the sample .

Measure core resistance (R_c) using the same steps as outlined above for measuring resistance of brine solution: Clean & dry the rock sample. Measure the porosity of the rock sample with helium or with a fluid saturation technique. Saturate rock with a conductive fluid if not already done in the porosity determination step. Measure the bulk resistivity of the rock saturated with the fluid. Measure the resistivity of the fluid that saturates the rock in a separate vessel. Rearrange & apply "Archie's first law (formation factor): $R_o = FR_w$", to obtain the formation factor. Rearrange & apply "Modification of Archie's first law: $R_o = R_w \phi^{-m}$", to obtain the cementation exponent [12] [13].

Methods of d value, erecting the "*m*" value: A log-log plot of F versus ϕ yields a straight line that can be extra plotted to $\phi = 1$ to find (a). The slope of the line (red) is $-m$ (Due to that Log ϕ always will be with (-value). A best fit line drawn through the points intersects the representing $\phi = 1$, at a value. The slope of the line is $-m$. "*a*" value is detected at the point of the intersection between the drawn line and (X = 1). Different "*m*" values affect the water saturation dramatically and of course leads to completely unreliable in "*a*" or (n) values does not affect the water saturation as much as "*m*" [6].

DATA ANALYSIS & RESULTS

Lithology: The Lithology of core-1 (Begumganj # 3) is mainly sandstone. The details lithological information of this core is shown in table-1.

Table-1: Lithological description from experimental data.

Whole Core No	Position	Depth	Lithological Description
4	Top	2893.20-94.20	Inter beded with thinly laminated siltstone; hard & compact, non-calcarious sandstone 60%; Shale 40%
	Middle		Sandstone 60%; Shale 40%
	Bottom		Sandstone 60%; Shale 40%
5	Top	2894.20-95.20	Sandstone with shale partings, micaceous, non-calcarious sandstone 60%; Shale 40%
	Middle		Sandstone 60%; Shale 40%
	Bottom		Sandstone 60%; Shale 40%
6	Top	2895.20-96.20	Sandy shale with sand lens, micaceous, non calcarious sandstone 60%; Shale 40%
	Middle		Sandstone 60%; Shale 40%
	Bottom		Sandstone 60%; Shale 40%
7	Top	2896.20-97.20	Sandstone with mica lamination, non calcarious sandstone 70%; Shale 30%
	Middle		Sandstone 60%; Shale 40%, pseudo laminated
	Bottom		Sandstone 60%; Shale 40%

The average sandstone of this core is 60% and shale is 40%. But whole core no.7 of upper portion has large amount of sandstone that is 70%.

Routine Core Analysis: The analyzed result of Begumganj (well no.3) (depth 2893-2897 m) by routine core analysis. Routine core analysis database is given table-2.

Table-2: Routine core analysis data.

Depth	Sample No	Grain density (g/cc)	ϕ_t(%)	ϕ_e(%)	K_{air}(mD)	K_∞(mD)	Bulk density (g/cc)
2896.9	17	2.04236	13.9069	13.07684	28.5793445	25.78915127	2.125732187
2895.6	08	1.676116	10.4481	9.558554	12.8553364	11.19721064	2.131136575
2894.9	06	3.68911	17.2632	16.55014	64.1801579	59.16011114	2.069490724
2893.1	05	3.171679	16.2229	15.47164	93.5512939	85.52363364	2.06537027
2895.1	10	3.228874	15.2049	14.4171	49.5237319	45.26678129	2.073572053
2896.5	11	2.704515	13.791	12.95752	34.9082999	31.40075734	2.089865061
2896.8	16	2.505502	13.2774	12.42969	32.1326722	28.87645282	2.128251572

The average porosity of core is 14.3%. This porosity denoted that core is moderate or fair for reservoir rock. In individual analysis, sample no. 05, 06, 10 is better than other sample. Because of porosity of 05, 06, 10 are good category for reservoir rock.

Special core analysis: The average permeability of core-1 is 45.1 mD. This permeability refers to core is moderate or fair for reservoir rock. In this core has medium permeability. In individual analysis, sample no. 08, 17 has low permeability that means it is formed by shale and little amount of sandstone. Sample no. 05 has large permeability so that fluid transmitted in this plug is very quickly.

The average water saturation of the core-1 is 32%. That is why the amount of gas saturation is high. In individual analysis of core plug, sample no.3 has 54% water saturation that means it has large volume of water in the pore. Other core plug has low water saturation so that saturation of gas is high that is near by 67-68%.

The empirically calculated capillary pressure data of core-1 reveals good environment to flow if hydrocarbon is present. Graphically show that, there is quite weak linear inverse relation between porosity and formation factor of the core.

According to theory of cementation factor, cementation factor is deviated from 1.3 to 2.24. Sample no. 5, 8, 16 are crossed the cementation factor range that means this sample are very compacted due to the presence of highly calcareous sandstone. On the other hand, cementation factor value of sample no. 3, 5, 11, 16 are into the range.

Saturation exponent range is 1.4-2.2 but all of core sample (except 18) are beyond the range.

Table-3: special core analysis data.

RW Cell (Dip Cell) factor determination with reference brine						
Brine name	**Salinity**(ppm)	**Resistivity @ 20°C**(Ohm.m)	**Brine Temp**°C	**Measured Resistance @ temp**(Ohm)	**Resistivity @ temp**(Ohm.m)	**RW Cell Factor @ 20°C**(m)
Known NaCl	25,000		19	19.74	0.068	0.00344

Sample			**Rw with actual brine**	**Sample Saturated with test brine**	**Sample Desaturated**		**Results**				
Depth	**Sample No**	**Porosity ϕ**	(ohm)	**R_0 @ 20°C** (ohm.m)	**Saturation S_w**(%Vp)	**R_t @ 20°C** (ohm.m)	**Formation Factor F_r**	**Cementation factor *m*** vs Porosity	**Tortuosity** vs Porosity	**Saturation exponent *n*** versus S_w	**Resistivity Index I_r** versus S_w
2894.5	3	4.09%	19.033	28.21	52.00%	223.381	440.927	1.904	18.017	3.164	7.919
2893.1	5	15.24%	18.69	18.998	28.00%	14.045	302.389	3.036	46.074	-0.237	0.739
2894.9	6	12.89%	19.2	15.441	35.90%	85.451	239.254	2.674	30.84	1.67	5.534
2895.6	8	12.18%	19.179	48.69	26.00%	18.009	755.255	3.148	91.986	-0.738	0.37
2896.5	11	14.14%	18.674	13.151	29.00%	34.681	209.499	2.732	29.617	0.783	2.637
2896.8	16	13.55%	18.661	41.91	32.00%	66.8	668.12	3.254	90.527	0.409	1.594
2896.1	18	12.01%	18.819	10.431	22.00%	117.788	164.9	2.409	19.809	1.601	11.292

Table-4: Summery of all experimental data

Core Properties	Minimum	Maximum	Average
Porosity %	10.44	17.26	14.3
Permeability (H) mD	12.85	93.55	45.1
Formation Factor	164.90	755.25	396.85
Water Saturation %	22.00	52.00	32

Log data:

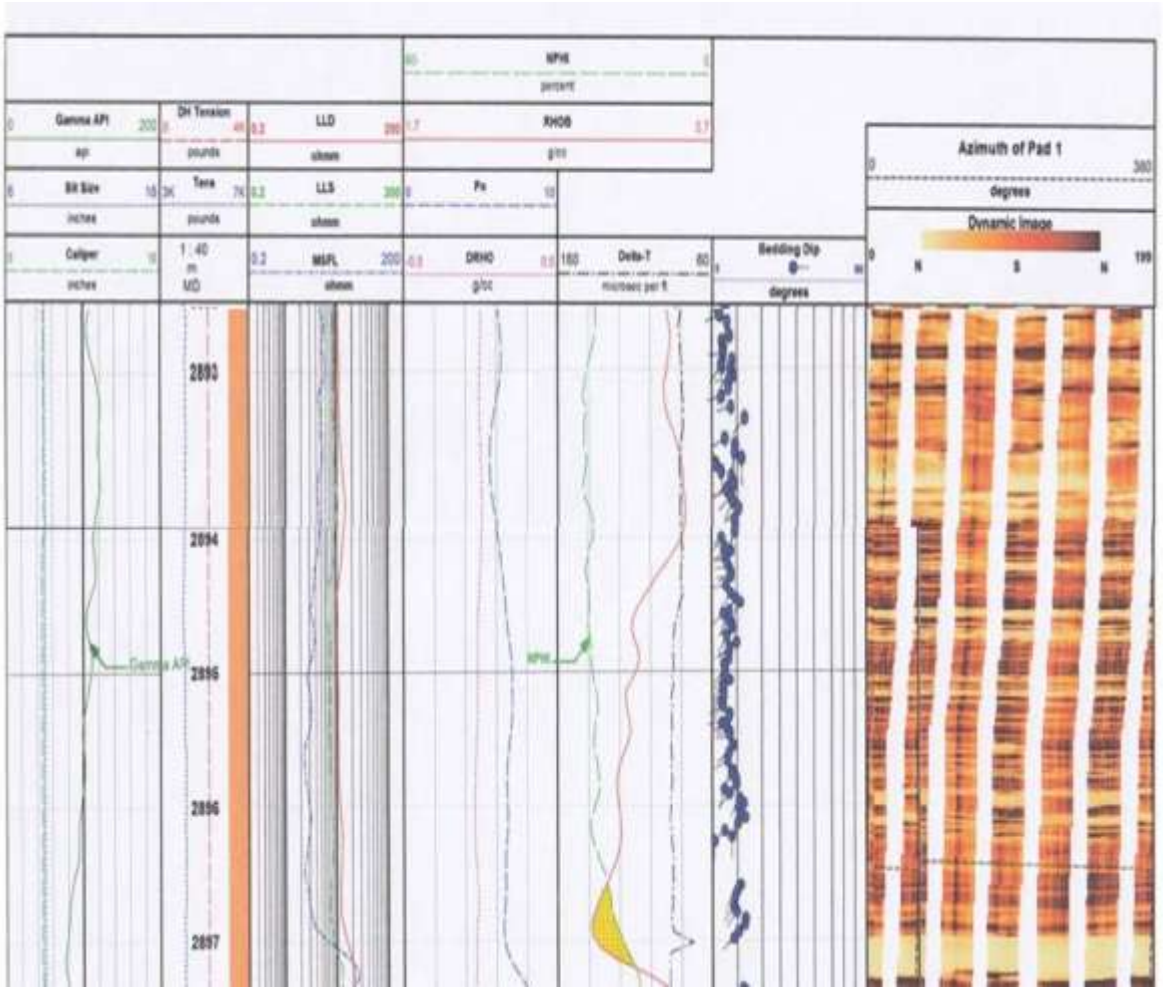

Figure: log of Begumganj (well no. 3) [6].

Cored interval image log of core-1 reveals both sandstone and shale bedding and core interval composite log of core-1 show moderate to good value of porosity and medium permeability. But, around at some lower part of the core may be dissolute. Cored interval composite log (2893-2897m MD): Composite log of the core indicate

at the depth of 2893m MD, permeability do not show same trend or deflection of against porosity, that is in here, dissolution is prevailed around 2893m MD. Core interval image log (2893-2897m MD): Gamma log is high, Neutron log is low to medium, Density value is high at 2895m which represent shale bedding, but 2893 m to 2894 m the density value is low and neutron log value is medium that represent sandstone at this zone. In this log represent that, the hydrocarbon bearing zone range from 2896.5 to 2897.5. Here positive intersection between neutron porosity log and sonic log

Graphical representation of core data

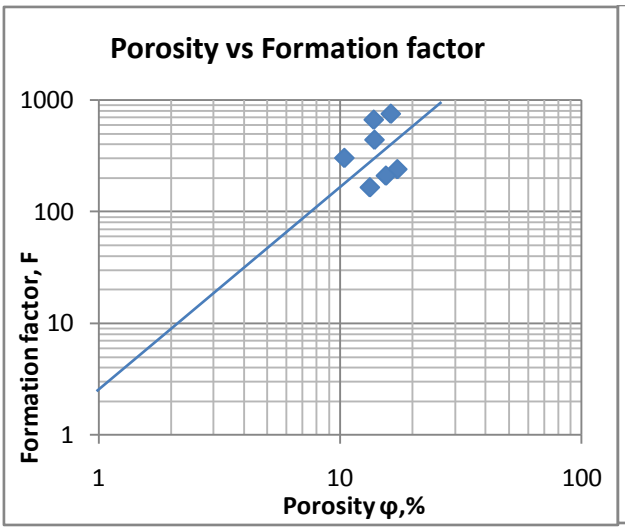

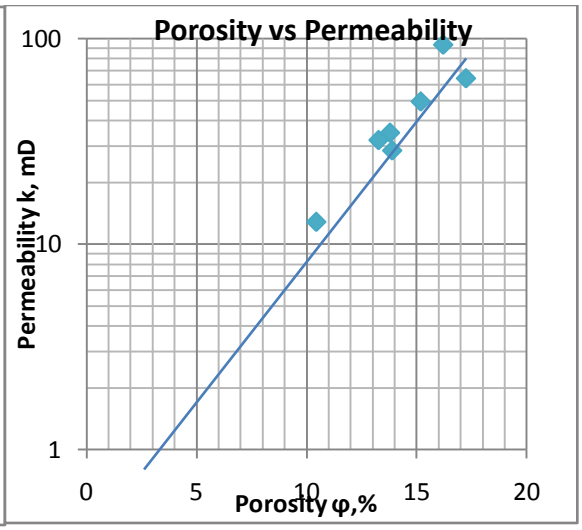

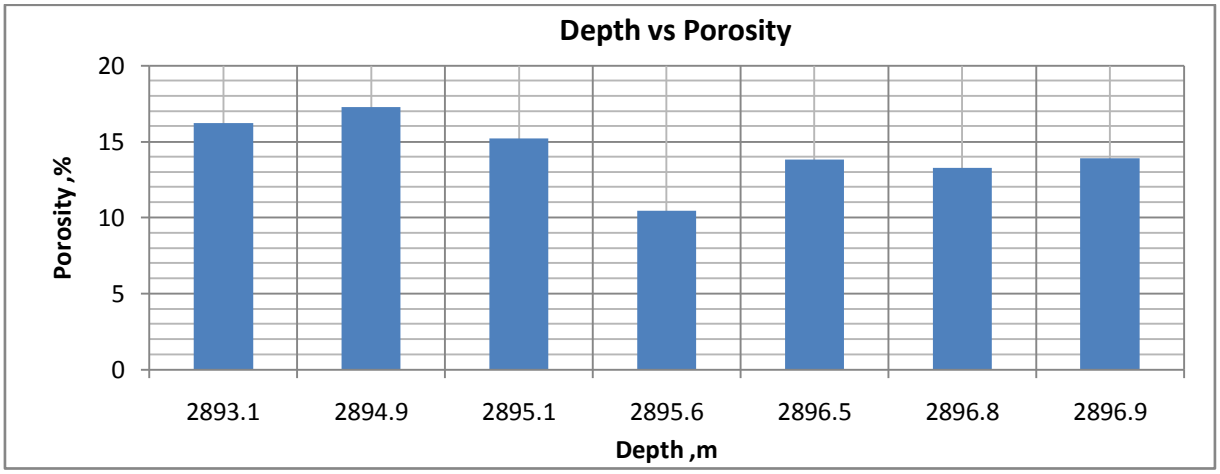

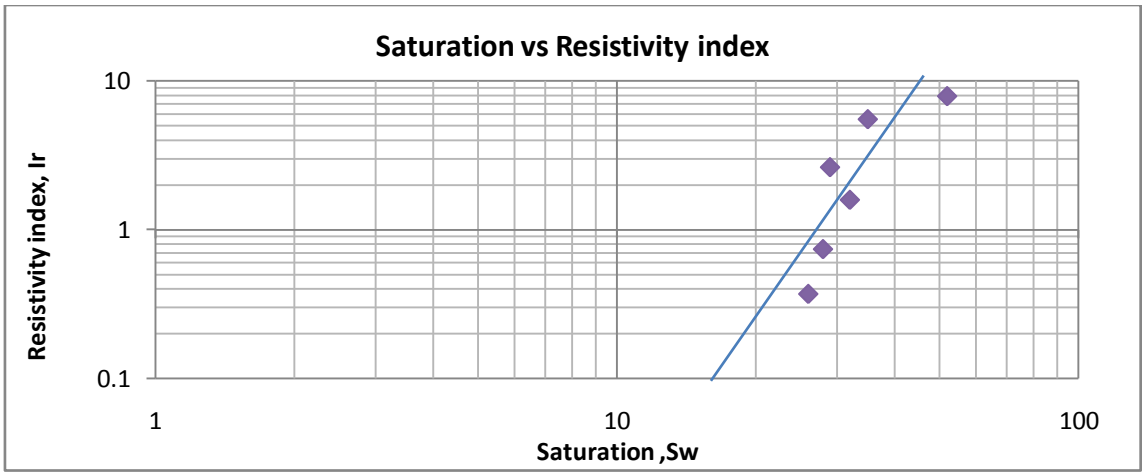

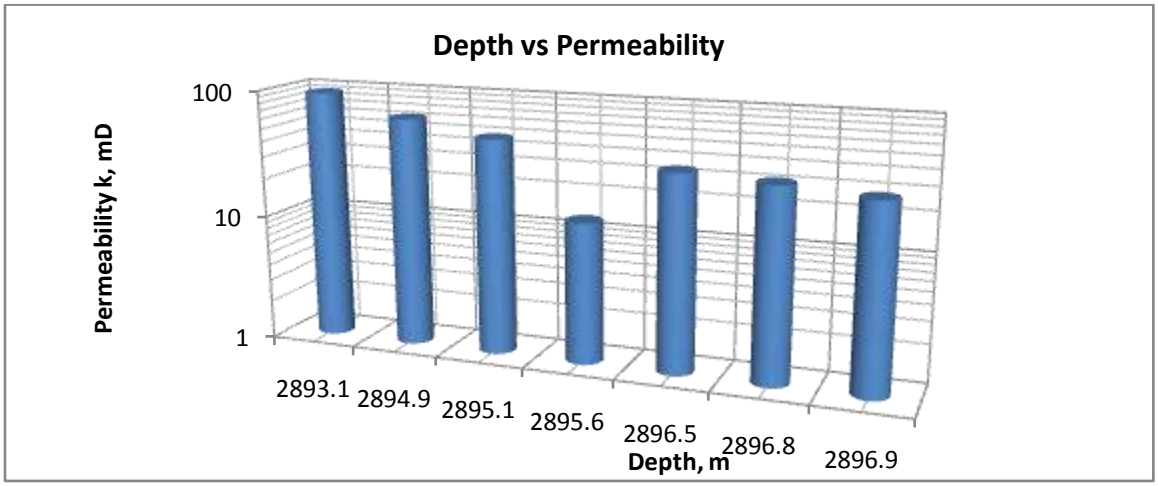

CONCLUSION

Seven number of depth points of the core have been selected for the study of petrophysical analysis and one or more sample of each depth point have been analyzed for petrophysical study to find out the data for effective porosity, permeability (both horizontal and vertical), rock density (both grain & bulk), fluid saturation (water), rock resistivity (both total and overall), formation resistivity factor and index, tortuosity and cementation factor which are shown in tabulated core analysis result sheets. Capillary pressure is measured not experimentally but empirically from porosity and permeability. Among conclusive depth interval of the core, the porosity is moderate or fair, permeability is moderate. The formation resistivity factor verses cementation factor may be used in reservoir rock estimation and interpretation. These two-factorial sketches indicate the conclusive sequence of the core is quite fracture. Log data is also analyzed and that's graphically represented. Hence, core analysis results are represented to moderate reservoir zone.

REFERENCES

[1] Ali, M. A., Baul, M. A., Murtaza, A. G., 1984, Reserve estimation report of Begumganj Gas Field. 19p.

[2] Alam MK, Hasan AKM, Khan MR & Whitney JW (1990) Geological map of Bangladesh. Published by Ministry of Energy and Mineral Resources, Geological Survey of Bangladesh with cooperation of U S Geological Survey.

[3] Petrobangla, 2009. Begumgonj Geological study, (Unpublished), 25p.

[4] Source: www.Wikipedia.com/begumganj upazila. Date of access: 3 September, 2015.

[5] An introduction to analysis for reservoir evaluation – core laboratories intentional inc, (August 1986). http://www.corelab.com/

[6] Reports on petrophysical parameters of reservoir rock of different geological structure of Bangladesh-petrophysical & reservoir study dept. Laboratory division, BAPEX, (Unpublished), pp 13-60.

[7] Conventional and special core analysis-R. Lenormand, version: 13, May 2006, pp 44-52.

[8] Resistivity theory-Dr.paul Glover, petrophysics MSc course note, pp 94-103.

[9] Petroleum Reservoir Engineering, J.R.Ursin & A.B. Zolotukhin Stavanger, 1997, pp 50-80.

[10] Laboratory methods of reservoir rock analysis, PMRE Dept. BUET (April-2003).

[11] American Petroleum Institute (API) recommended practices (40) for core analysis, 2nd edition, February 1998, pp 20-40, 123-200.

[12] Archie, 1942 Archie, G. E., The electrical resistivity log as an aid in determining some reservoir characteristics, Petroleum Transactions of the AIME 146, 1942, pp 54-62.

[13] Operation manual of all petroleum reservoirs engineering service of core analysis laboratories Inc, Dallas, Texas, USA, (September- January 1985).